



UNIVERSITAS INDONESIA

**MODIFIED GRAVITY ON COMPACT OBJECT AND ULTRA-COMPACT
OBJECT**

DISSERTATION

**ILHAM PRASETYO
1906340716**

**FACULTY OF MATHEMATICS AND NATURAL SCIENCES
PHYSICS BY RESEARCH PROGRAM
DEPOK
NOVEMBER 2021**

This page intentionally left blank



UNIVERSITAS INDONESIA

**MODIFIED GRAVITY ON COMPACT OBJECT AND ULTRA-COMPACT
OBJECT**

DISSERTATION

**Proposed in accordance to one of the requirements for the degree of
DOCTOR OF PHYSICS**

ILHAM PRASETYO

1906340716

**FACULTY OF MATHEMATICS AND NATURAL SCIENCES
PHYSICS BY RESEARCH PROGRAM**

DEPOK

NOVEMBER 2021

This page intentionally left blank

HALAMAN PERSETUJUAN

Judul : Modifikasi Gravitasi pada Objek Kompak dan Ultra-kompak

Nama : Ilham Prasetyo

NPM : 1906340716

Laporan Disertasi ini telah diperiksa dan disetujui.

13 November 2021



Prof. Dr. Anto Sulaksono

Promotor



Handhika Satrio Ramadhan, Ph.D

Kopromotor

This page intentionally left blank

HALAMAN PERNYATAAN ORISINALITAS

**Disertasi ini adalah hasil karya saya sendiri,
dan semua sumber baik yang dikutip maupun dirujuk
telah saya nyatakan dengan benar.**

Nama : Ilham Prasetyo

NPM : 1906340716

Tanda Tangan :



Tanggal : 13 November 2021

This page intentionally left blank

HALAMAN PENGESAHAN

Disertasi ini diajukan oleh :

Nama : Ilham Prasetyo
NPM : 1906340716
Program Studi : Ilmu Fisika
Judul Disertasi : Modifikasi Gravitasi pada Objek Kompak dan Ultra-kompak

Telah berhasil dipertahankan di hadapan Dewan Penguji dan diterima sebagai bagian persyaratan yang diperlukan untuk memperoleh gelar Doktor Fisika pada Program Studi Ilmu Fisika, Fakultas Matematika dan Ilmu Pengetahuan Alam, Universitas Indonesia.

DEWAN PENGUJI

Promotor	:	Prof. Dr. Anto Sulaksono	()
Kopromotor	:	Handhika Satrio Ramadhan, Ph.D	()
Penguji 1	:	Muhammad Aziz Majidi, Ph.D	()
Penguji 2	:	Prof. Dr. rer. nat. Terry Mart	()
Penguji 3	:	Dr. rer. nat. Agus Salam	()
Penguji 4	:	Dr. Adam Badra Cahaya	()
Penguji 5	:	Andy Octavian Latief, Ph.D	()

Ditetapkan di : Depok

Tanggal : 13 November 2021

This page intentionally left blank

ACKNOWLEDGEMENT

Thanks to Allah SWT. because of Him, I could finish this master thesis. Also thanks to Rasulullah Muhammad SAW. for his teachings, his family, his close friends and followers whose way of life become the examples of how to behave and do just in the Islamic way.

This thesis is written to fulfill the requirements to obtain the degree of doctoral in science (Dr.) from Math and Natural Science Faculty in Universitas Indonesia. I realize that in writing this dissertation, I have been supported by lots of people. Here I thank them, especially

1. my father Aba Badrudin, my mother Sri Susilowati, and my older brother Dhion Cahyo Pratomo for their endless support and encouragement;
2. my dissertation advisors Anto Sulaksono and Handhika Satrio Ramadhan for their encouragement and patience;
3. my academic advisor Muhammad Aziz Majidi for his support, valuable advice, and patience;
4. my friends at our theoretical lab: Adit, Byon, Reyhan, Sayyid, Agya, Gerwin, Lala, Andri, Ridwan, Haris, and many more that I cannot mention here.

I dedicate this dissertation to my family and my dear friend Muhammad Iqbal, who had passed away while pursuing his doctoral degree. I hope this dissertation is useful for newcomer researchers.

Tangerang Selatan, 28 December 2021

Ilham Prasetyo

This page intentionally left blank

HALAMAN PERNYATAAN PERSETUJUAN PUBLIKASI TUGAS AKHIR UNTUK KEPENTINGAN AKADEMIS

Sebagai sivitas akademik Universitas Indonesia, saya yang bertanda tangan di bawah ini:

Nama : Ilham Prasetyo
NPM : 1906340716
Program Studi : Ilmu Fisika
Fakultas : Matematika dan Ilmu Pengetahuan
Alam
Jenis Karya : Disertasi

demi pengembangan ilmu pengetahuan, menyetujui untuk memberikan kepada Universitas Indonesia **Hak Bebas Royalti Noneksklusif (Non-exclusive Royalty Free Right)** atas karya ilmiah saya yang berjudul:

Modifikasi Gravitasi pada Objek Kompak dan Ultra-kompak

beserta perangkat yang ada (jika diperlukan). Dengan Hak Bebas Royalti Noneksklusif ini Universitas Indonesia berhak menyimpan, mengalihmedia/formatkan, mengelola dalam bentuk pangkalan data (database), merawat, dan memublikasikan tugas akhir saya selama tetap mencantumkan nama saya sebagai penulis/pencipta dan sebagai pemilik Hak Cipta.

Demikian pernyataan ini saya buat dengan sebenarnya.

Dibuat di : Depok
Pada tanggal : 13 November 2021
Yang menyatakan



(Ilham Prasetyo)

This page intentionally left blank

ABSTRAK

Nama : Ilham Prasetyo
Program Studi : Ilmu Fisika
Judul : Modifikasi Gravitasi pada Objek Kompak dan Ultra-kompak

Dalam disertasi ini, dua jenis model gravitasi termodifikasi dipelajari dan dampaknya ditinjau pada beberapa sifat bintang neutron. Model pertama adalah gravitasi semi-klasik (SCGrav) yang diajukan oleh Carballo-Rubio [PRL 120, 061102 (2018)] dan model kedua adalah model gravitasi Eddington-inspired Born Infeld (EiBI) yang dipopulerkan oleh Banados dan Ferreira [PRL 105, 011101 (2010)]. Dalam model SCGrav terdapat parameter l_p yang merupakan konstanta kopling untuk sebuah suku tambahan pada bagian materi di persamaan medan Einstein. Dalam EiBI terdapat κ , merupakan parameter yang secara skematis mengatur kekuatan dari suku-suku tensor Ricci nonlinear dalam Lagrangian ($\mathcal{O}(R^{n+1})$, $n \geq 1$), dan λ , yang berelasi dengan konstanta kosmologi biasa Λ_c . Pada model SCGrav, efek l_p menjadi fokus studi dan kami bandingkan dengan sistem persamaan Tolman-Oppenheimer-Volkoff (TOV) standar dalam relativitas umum (GR). Dari analisis kami pada SCGrav, kami mendapatkan bahwa efek l_p tidak signifikan jika dibandingkan dengan TOV GR. Sementara itu, pada model EiBI, kami berfokus pada efek Λ_c terhadap momen inersia I dan parameter deformabilitas tidal Λ . Konstanta kosmologi Λ_c dari hasil observasi digunakan dan dibandingkan hasilnya dengan data-data yang diekstraksi dari hasil analisis beberapa literatur yang meninjau data-data observasi tidak langsung dari berbagai bintang neutron bermassa $1.4M_\odot$. Dari analisis terhadap konstanta kosmologi hasil pbservasi, massa maksimum yang diraih hanya sekitar $2.1M_\odot$.

Kata Kunci:

gravitasi semi-klasik, gravitasi Eddington-inspired Born Infeld, bintang neutron, objek kompak, objek ultra-kompak

ABSTRACT

Name : Ilham Prasetyo

Program : Physics

Title : Modified Gravity on Compact Object and Ultra-compact Object

In this dissertation, we investigate two kinds of modified gravity models and their impact on some properties of a neutron star. The first model is the semiclassical gravity (SCGrav) proposed by Carballo-Rubio [PRL 120, 061102 (2018)] and the second model is the Eddington-inspired Born Infeld gravity (EiBI) popularized by Banados and Ferreira [PRL 105, 011101 (2010)]. In the SCGrav model, there is a parameter l_p which is a coupling constant for an additional term on the matter part of the Einstein field equation. In EiBI there are κ , which is the parameter that schematically set the strength of the nonlinear Ricci tensor terms in the Lagrangian ($\mathcal{O}(R^{n+1})$, $n \geq 1$), and λ , which is related to the usual cosmological constant Λ_c . In the SCGrav model, we focused on studying the effect of l_p and we compare it with the standard Tolman-Oppenheimer-Volkoff equation (TOV) in general relativity (GR). From our analysis on SCGrav, we obtain that the effect of l_p is not significant if compared to TOV GR. On the other hand, in the EiBI model we focus on the effect of cosmological constant Λ_c towards the moment of inertia I and tidal deformation parameter Λ . We use Λ_c from observation and compare the results with observational data from neutron stars with mass $1.4M_\odot$. From our analysis, the maximum mass which can be reached is only around $2.1M_\odot$.

Keywords:

semiclassical gravity, Eddington-inspired Born Infeld gravity, neutron star, compact object, ultracompact object

CONTENTS

TITLE PAGE	i
LEMBAR PERSETUJUAN	iii
LEMBAR PERNYATAAN ORISINALITAS	v
LEMBAR PENGESAHAN	vii
ACKNOWLEDGEMENT	ix
LEMBAR PERSETUJUAN PUBLIKASI ILMIAH	xi
ABSTRAK	xiii
CONTENTS	xv
LIST OF FIGURES	xvii
LIST OF TABLES	xviii
1 INTRODUCTION	1
1.1 Background and Motivation	1
1.2 The Outline	2
2 A BRIEF REVIEW OF GENERAL RELATIVITY	5
3 COMPACT AND ULTRA-COMPACT OBJECTS	13
4 NEUTRON STARS	17
4.1 Neutron Stars	17
4.2 The $\sim 2.6M_{\odot}$ NS from GW190814 event	19
5 RELATIVISTIC MEAN FIELD	21
5.1 Relativistic Mean Field	21
5.2 The Neutron Star Matter's Equation of State	26

6 ULTRA-COMPACT OBJECT FROM SEMI-CLASSICAL GRAVITY	33
6.1 A Short Introduction to The Semi-classical Gravity	33
6.2 Theory of a Compact Star in Semi-classical Gravity	35
6.3 Analysing the Negative Branch	37
6.4 Numerical Results	44
6.5 Numerical Verification	50
6.5.1 Numerical solutions from negative branch	50
6.5.2 Forward and backward integration solutions from positive branch	54
6.5.3 Comparison of our numerical results with the density for regular geometry part of Ho-Matsuo model	55
6.6 Conclusions	60
7 MOMENT OF INERTIA AND TIDAL DEFORMATION IN EDDINGTON-INSPIRED BORN INFELD THEORY OF GRAVITY	63
7.1 Introduction	63
7.2 The Eddington-inspired Born-Infeld Theory of Gravity	65
7.2.1 Vacuum solution	66
7.2.2 Moment of Inertia	67
7.2.3 Tidal Deformation	70
7.2.3.1 The vacuum case	71
7.2.3.2 The Non-vacuum case	76
7.3 Numerical Results and Discussions	78
7.4 Conclusions	87
8 CONCLUSIONS	89
8.1 First part	89
8.2 Second part	90
REFERENCES	91
APPENDIX	I
A TETRAD METHOD	III
PENYANDANG DANA DAN PUBLIKASI ILMIAH TERKAIT DISERTASI	IX
BIOGRAFI PENULIS	X

LIST OF FIGURES

1.1	Flowchart connecting 1st work and 2nd work	3
5.1	Binding energy comparison between EoSs	28
5.2	Pressure comparison between EoSs	29
5.3	Variations of G3 RMF EoS by adding hyperon or speed of sound constraint	31
5.4	M-R result from variations of G3 RMF EoS	32
6.1	Profiles from varying w	45
6.2	Here are the M-R curves from variations of w	46
6.3	Here are the M-R curves from variations of B . If B is decreased, it produces higher mass and larger radius.	47
6.4	Here are the M-R curves from variations of α	48
6.5	Here are the M-R curves from variations of l_p	49
6.6	The backward and forward integration results on the negative branch . .	53
6.7	Profiles of pressure in the positive branch from backward integration, forward integration, and the comparison between them	56
6.8	Negative central mass leads to near black hole limit	58
6.9	Zero central mass leads to near and beyond Buchdhal limit	59
7.1	Effect from varying κ	79
7.2	Effect of using observed Λ_c to M-R relation for different EoSs	80
7.3	Effect of using observed Λ_c to moment of inertia	81
7.4	Effect of using observed Λ_c to tidal deformability	82
7.5	M-R relation by variations of Λ_c	83
7.6	These are M-R curves from different EoSs	84
7.7	The result from varying κ and Λ_c on the unphysical case	85
7.8	Moment of inertia within EiBI obtained from G3 WHSS EoS with variations of κ and very large and negative Λ_c	85
7.9	The tidal deformation with κ varied and negative with very large value of Λ_c	86

LIST OF TABLES

6.1 The tabulated compactness data from variations of w , B , and p_c , with $m_c = 0$	60
---	----

CHAPTER 1

INTRODUCTION

1.1 Background and Motivation

The gravitational wave (GW) astronomy by The Laser Interferometer Gravitational-Wave Observatory (LIGO) collaboration [1] gave rise to many studies about what kind of massive bodies produce such waves in the fabric of space-time. The studies are not only limited to “relativist” but also include contributions from other fields of study, especially astronomy. The process of two massive bodies orbiting each other until they combine gives GW signals. If the two bodies are not black holes (BHs), then electromagnetic waves are also produced, which are detected by radio telescopes and so on. From these, people can measure many astronomical properties. From the point of view of astronomy, the coalescing process of two neutron stars can synthesize heavy metals, e.g., silver and platinum. The matter properties of neutron stars, which are still mysterious, can then be examined quite directly.

From the theoretical physics point of view, the GW is the playground. If the resulting object after the ringdown phase, the phase after the two objects coalesce, gave an object other than a black-hole dan has compactness larger than a third ($GM/R > 1/3$, with G the Newton constant, M the mass, and R the radius), it is said that there will be a series of GW echo [2]. Motivated by this, many papers had discussed such horizonless ultra-compact objects (UCOs), which is more massive than a neutron star (NS) because its compactness is less than NS’ ($1/6 < GM/R < 1/3$), and their main way to detect a UCO is by the GW echo. One such proposal is called gravastar [3, 4], where the surface of the star acts like a shield that divides de-Sitter space-time inside and the Schwarzschild space-time outside. The surface is said to be a thin shell of ultra-relativistic matter. Interestingly, Carballo-Rubio [5] had proposed how to produce the said star using semiclassical gravity theory (SCGrav). SCGrav can be seen as a modified theory of gravity by adding a term called renormalized stress-energy tensor (RSET) with its strength determined by a coupling constant l_p .

In this dissertation, we shall discuss SCGrav. Usually, SCGrav is used to discuss BHs, but in our work here we choose compact objects (COs). The theory predicts two branches of equations called positive and negative branches. The negative branch goes to the standard Tolman-Oppenheimer-Volkoff (TOV) equation in general relativity (GR) in the limit $l_p \rightarrow 0$, while the positive branch does not. We focus on the negative branch and compare

its differences with TOV GR because the positive branch predicts the combination of a black star and a gravastar, which are exotic objects with an exotic type of matter. This theory is interesting because not only the TOV equation is modified but the differential equation for the mass itself is also modified significantly. This modification restricts what type of equation of state (EoS) of the nuclear matter inside the NS.

On the other hand, the recent GW190814 event [6] triggers another excitement. They found a new mysterious compact object whose mass is around $2.6M_{\odot}$ (M_{\odot} is the solar mass). There are various studies that try to determine the nature of this object. It is known that the mass of the most massive neutron star PSR J0740+6620 is around $2.1M_{\odot}$ [7]. This $0.4M_{\odot}$ gap leads people to investigate what mechanism that allows such object to exist. Some proposed that either it is a black hole (BH) [6, 8, 9, 10] or a fast rotating neutron star (NS) [6, 11, 12, 13, 14]. Other exotic objects are also proposed, e.g., quark star [15, 16, 17, 18, 19, 20, 21] or hybrid star [22, 23], with or without rotation. Some others also proposed that it is possible to obtain an NS with mass around $2.6M_{\odot}$ using modified gravity theories [24, 25, 26, 27].

To tackle this $2.1M_{\odot}$ problem, we shall use another modified gravity called Eddington-inspired Born Infeld gravity (EiBI) [28, 29, 30, 31, 32]. The EiBI parameters κ and λ can be used to increase or decrease the maximum mass M and radius R of an NS. The cosmological constant Λ_c is related to λ by $\lambda = \kappa\Lambda_c + 1$. In Ref. [33], the role of κ has been discussed extensively with λ set to unity or equivalently $\Lambda_c = 0$. We shall discuss what is happening to an NS if we set $\Lambda_c \neq 0$. Then our calculations extract the moment of inertia I of the NS if it is slowly rotating and its tidal deformability Λ if the NS is perturbed. The results are compared with the various known observations.

1.2 The Outline

In this dissertation, we present our results in two parts. The first part is the result of applying a linear EoS, which corresponds to a UCO, in the SCGrav theory. From this, we analyze the effect of parameter l_p compared to the standard TOV in GR. The second part is the result of calculating the moment of inertia and the tidal deformation aspect from an NS whose matter is described by Relativistic Mean Field theory (RMF) using the G3 parameter set from Ref. [34]. We compare the results with the observed data from various papers and analyze its behaviors if we vary the value of both κ and Λ_c .

This dissertation is organized as follows. In chapter 1, we briefly discuss the background of our research, the specific problems that we investigate, and the goals. In chapter 2, we briefly explain the tools we use from GR. In chapter 3, we briefly introduce the notion of CO and UCO including their current status in the research community. In chapter

4, we briefly introduce the notion of NS and we include its current status in the research community. In chapter 5, we shall very briefly discuss the Relativistic Mean Field theory (RMF), which is the tool to produce the EoS for the second part of this work, which will be important to describe the matter content in a particular massive object. In chapter 6, we show the first part of our results, i.e., our analysis of SCGrav. In chapter 7, the second part of our results is shown, i.e., our analysis of the moment of inertia and tidal deformation in EiBI. Lastly, in chapter 8, we discuss the conclusions from both parts of our work. We also include Appendix A which, respectively, are essential for the second part of our work. Fig. 1.1 may help explain the connection behind the two works.

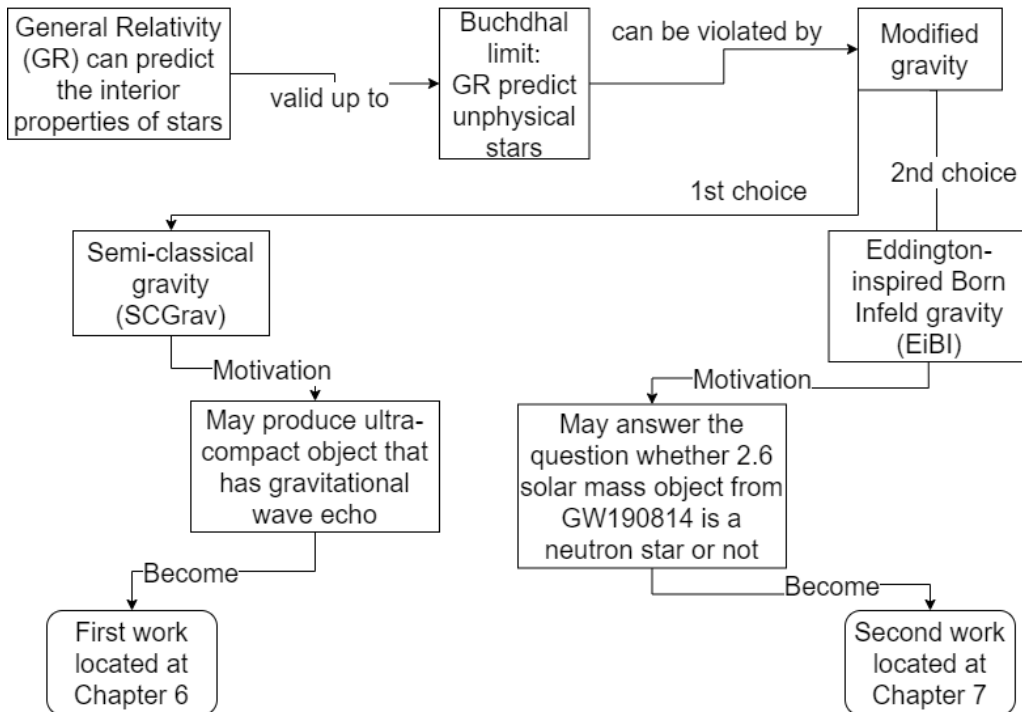


Figure 1.1: This is the flowchart that show the motivation on why we do the two works.

This page intentionally left blank

CHAPTER 2

A BRIEF REVIEW OF GENERAL RELATIVITY

In this chapter, we revisit some tools in general relativity (GR) that are necessary for our work. This review is not comprehensive, so the readers are referred to some literature listed as follows:

- Some great introductory books: Ryder [35], Carroll [36], and D’Inverno [37];
- A haven for tools, many are not explained in other books: Poisson [38];
- A very popular encyclopedia covering many topics in GR, both theoretical and experimental: Misner, Thorne, and Wheeler [39];
- A haven for tools that contain many other things which are more mathematically oriented, e.g., differential geometry: Nakahara [40] and Baez and Muniain [41];
- Full of elegant derivations but quite advanced and contains the short version of singularity theorems: Wald [42];
- Hailed as the classic which contains very mathematical treatment on both black holes and cosmology, very comprehensive discussions on black holes, and the full version of the singularity theorems: Hawking and Ellis [43];
- A classic book on differential geometry with physicists as the target audience: Nash and Sen [44];
- Covering the origin of the Hawking temperature obtained by SCGrav approach, i.e., quantum field theory employed alongside GR: Birrell and Davies [45], Parker and Toms [46], and Wald [47];
- The books for astrophysicists and nuclear scientists studying NS and other COs: Glendenning [48], Weber [49], and Poisson and Will [50].
- A very detailed book to study black-holes and their perturbation aspects: Chandrasekhar [51].

We start with a few discussions about the physical phenomena in GR. The gravitational field exerted by a typical neutron star (NS) is considerably different compared to the flat space-time, where the special relativity holds and the gravity is still Newtonian. An NS with mass M around $1.5M_{\odot}$ and radius R around 10 km has compactness

$C = GM/R$ (with G the Newton constant) much larger than the Sun and the Earth, i.e., $2C \sim 0.4$ for NS, $2C \sim 10^{-6}$ for the Sun, and $2C \sim 10^{-9}$ for the Earth.

Furthermore, if any massive bodies are rotating, the phenomenon of frame dragging (known as the Lense-Thirring effect) happens. This effect is not intuitive since it has no analogy in Newtonian physics. When Newton first investigates the role of rotation on a bucket filled with water in 1686, he was interested in whether non-uniform motion is relative or not to its surroundings. Newton argued that the water is forced to rise the sides of the bucket due to centrifugal force, so the bucket's rotation is absolute. E. Mach reexamined this argument in 1883 in an attempt to better understand how inertial force arises. He asked if the bucket is fixed and the universe is rotating about it then what causes the water to rise. This is known as Mach's principle. He suggested that if the vessel's thickness and mass are sufficiently large, the surface of the water may depend on the rotation of the vessel. Lense and Thirring [52] in 1918 answered such a question with Einstein's formulation of gravity, which was finished a couple of years earlier.

In the following passage, we try to explain what the Lense-Thirring effect is. A gyroscope is an apparatus that can automatically orient itself, which is why it is used in airplanes to orient itself to the Earth. In special relativity, the precession of a gyroscope—called Thomas precession—is dependent on the force which influences the gyroscope. In GR, on the other hand, there exist two more precisions called de-Sitter precession and Lense-Thirring precession. The de-Sitter precession is similar to the Thomas precession with the force replaced by gravitational force with a factor of 3. The Lense-Thirring precession, on the other hand, depends not on the force but the angular momentum from the rotating massive body [35]. This effect is tested by the Gravity Probe B satellite.

Now that we can somehow see that the fabric of space-time is real due to the Lense-Thirring effect, we turn to the mathematical description of such a thing. The origin of the tools was already been developed by Riemann and other mathematicians, and it is connected to physics by Einstein. It came from a branch of study in mathematics called differential geometry. Differential geometry turns out not only useful for gravity but also useful as a tool to study other things, such as the topological nature of both the Aharonov-Bohm phenomenon and the Yang-Mills field. But in this dissertation, we intend to restrict our review of GR only to the tools necessary for our work.

Suppose a particle's trajectory in a space is a line denoted by a function $f(s)$ with an auxilliary parameter s . The position of the particle in that line can be denoted as a vector. In Newtonian mechanics, this vector is basically a triple of real numbers denoted as $x^i = (x^1, x^2, x^3)$. In special relativity, time is not an arbitrary parameter anymore, so it is included as $x^0 = ct$, with c the speed of light in vacuum, in a 4-vector $x^\mu =$

(x^0, x^1, x^2, x^3) or more generally,

$$\vec{x} = x^0 \hat{e}_0 + x^1 \hat{e}_1 + x^2 \hat{e}_2 + x^3 \hat{e}_3 \equiv x^\mu \hat{e}_\mu. \quad (2.1)$$

Here \hat{e}_μ is called *vector basis*. We omit the summation symbol in the last equality because we use the Einstein summation convention. The component of this vector, x^μ denoted by a superscript index, is called *contravariant* quantity. The particle should have the “speed” when moving along the line. This can be extracted by the chain rule

$$\frac{d}{ds} f = \left(\frac{dx^0}{ds} \frac{\partial}{\partial x^0} + \frac{dx^1}{ds} \frac{\partial}{\partial x^1} + \frac{dx^2}{ds} \frac{\partial}{\partial x^2} + \frac{dx^3}{ds} \frac{\partial}{\partial x^3} \right) f = \frac{dx^\mu}{ds} \frac{\partial}{\partial x^\mu} f. \quad (2.2)$$

The form of d/ds in the left hand side, in mathematics, is called *the* vector, which is locally shown with the vector basis $\hat{e}_\mu = \partial/\partial x^\mu$. So in a sense, the vector basis acts like an operator acting on a scalar function. Because the scalar functions should be differentiable, this mathematical construction motivates the notion of *differential geometry*.

In physics, we usually denote an infinitesimal quantity of, say a function $F(x^\mu)$, as

$$dF = \frac{\partial F}{\partial x^\mu} dx^\mu. \quad (2.3)$$

The components can be relabeled as $\omega_\mu = \partial F / \partial x^\mu$. This quantity, with subscript index, is called *covariant* quantity. In mathematics, a quantity resembling dF is called covector and dx^μ is called *covector basis*. In general, covector basis is denoted as something with superscript index ($\hat{\omega}^\mu$) while the vector basis use subscript index (\hat{e}_μ):

$$\boldsymbol{\omega} = \omega_\mu \hat{\omega}^\mu, \quad \vec{V} = V^\mu \hat{e}_\mu. \quad (2.4)$$

The definition of covector and vector is necessary to define the generalisation of dot product. While the vector basis act like an operator to a scalar function, the covector basis act like an operator to the vector basis. This condition

$$\hat{\omega}^\mu(\hat{e}_\nu) = \delta_\nu^\mu \quad (2.5)$$

is necessary to obtain the dot product between a covector $\boldsymbol{\omega}$ and a vector \vec{V}

$$\boldsymbol{\omega}(\vec{V}) = \omega_\mu V^\mu. \quad (2.6)$$

From now on, we shall call something with superscript (subscript) index, e.g., V^μ (ω_μ), as a vector (covector).

Another way to obtain a dot product of two vectors can be done via the so-called

metric tensor $g_{\mu\nu}$. In a *finite* dimensional space-time, we can obtain the covector of V^μ by

$$V_\mu = g_{\mu\nu} V^\nu. \quad (2.7)$$

In physics, this metric tensor is usually introduced by the infinitesimal length of a flat space-time in Cartesian coordinate

$$ds^2 = -c^2 dt^2 + dx^2 + dy^2 + dz^2 = g_{\mu\nu} dx^\mu dx^\nu. \quad (2.8)$$

So the metric $g_{\mu\nu}$ can be visualized as a 4×4 matrix, whose diagonal components has sign $(-, +, +, +)$. Its inverse is denoted as $g^{\mu\nu}$, which can be used to make a subscript index become superscript index

$$V^\mu = g^{\mu\nu} V_\nu. \quad (2.9)$$

This bijective map between vectors and covectors requires that the dimension of the space-time is finite.

Now we introduce the notion of tensors. A scalar f , vector V^μ , covector ω_μ , metric $g_{\mu\nu}$ and inverse metric $g^{\mu\nu}$, respectively, are tensor rank $(0, 0)$, $(1, 0)$, $(0, 1)$, $(0, 2)$, and $(2, 0)$. Except for the scalar, the tensor indices denote the *local* version of the tensor. In mathematics a tensor T rank $(1, 1)$ is written locally in a coordinate system x^μ as

$$T = T^\mu{}_\nu \left(\frac{\partial}{\partial x^\mu} \otimes dx^\nu \right). \quad (2.10)$$

The entity inside the round bracket can be thought of as the basis of the said tensor. If we choose another coordinate system, say x'^μ , we write the tensor as

$$T = T^{\mu'}{}_{\nu'} \left(\frac{\partial}{\partial x'^\mu} \otimes dx'^\nu \right). \quad (2.11)$$

The tensor T is still the same but described with different set of coordinates. The two coordinates are related to each other by $x'^\mu = x'^\mu(x^\nu)$. With the chain rule, the vector and the covector basis can be related to each other by

$$\frac{\partial}{\partial x^\alpha} = \left(\frac{\partial x'^\mu}{\partial x^\alpha} \right) \frac{\partial}{\partial x'^\mu}, \quad dx^\alpha = \left(\frac{\partial x^\mu}{\partial x'^\alpha} \right) dx'^\alpha, \quad (2.12)$$

Since the round bracketed entities above are scalars, then we obtain

$$T^{\mu'}{}_{\nu'} = T^\alpha{}_\beta \frac{\partial x'^\mu}{\partial x^\alpha} \frac{\partial x^\beta}{\partial x'^\nu}. \quad (2.13)$$

This is the *coordinate transformation condition* that should be satisfied by any tensor.

A tensor can have either symmetric or antisymmetric properties in its indices. The symmetric property is denoted by round brackets and the antisymmetric property by square brackets. For example, a tensor rank $(2, 0)$ is symmetric if

$$T^{(\mu\nu)} = \frac{1}{2!}(T^{\mu\nu} + T^{\nu\mu}), \quad (2.14)$$

or antisymmetric if

$$T^{[\mu\nu]} = \frac{1}{2!}(T^{\mu\nu} - T^{\nu\mu}). \quad (2.15)$$

Now we introduce the Lie derivative. We shall denote partial derivative over x^μ as ∂_μ . Since a vector, intuitively, has magnitude and orientation, covector and tensors, in general, have their magnitude and orientation. Suppose we have a curved space-time and suppose there is a tensor $T^{\mu\nu}(x)$ and a vector X^μ where both are “attached” at the same point p in the space-time. The tensor is then moved in a direction of a vector \vec{X} to a new position q , which became $T'^{\mu\nu}(x')$ and the new position is

$$x'^\mu = x^\mu + X^\mu(x)\delta u, \quad (\delta u \text{ is a small constant}). \quad (2.16)$$

By the coordinate transformation condition, we have

$$T'^{\alpha\beta}(x') = T^{\mu\nu}(x) \frac{\partial x'^\alpha}{\partial x^\mu} \frac{\partial x'^\beta}{\partial x^\nu} = T^{\mu\nu}(x) + [\partial_\mu X^\alpha T^{\mu\beta}(x) + \partial_\nu X^\beta T^{\alpha\nu}(x)], \quad (2.17)$$

where we omit $\mathcal{O}(\delta u^2)$. Now we want to compare it with the original tensor $T^{\mu\nu}(x')$ with its origin is at q . By Taylor expansion up to first order, we have

$$T'^{\alpha\beta}(x') = T^{\mu\nu}(x^\alpha + X^\alpha(x)\delta u) = T^{\mu\nu}(x) + \delta u X^\alpha \partial_\alpha T^{\mu\nu}(x). \quad (2.18)$$

The definition of the *Lie derivative*, in our case here, is just the difference between $T^{\mu\nu}(x')$ and $T'^{\mu\nu}(x')$ as $\delta u \rightarrow 0$,

$$\mathbf{L}_{\vec{X}} T^{\mu\nu} = \lim_{\delta u \rightarrow 0} \frac{T^{\mu\nu}(x') - T'^{\mu\nu}(x')}{\delta u}. \quad (2.19)$$

This gives us

$$\mathbf{L}_{\vec{X}} T^{\alpha\beta} = X^\mu \partial_\mu T^{\alpha\beta} - \partial_\mu X^\alpha T^{\mu\beta} - \partial_\nu X^\beta T^{\alpha\nu}. \quad (2.20)$$

To find $\mathbf{L}_{\vec{X}} T_{\alpha\beta}$, one can use $x'^\mu = x^\mu + X^\mu(x')\delta u$, which gives

$$\mathbf{L}_{\vec{X}} T_{\alpha\beta} = X^\mu \partial_\mu T_{\alpha\beta} + \partial_\alpha X^\mu T_{\mu\beta} + \partial_\beta X^\mu T_{\alpha\mu}. \quad (2.21)$$

If the Lie derivative acts on a scalar, it behaves like a partial derivative

$$\mathbf{L}_{\vec{X}} f = X^\alpha \partial_\alpha f. \quad (2.22)$$

Now a *Killing vector* $\vec{\xi}$ is a vector that satisfies

$$\mathbf{L}_{\vec{\xi}} g_{\mu\nu} = 0. \quad (2.23)$$

This vector is special since, along $\vec{\xi}$, the metric is unchanged, thus the space denoted by the metric is also unchanged. $\vec{\xi}$ describes what type of *isometry* from the given metric. For example, the surface of a ball with radius R , whose metric is $ds^2 = R^2(d\theta^2 + \sin^2 \theta d\phi^2)$, is of course does not change its shape if we rotate it along ϕ , so $\vec{\xi} = \partial_\phi$.

Next is the affine connection, or simply, the connection. The connection is defined such that the result of applying *covariant derivative* ∇_μ over any tensor is a tensor. The covariant derivative is related to the partial derivative through the *connection* $\Gamma_{\mu\nu}^\alpha$. For example,

$$\nabla_\mu T_\beta^\alpha = \partial_\mu T_\beta^\alpha + \Gamma_{\mu\nu}^\alpha T_\beta^\nu - \Gamma_{\mu\beta}^\nu T_\nu^\alpha. \quad (2.24)$$

If the covariant derivative act on a scalar, it became partial derivative

$$\nabla_\alpha f = \partial_\alpha f. \quad (2.25)$$

From the definition of $\nabla_\mu T^\alpha$ above and the coordinate transformation condition, one can obtain

$$\Gamma'{}^\beta_{\alpha\sigma} = \frac{\partial x^\rho}{\partial x'^\sigma} \frac{\partial x^\lambda}{\partial x'^\alpha} \frac{\partial x'^\beta}{\partial x^\gamma} \Gamma'{}^\gamma_{\lambda\rho} - \frac{\partial x^\lambda}{\partial x'^\alpha} \frac{\partial x^\rho}{\partial x'^\sigma} \frac{\partial^2 x'^\beta}{\partial x^\lambda \partial x^\rho}. \quad (2.26)$$

The second term tells us that the connection is not a tensor. There is the so-called *torsion tensor* $T_{\mu\nu}^\alpha$ which is the antisymmetric part of connection

$$T_{\mu\nu}^\alpha = \Gamma_{\mu\nu}^\alpha - \Gamma_{\nu\mu}^\alpha. \quad (2.27)$$

GR is torsionless, so the connection is symmetric

$$\Gamma_{\mu\nu}^\alpha = \Gamma_{\nu\mu}^\alpha. \quad (2.28)$$

From now on, we shall focus on zero torsion theory. The explicit expression of $\Gamma_{\mu\nu}^\alpha$ can be obtained by the fact that the metric vanishes if a covariant derivative acts on it,

$$\nabla_\alpha g_{\mu\nu} = 0. \quad (2.29)$$

From this, one can obtain

$$\Gamma_{\mu\nu}^\alpha = \frac{1}{2} g^{\alpha\beta} (\partial_\mu g_{\beta\nu} + \partial_\nu g_{\beta\mu} - \partial_\beta g_{\mu\nu}). \quad (2.30)$$

An *affine geodesic* is a curve in the space-time whose tangent vectors are parallel to the curve itself. Suppose that the curve, whose auxilliary parameter is u , is located at x^μ and its tangent vector is $X^\mu = dx^\mu/du$, then it is an affine geodesic if

$$X^\alpha \nabla_\alpha X^\beta = \lambda X^\beta. \quad (2.31)$$

If there is an auxilliary parameter s that is defined such that all the tangent vectors have same length, then s become *affine parameter* and the above equation becomes *geodesic equation* (same as above but $\lambda = 0$).

Now we turn to the *Riemann tensor* which contains all the information about the curvature of space-time. It is defined locally as

$$R^\alpha{}_{\mu\beta\nu} = \partial_\beta \Gamma^\alpha_{\mu\nu} - \partial_\nu \Gamma^\alpha_{\mu\beta} + \Gamma^\alpha_{\beta\delta} \Gamma^\delta_{\mu\nu} - \Gamma^\alpha_{\nu\delta} \Gamma^\delta_{\mu\beta}. \quad (2.32)$$

It has four properties:

1. $R_{\alpha\mu\beta\nu} = -R_{\alpha\mu\nu\beta} = -R_{\mu\alpha\beta\nu}$,
2. $R_{\alpha\mu\beta\nu} = R_{\beta\nu\alpha\mu}$,
3. the *first Bianchi identity* $R^\alpha{}_{[\mu\beta\nu]} = 0$,
4. and the *second Bianchi identity* $R^\alpha{}_{\mu[\beta\nu;\kappa]} = 0$, with $T_{\alpha;\kappa} = \nabla_\kappa T_\alpha$.

The Riemann curvature is also named as the *intrinsic curvature*, because an observer can now see the curvature of a d -dimensional space-time \mathcal{M} even though he/she lives in \mathcal{M} itself. Then there is the so-called *Ricci tensor*, which is the trace of the Riemann tensor

$$R_{\mu\nu} = R^\beta{}_{\mu\beta\nu}. \quad (2.33)$$

The Ricci tensor does not contain all the information about the intrinsic curvature. This missing information is contained in the *Weyl tensor*

$$\begin{aligned} C_{\alpha\beta\mu\nu} &= R_{\alpha\beta\mu\nu} + \frac{1}{d-2} (R_{\alpha\nu} g_{\beta\mu} + g_{\alpha\nu} R_{\beta\mu} - R_{\alpha\mu} g_{\beta\nu} - g_{\alpha\mu} R_{\beta\nu}) \\ &\quad + \frac{R}{(d-2)(d-3)} (g_{\alpha\mu} g_{\beta\nu} - g_{\alpha\nu} g_{\beta\mu}), \end{aligned} \quad (2.34)$$

with d the dimension of the space-time. We can see that $C^\beta{}_{\mu\beta\nu} = 0$.

Now that all basic ingredients are in place, we can discuss the Einstein Field Equation (EFE)

$$R_{\mu\nu} - \frac{1}{2}Rg_{\mu\nu} = \frac{8\pi G}{c^4}T_{\mu\nu}. \quad (2.35)$$

The stress-energy tensor (or stress tensor for short) $T_{\mu\nu}$ contains the information about the matter. In general $T^{00} = \epsilon/c^2$ where ϵ the energy density, T^{0i} = the momentum density, $T^{ij} = p$ with p the pressure, and T^{ij} = the shear stress ($i \neq j$). If one use Lagrangian density \mathcal{L} to describe the matter, then one can use

$$T_{\mu\nu} = -2\frac{\partial \mathcal{L}}{\partial g^{\mu\nu}} + g_{\mu\nu}\mathcal{L} \quad (2.36)$$

to obtain the stress-energy tensor components. One can derive the identity $\nabla_\mu G^{\mu\nu} = 0$ from $R^\alpha_{\mu[\beta\nu;\kappa]} = 0$ by first contracting α with β then contracting μ with ν . By EFE, this implies the covariant conservation equation

$$\nabla_\mu T^{\mu\nu} = 0. \quad (2.37)$$

This equation is necessary since both the continuity equation and the Euler equation can be derived from it [50]. The EFE can be derived from the Einstein-Hilbert action

$$S_{\text{EH}} = \int d^4x \sqrt{-g} \left(\frac{c^4}{18\pi G} R + \mathcal{L} \right), \quad (2.38)$$

$g = \det(g_{\mu\nu})$ and \mathcal{L} the Lagrangian density for the matter. But it will be a long dicussion so we refer the readers to Ref. [38] for the details. We only show the useful relations for varying the action [45, 46, 37, 35]:

$$\delta g_{\mu\nu} = -g_{\mu\alpha}g_{\nu\beta}\delta g^{\alpha\beta}, \quad (2.39)$$

$$\delta\sqrt{-g} = -\frac{1}{2}\sqrt{-g}g_{\mu\nu}\delta g^{\mu\nu}, \quad (2.40)$$

$$\delta R = R_{\mu\nu}\delta g^{\mu\nu} + g^{\rho\sigma}g^{\mu\nu}(\delta g_{\rho\mu;\sigma\nu} - \delta g_{\rho\sigma;\mu\nu}), \quad (2.41)$$

$$\delta R^\alpha_{\mu\beta\nu} = (\delta\Gamma^\alpha_{\mu\nu})_{;\beta} - (\delta\Gamma^\alpha_{\mu\beta})_{;\nu}, \quad (2.42)$$

$$\delta\Gamma^\lambda_{\mu\nu} = \frac{1}{2}g^{\lambda\beta}\left[(\delta g_{\beta\nu})_{;\mu} + (\delta g_{\beta\mu})_{;\nu} - (\delta g_{\mu\nu})_{;\beta}\right]. \quad (2.43)$$

One can obtain the Riemann tensor components using an algebraic program, e.g., *Mathematica*. There is another method, which uses differential forms rather than $\Gamma^\mu_{\nu\rho}$, called *tetrad method*. We show its steps in the Appendix.

CHAPTER 3

COMPACT AND ULTRA-COMPACT OBJECTS

The excitement over GW astronomy by LIGO and Virgo [1] in the last 5 years since the GW150914 event gave rise to many investigations on what mechanisms produce the GW. From the astronomical point of view, there is an emphasis on the possibility of finding the synthesizing process of heavy metals, e.g, silver, and platinum. This hypothesis can be tested from the collision of two NSs at the GW170817 event. From the theoretical physics point of view, some investigations ask what kind of heavy objects may mimic black holes. These objects are horizonless and usually called ultra-compact objects (UCOs). These objects are more compact than the known compact objects, e.g., NSs or white dwarfs. The existence of UCOs, if they are the final state after the ringdown phase of two massive bodies colliding that produce GW, can be detected by the existence of the so-called GW echo.

As we have known, black holes (BHs) cannot be observed directly and their existence is usually confirmed by their intense gravity effects. One such effect is the famous light deflection, known since the observation of a total solar eclipse at the island of Principe at Sobral on 29 May 1919 by Eddington and his colleagues. Since Eddington only measures the deflection by the Sun, the deflection of black holes is much more tremendous so the visualization is very weird. One can see an approximate illustration of such rotating black holes in the film Interstellar, which includes Kip Thorne as its consultant.

The other effect that triggers recent excitement is the GW. One such apparatus is the LIGO, the abbreviation of Laser Interferometer Gravitational-Wave Observatory. The success of detecting the GW150914 event at 09.51 UTC on 14 September 2015 led Rainer Weiss, Kip Thorne, and Barry C. Barish, the initiators of the LIGO project, as the receiver of the Nobel Prize in Physics in 2017. This achievement opens the possibility to observe the universe not only by using electromagnetic waves—which is done a long time ago by astronomers—but also by looking at ripples of space-time.

When two massive objects going revolve around each other and they are going closer and closer, the curve of space-time around these two undergoes rapid changes. This change is like a perturbed fabric of elastic sheets, which will produce waves. These waves can be detected by a laser interferometer, whose unperturbed configuration is such that the two separated lights annihilate each other on a screen, hence light will appear when a GW passes by. When a GW passes by, the interferometer can detect two types of waves depending on their polarization. One of them is called the plus-polarized GW and the

other is the cross-polarized GW. This makes one of the arms of the interferometer slightly shorter and the other slightly longer. When this happens, light appears on the screen and its intensity oscillate.

In the ring-down phase, i.e., when the two massive objects had combined, the wave died down so quickly into complete silence if the final object is a BH. On the other hand, if the final object is a UCO, it has been calculated that the silence will be followed by echoes. As an illustration of how massive these UCOs are, they are much heavier and their size is smaller than an NS but still lighter than a BH. The compactness $C = GM/R$ of an NS is ~ 0.2 , but for a black-hole $C = 1/2$, so there is a large gap between NS and BH. In general, massive objects are categorized by compactness as follows [2]:

- if $2C > 1/3$, then it is a compact object (CO),
- if $2C > 2/3$, then it is an ultra-compact object (UCO),
- if $2C > 8/9$, then it violates the Buchdhal limit—the limit of GR,
- if $2C > 1/(1 + 0.019)$, then it is a clean-photon sphere objects (ClePhO), and
- if $2C > 1/(1 + 10^{-40})$, then it is a near-horizon quantum structure.

The compact object criteria are fulfilled if the spherical object has an innermost stable circular orbit (ISCO) at $r = 6GM$. The UCO criteria are fulfilled if the spherical object has an unstable light ring (or photon sphere) at $r = 3GM$. The Buchdhal limit $C = 4/9$ is the limit of GR as a prediction of any horizonless massive object. This came from the Buchdhal theorem, which roughly says that the pressure at the center goes to infinity if the system satisfies the following conditions:

1. GR is the correct theory of gravity,
2. the solution is spherically symmetric,
3. the matter is described by a single perfect fluid,
4. the fluid is isotropic or mildly anisotropic $p_r \geq p_t$,
5. the radial pressure and the energy density are both nonnegative ($p_r \geq 0, \rho \geq 0$), and
6. from the center to the surface of the star, the energy density decreases $\rho'(r) < 0$.

The ClePho has the following unique signature, i.e., its gravitational wave behavior is identical to black holes at early times but displays unique signatures of its surface at late

times. The near-horizon quantum structure came from looking at the tidal Love number k_2 , which is estimated to be $k_2 \sim 1/|\log \epsilon| \sim \mathcal{O}(10^{-3} - 10^{-2})$, where $\epsilon = 1/2C - 1$. As a comparison, this number is very small compared to a typical neutron star who has $k_2 \sim 200$.

For the echo to exist, the final object from the coalesce should at least have compactness $C > 1/3$. This is because the effective potential V_{eff} that produces the GW echo has a spherical barrier located at the so-called unstable photon sphere at $r = 3GM$ [53]. (The unstable term is due to both $V'_{eff}(3GM) = 0$ and $V''_{eff}(3GM) < 0$.) The photon sphere's existence can be derived from the geodesic of massless particles in the space-time with Schwarzschild metric, but it does not imply that GW echo can be produced. The GW came from the TT-tensor (transverse traceless) part of metric perturbation. From the perturbation calculation, we can obtain the effective potential V_{eff} .

The GW echo frequency f_{echo} can be calculated using the object's compactness by the proper time delay [54]

$$\tau_{echo}^{(num)} = \int_0^{3GM} \sqrt{-\frac{g_{rr}}{g_{tt}}} dr. \quad (3.1)$$

This formula needs the complete information of the interior of the object. The integration from $r = 0$ to $r = 3GM$ means that the waves are trapped at a region between $r = 3GM$ and $r = 0$, assuming that the gravitational wave penetrates the UCO. When the wave cannot penetrate and being reflected by the object's surface, integrating Eq. (3.1) from $r = R$ rather than $r = 0$ will produce [2]

$$\tau_{echo}^{(approx)} \sim 4M|\log \epsilon|, \quad (3.2)$$

with $\epsilon = 1/2C - 1$ and $f_{echo} = \pi/\tau_{echo}$. Eq. (3.2) is sufficient to estimate the order of magnitude of the frequency.

The existence of such echo had been observed. The GW170817 event, a merger of two neutron stars that produce a BH remnant with mass around $2.6\text{-}2.7 M_\odot$ and dimensionless spin around 0.84-0.87, produced an echo which had been calculated in Ref. [55] and the result is $f_{echo} \simeq 72$ Hz. This was predicted in Ref. [56] to be compatible with a toy model of an incompressible star with a mass of around $2\text{-}3M_\odot$.

Many UCO proposals are compiled in a review by Cardoso and Pani [2]. One of them is called gravastars [3, 4]. Inside the surface of the gravastar lies another de-Sitter space connected to the Schwarzschild space-time by a thin shell of ultrarelativistic matter. Carballo-Rubio [5] utilized the theory of semi-classical gravity to obtain a different type of TOV-like equation and the result has many similar features with gravastar. In the next chapter, we shall present our analysis on the Carballo-Rubio model [5].

This page intentionally left blank

CHAPTER 4

NEUTRON STARS

4.1 Neutron Stars

In this chapter, we shall review some features of neutron stars (NSs). Our discussion will be very short and basic. For comprehensive discussions, readers are referred to Glendenning [48].

Chadwick in 1932 discovered the neutron particle. One year later, Baade and Zwicky investigate supernovae and they conceived the notion of NS. When the presupernova star's core became heavier by the production of iron from nuclear fusion, the mass increases until the gravitational force wins over the pressure from the matter, hence the core collapsing. But then the collapse is stopped by neutrons in the core of the star, the matter bounces off the hard iron core, making the supernova explosion. So the type II supernova explosion release so much debris due to the highly compact object formed in the center of the presupernova star called NS. (Type Ia supernova is the result of mergers of two white dwarfs, so its process is different and it happens very rarely.)

NSs are partially supported by neutron degeneracy pressure, an effect caused by the Pauli exclusion principle (similar to electron degeneracy pressure in white dwarfs). This pressure is only able to negate the gravitational pull if the mass is no more than $0.7M_{\odot}$. Beyond this, repulsive nuclear forces are needed. This mechanism gives the so-called the Tolman-Oppenheimer-Volkoff (TOV) limit $M \lesssim 2.0M_{\odot}$. Beyond this, the matter collapses into a more dense star, e.g., quark star, or black-hole. (In the case of the white dwarf, the Chandrasekhar limit $M \lesssim 1.4M_{\odot}$ is the boundary between the white dwarf and neutron star.)

How about protons? It is common to assume neutral net charge distribution for massive objects. So the pre-collapsed star should have the net charge from electrons equal to the net charge of the protons. If the mass exceeds the Chandrasekhar limit, the electron degeneracy pressure is lost against the gravitation, so the electrons, protons, and neutrons are packed together. Then due to the inverse beta decay process, protons and electrons combined produce neutrons and electron neutrinos. Even though the neutrons are unstable due to the beta decay, the inverse beta decay stabilizes it so the neutrons dominate the matter.

The TOV limit, if the strong forces are included, is actually in the range of $1.5 - 3M_{\odot}$. This large uncertainty exists because the EoS for extremely dense matter is unknown.

So to make the range narrower, people use observations. The empirical upper bound on the TOV limit is usually taken from the mass of PSR J0348+0432, which is $2.01 \pm 0.04 M_{\odot}$. On the other hand, NS radius is somehow harder to know for different masses of NSs. Usually, the radius is obtained from canonical NS with mass $1.4 M_{\odot}$. There are calculations by Landry et al [57] and Jiang et al [58] whose result is $R_{1.4} = 12.32^{+1.09}_{-1.47}$ km and $R_{1.4} = 12.1^{+1.2}_{-0.8}$ km, respectively. The most stringent one is calculated by Capano et al [59] whose result is $R_{1.4} = 11.0^{+0.9}_{-0.6}$ km.

The pre-supernova star is generally rotating, so the NS produced should also rotate faster since the radius is smaller due to the conservation of angular momentum. An NS cannot have a period of (uniform) rotation such that its frequency is more than the so-called Kepler frequency [48]

$$\Omega_K \approx 0.625 \sqrt{M/R^3}. \quad (4.1)$$

The Kepler frequency is the absolute limit of rotation, where beyond the matter will fall apart due to centripetal force. Although this result is Newtonian, it was justified by GR since it is accurate to better than 10%. This absolute limit gives the lowest possible period, called the Kepler period

$$P_K = \frac{2\pi}{\Omega_K} \approx 0.0276 \sqrt{\frac{(R/\text{km})^3}{M/M_{\odot}}} \text{ ms}. \quad (4.2)$$

This period is also called the mass-shedding limit. From Fig. 7.2 in Ref. [48], we see that the NS with $1.442 M_{\odot}$ cannot have a rotational period less than 0.33 ms. The region forbidden by GR is denoted by the following constraint:

$$P > 0.167 \frac{M}{M_{\odot}} \text{ ms}, \quad (4.3)$$

assuming that $GM/R < 4/9$. For a star with mass equal to that of PSR 1931+16, i.e., $M = 1.441 M_{\odot}$, it yields $P > 0.24$ ms.

There are at least two stability conditions for NS. The first one is $dM/d\rho_c > 0$, i.e., the mass increases as one increases the central energy density. The maximum mass is usually located at the point where $dM/d\rho_c = 0$. The other criteria are from radial perturbation analysis. By this method, one can see the possibility of the star will expand or contract if it is perturbed along the radial direction. If it tends to either expand or contract after a little nudge, then it is unstable.

4.2 The $\sim 2.6M_{\odot}$ NS from GW190814 event

The most recent known problem in compact object is the nature of $2.50 - 2.67M_{\odot}$ massive secondary object detected in the gravitational wave (GW) by LIGO and Virgo collaboration in their GW190814 event [6].¹ This object has no measurable signature of tidal deformation, and also there is no electromagnetic counterpart on the gravitational wave-front. Much discussions had been published about this object, such as, whether it is a lightest black hole (BH) [6, 8, 9, 10], a fast rotating neutron star (NS) [6, 11, 12, 13, 14], a quark star [15, 16, 17, 18, 19, 20, 21] or a hybrid star [22, 23]. However, one could not exclude the possibility that the secondary object of GW190814 is a super-massive static or at least a slow rotating NS [8, 60, 61]. The latter possibility triggers other discussions about the appropriate type of equation of state (EoS) of the super-massive NS that satisfies observational constraints [62, 63, 64, 65, 60, 61]. Furthermore, several attempts have been done to explain the source of the secondary object's mass in the GW190814 event using, e.g., anisotropic pressure [66, 67, 68], the possibility of it being a primordial black hole [69], the indication of a dark matter candidate called mirror world [70], and some modified gravity theories [24, 25, 26, 27].

Here we mention some developments on the properties of NS by observations. The maximum mass of NS around $2.0 M_{\odot}$ came from accurate measurements of massive pulsars such as PSR J0348+0432, PSR J0740+6620, and PSR J6114-2230 [71, 72, 73, 7, 74]. NICER [75] measured the X-ray emissions from the hot spots on the surface of NS, which provide simultaneous pieces of information about the mass and radius of some pulsars. The recent NICER investigations report the mass and radius constraints for PSR J0030+0451 [76, 77, 78]. On the other hand, GW analysis by LIGO and Virgo collaboration from the remnant of two NSs had measured the tidal deformability of the NSs. This analysis can survey a wide range of NS masses and its corresponding central density [79, 80, 81, 6]. The two GW events from the coalescence of two NSs, i.e., GW170817 [79, 80] and GW190425 [6], have been reported. The analysis from these events can provide a stricter constraint to mass and radius of canonical NS (i.e., with a mass around $1.4M_{\odot}$) and thus also restrict the EoS of NS.

Moreover, other studies have been performed to extract accurate information on the properties of the EoS of NSs [57, 58, 82, 83, 84, 85]. These studies are done by systematically examining NS observable measurements and other observable measurements, e.g, NS moment of inertia and nuclear properties. We need to note that to describe NS matter, some use non-relativistic models while others use relativistic models. Several models of NS matter are already proposed, e.g., the relativistic mean-field (RMF) models. Dutra

¹Actually, the most recent one is $2.8 M_{\odot}$ from GW200210_092254, which came after we finished defending this dissertation.

et al. [86] had reported that they found only 34 from 263 RMF parameter sets that satisfy constraints from nuclear matter. Furthermore, only 15 out of 35 parameter sets in isotropic NS without hyperons that predict maximum mass around $2.0 M_{\odot}$. However, none of them satisfy the latter constraint if the model includes hyperons and other exotic particles. (For details, please see Ref. [87] and the references therein.) This is known as the “hyperon puzzle”.

We need to emphasize that the tension between nuclear physics persists. Some results from NS observations imply that the models of NS EoS should be relatively stiff so that they can produce NS with a maximum mass around $2.0 M_{\odot}$. On the other hand, the recent result on the radius of NS with canonical mass, like the one predicted by GW170817, is more in favor of a softer EoS. This issue turns out can be resolved by introducing anisotropic pressure [88]. The drawback of using anisotropic pressure is that the source of the anisotropy itself is still merely a mathematical possibility, not a phenomenological one. Moreover, the tension will remain tight if the secondary object in another GW event, i.e., GW190814, is a static or slow rotating NS.

CHAPTER 5

RELATIVISTIC MEAN FIELD

5.1 Relativistic Mean Field

Since the second part of our work relies on EoS from Relativistic Mean Field (RMF) with G3 parameter, in this chapter we shall briefly revisit RMF to illustrate the main algorithm on how to obtain the needed EoS. The EoS is usually extracted as two columns of data: energy density and pressure. This data will then be the input in the code that calculates the TOV equation in form of the following. The data is fitted as a polynomial function of pressure and the fitting result is used as input in the TOV solver.

As a disclaimer, this chapter is by no means comprehensive. Interested readers are referred to other more comprehensive literature such as Ref. [48]. For more pedagogical ones, we refer to Refs. [89, 90].

In this work we actually use the Lagrangian from Ref. [91]. But to make this chapter as simple as possible, we consider the most simple model in RMF called the $\sigma - \omega$ model, whose Lagrangian is

$$\mathcal{L} = \mathcal{L}_B^{\text{free}} + \mathcal{L}_M^{\text{free}} + \mathcal{L}_{BM}^{\text{lin}}. \quad (5.1)$$

This Lagrangian describes baryons interacting with each other through σ and ω mesons and the mesons also are not self-interacting. The baryons considered here are the proton and neutron $B = p, n$. The free baryon term is

$$\mathcal{L}_B^{\text{free}} = \sum_{B=p,n} \bar{\psi}_B [i\gamma^\mu \partial_\mu - M_B] \psi_B. \quad (5.2)$$

The free meson term is

$$\mathcal{L}_M^{\text{free}} = \frac{1}{2} (\partial^\mu \sigma \partial_\mu \sigma - m_\sigma^2 \sigma^2) - \frac{1}{4} \omega^{\mu\nu} \omega_{\mu\nu} + \frac{1}{2} m_\omega^2 \omega^\mu \omega_\mu \quad (5.3)$$

The linear baryon-meson interaction term is

$$\mathcal{L}_{BM}^{\text{lin}} = \sum_B \bar{\psi}_B [g_{\sigma B} \sigma - \gamma_\mu g_{\omega B} \omega^\mu] \psi_B. \quad (5.4)$$

This Lagrangian will produce equations of motions that are too complicated to solve since they are partial differential equations. The RMF approximation uses the fact that the system is in the ground state and the following four assumptions are used in the system:

(1) translation invariance, (2) rotation invariance, (3) staticity, and (4) definite spin and parity. These conditions imply that the mesons all behave like constants:

$$\begin{aligned}\sigma(x) &\longrightarrow \langle\sigma(x)\rangle = \sigma_0, \\ \omega^\mu(x) &\longrightarrow \langle\omega^\mu(x)\rangle = \omega^\mu.\end{aligned}$$

Using the Euler-Lagrange equation on the Lagrangian and employing the RMF approximation, we obtain one equation of motion and three constraints

$$[i\gamma^\mu\partial_\mu - M_B + g_{\sigma B}\sigma_0 - \gamma_\mu g_{\omega B}\omega^\mu] \psi_B = 0, \quad (5.5)$$

$$-m_\sigma^2\sigma_0 + \sum_B g_{\sigma B} \langle \bar{\psi}_B \psi_B \rangle = 0, \quad (5.6)$$

$$m_\omega^2\omega_0 - \sum_B g_{\omega B} \langle \psi_B^\dagger \psi_B \rangle = 0, \quad (5.7)$$

$$m_\omega^2\omega_i - \sum_B g_{\omega B} \langle \bar{\psi}_B \gamma_i \psi_B \rangle = 0. \quad (5.8)$$

We also need the pressure p and energy density ϵ using the canonical definition of the stress-energy tensor

$$T_\nu^\mu = \frac{\partial \mathcal{L}}{\partial(\partial_\mu \phi_a)} \partial_\nu \phi_a - \delta_\nu^\mu \mathcal{L}. \quad (5.9)$$

The energy density and the pressure are from $\rho = T_0^0$ and $p\delta_j^i = -T_j^i$, respectively. Since we use the RMF approximation, the fields ϕ_a are just ψ_B so we obtain

$$\epsilon = \sum_B \langle \bar{\psi}_B \gamma_0 e_B(\vec{k}) \psi_B \rangle - \langle \mathcal{L} \rangle, \quad (5.10)$$

$$p = \frac{1}{3} \sum_B \langle \bar{\psi}_B \vec{\gamma} \cdot \vec{k} \psi_B \rangle + \langle \mathcal{L} \rangle, \quad (5.11)$$

with

$$\langle \mathcal{L} \rangle = -\frac{1}{2} m_\sigma^2 \sigma_0^2 + \frac{1}{2} m_\sigma^2 (\omega_0^2 - \vec{\omega}^2). \quad (5.12)$$

Since the mean field approximation makes the nucleon has no x dependent term, we have ψ in the form of

$$\psi_B(x) = \psi_B(k) e^{i\vec{k} \cdot \vec{x} - ie_B(\vec{k})t}. \quad (5.13)$$

Substitute this into Eq. (5.5) we obtain

$$\left[\gamma_0 e_B(\vec{k}) - \gamma_0 g_{\omega B} \omega_0 \right] = \left[\vec{\gamma} \cdot \left(\vec{k} + g_{\omega B} \vec{\omega} \right) + M_B - g_{\sigma B} \sigma_0 \right] \quad (5.14)$$

Multiplying this with γ_0 from left and squaring both terms we have

$$e_B(\vec{k}) = g_{\omega B}\omega_0 \pm \sqrt{\left(\vec{k} + g_{\omega B}\vec{\omega}\right)^2 + (M_B - g_{\sigma B}\sigma_0)^2}. \quad (5.15)$$

We shall only use the positive sign in $e_B(\vec{k})$ since we consider the system consists of particles only, excluding the anti-particles.

Now the three constraints Eqs. (5.6)-(5.8), energy density and pressure needs the explicit expressions for their expectation value terms. This can be done using a method deviced by Glendenning in Ref. [48], using

$$\langle \bar{\psi}_B \Gamma \psi_B \rangle = \sum_s \int \frac{d\vec{k}}{(2\pi)^3} (\bar{\psi}_B \Gamma \psi_B)_{\vec{k},s} \Theta[\mu_B - e_B(\vec{k})]. \quad (5.16)$$

s is the (iso)-spin index, $(\bar{\psi}_B \Gamma \psi_B)_{\vec{k},s}$ is the expectation value of its single-particle state, μ_s is the Fermi energy or chemical potential, and Θ is the step function. The operator Γ can be obtained by manipulation the so-called Dirac Hamiltonian

$$H_D = i\partial_0 = \gamma_0 \vec{\gamma} \cdot (\vec{k} + g_{\omega B}\vec{\omega}) + \gamma_0(M_B - g_{\sigma B}\sigma_0) + g_{\omega B}\omega_0. \quad (5.17)$$

Now it is clear that

$$(\bar{\psi}_B H_D \psi_B)_{\vec{k},B} = e_B(\vec{k}). \quad (5.18)$$

By convention, $(\psi_B^\dagger \psi_B)_{\vec{k},B} = 1$, so if ζ is an arbitrary variable then

$$\frac{\partial}{\partial \zeta} \left(\psi_B^\dagger H_D \psi_B \right)_{\vec{k},B} = \left(\psi_B^\dagger \frac{\partial H_D}{\partial \zeta} \psi_B \right)_{\vec{k},B} = \frac{\partial e_B(\vec{k})}{\partial \zeta}. \quad (5.19)$$

So if $\Gamma = \gamma_0 \gamma_i$ then we use $\zeta = k^i$ so we have

$$\begin{aligned} \langle \psi_B^\dagger \gamma_0 \gamma_i \psi_B \rangle &= \sum_s \int \frac{dk^i dk^j dk^k}{(2\pi)^3} \frac{\partial}{\partial k^i} e_B(\vec{k}) \Theta[\mu_B - e_B(\vec{k})] \\ &= 2 \int \frac{dk^j dk^k}{(2\pi)^3} \int de_B(\vec{k}) = 0. \end{aligned} \quad (5.20)$$

This vanishes because e_B are constant anywhere on the boundary of the region where the integration is evaluated. This implies $\omega_i = 0$, so in the RMF approximation, we can use $\omega^\mu(x) \rightarrow \langle \omega^\mu(x) \rangle = \omega_0 \eta^{0\mu}$ from the start, with $\eta^{\mu\nu} = \text{diag}(1, -1, -1, -1)$. The others

can be calculated to obtain

$$\rho_B = \langle \psi_B^\dagger \psi_B \rangle = 2 \int_0^{k_{FB}} \frac{d\vec{k}}{(2\pi)^3} = 2 \int_0^{k_{FB}} \frac{k^2 dk}{2\pi^2} = \frac{k_{FB}^3}{3\pi^2}, \quad (5.21)$$

$$\langle \bar{\psi}_B \psi_B \rangle = 2 \int_0^{k_{FB}} \frac{k^2 dk}{2\pi^2} \frac{m^*}{\sqrt{k^2 + m^{*2}}}, \quad (5.22)$$

which can be substituted to Eqs. (5.6)-(5.7), and, in the energy density and pressure,

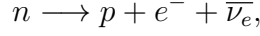
$$\langle \bar{\psi}_B \gamma_0 e_B(\vec{k}) \psi_B \rangle = g_{\omega B} \omega_0 \rho_B + 2 \int_0^{k_{FB}} \frac{k^2 dk}{2\pi^2} \sqrt{k^2 + m^{*2}}, \quad (5.23)$$

$$\langle \bar{\psi}_B \vec{\gamma} \cdot \vec{k} \psi_B \rangle = 2 \int_0^{k_{FB}} \frac{k^2 dk}{2\pi^2} \frac{k^2}{\sqrt{k^2 + m^{*2}}}. \quad (5.24)$$

The baryon density ρ —an important quantity—is defined as

$$\rho = \rho_n + \rho_p. \quad (5.25)$$

Three stability conditions are necessary for massive bodies such as NS. It is known that there is the beta decay process



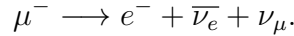
but since the large density and pressure inside an NS can trigger another reaction, namely



These two reaction compete each other creating the so-called beta-stability condition

$$\mu_n = \mu_p + \mu_e, \quad (5.26)$$

with $\mu_x = \partial\epsilon/\partial\rho_x$ and $\rho_x = k_x^3/(3\pi^2)$. For ultra-dense matter, electrons can have ultra-relativistic energies reaching the mass of muon, changing the electrons into muons by



So the other condition is

$$\mu_\mu = \mu_e. \quad (5.27)$$

The last condition came from the fact that massive bodies is electrically neutral, so

$$\rho_\mu + \rho_e = \rho_p. \quad (5.28)$$

One can numerically obtain the pressure and the energy density, which will be used as the EoS. They also satisfy the relation from thermodynamics

$$p = \rho^2 \frac{\partial}{\partial \rho} \frac{\epsilon}{\rho}. \quad (5.29)$$

Various quantities can be calculated from these equations, but here we only mention two. The first one is the symmetry energy coefficient

$$E_{\text{sym}} = \frac{1}{2} \frac{\partial^2}{\partial \delta^2} \left. \frac{\epsilon}{\rho} \right|_{\delta=0}, \quad (5.30)$$

where $\delta = (\rho_n - \rho_p)/\rho$ is measuring the deviation from the assumed isospin symmetry. In the semi-empirical mass formula, $E_{\text{sym}} = a_4$ which accompany the $(N - Z)^2/A^2$ term. To evaluate this, usually one use these relations:

$$\rho_n = \rho \frac{1 + \delta}{2}, \quad (5.31)$$

$$\rho_p = \rho \frac{1 - \delta}{2}. \quad (5.32)$$

The second quantity is the compressibility

$$K = 9\rho_s^2 \frac{\partial^2}{\partial \rho^2} \left. \frac{\epsilon}{\rho} \right|_{\rho=\rho_0}, \quad (5.33)$$

where ρ_0 is the so-called saturation density. The origin of ρ_0 is as follows. Since nuclear matter is a saturated system, we know that the strong force keep the nucleons clump together opposing the Coulomb force. This strong force is attractive at radius > 0.4 fm but become repulsive at radius ≤ 0.4 fm. Thus the density has a maximum value and this is called saturation density. The value of ρ_0 differ from a literature to the other, depending on the underlying theories and experiments: $\rho_0 = 0.148 \text{ fm}^{-2}$ from Ref. [90], $\rho_0 = 0.153 \text{ fm}^{-2}$ from Ref. [48], and $\rho_0 = 0.16 \text{ fm}^{-2}$ from Ref. [49].

The last quantity is the binding energy, defined as [49]

$$\frac{E}{A} = \frac{1}{\rho} \left(\epsilon - \sum_B M_B \rho_B \right). \quad (5.34)$$

By comparing with data from observations, one usually shows both the calculation results and the observation data in a plot where E/A and ρ/ρ_0 are the y and x -axis, respectively.

5.2 The Neutron Star Matter's Equation of State

Here, we discuss a summary of the RMF model that we use in Chapter 7. We also discuss the nuclear and NS matter predictions, which corresponds to the RMF model after a parameter set is used. Specifically, we show the reason why we use the G3 RMF parameter set to describe the core region of NSs.

We start by using the RMF Lagrangian density from Ref. [92]. The Lagrangian density includes σ , ω , and ρ as the non-strange mesons, ϕ as the strange meson, e^- and μ^- as the leptons, p and n as the nucleons, and Λ , Σ , Ξ as the hyperons. The tensors $\omega^{\mu\nu} = \partial^\mu\omega^\nu - \partial^\nu\omega^\mu$, $\phi^{\mu\nu} = \partial^\mu\phi^\nu - \partial^\nu\phi^\mu$ and $\rho^{\mu\nu} = \partial^\mu\rho^\nu - \partial^\nu\rho^\mu$ corresponds to ω , ϕ and ρ mesons, respectively. The explicit expressions is as follows:

$$\mathcal{L} = \mathcal{L}_B + \mathcal{L}_{BM} + \mathcal{L}_M + \mathcal{L}_L, \quad (5.35)$$

where the free lepton term with lepton mass M_L ($L = e^-, \mu^-$) is

$$\mathcal{L}_L = \sum_L \bar{\Psi}_L [i\gamma^\mu \partial_\mu - M_L] \Psi_L, \quad (5.36)$$

the free baryon term with baryon mass M_B ($B = N, \Lambda, \Sigma, \Xi$ with $N = p, n$) is

$$\mathcal{L}_B = \sum_B \bar{\Psi}_B [i\gamma^\mu \partial_\mu - M_B] \Psi_B, \quad (5.37)$$

the meson-baryon coupling terms are

$$\begin{aligned} \mathcal{L}_{BM} &= \sum_B \bar{\Psi}_B [g_{\sigma B} \sigma - \gamma_\mu g_{\omega B} \omega^\mu \\ &\quad - \frac{1}{2} \gamma_\mu g_{\rho B} \boldsymbol{\tau}_B \cdot \boldsymbol{\rho}^\mu - \gamma_\mu g_{\phi B} \phi^\mu] \Psi_B, \end{aligned} \quad (5.38)$$

the free and self interaction meson Lagrangian density

$$\begin{aligned} \mathcal{L}_M &= \frac{1}{2} (\partial_\mu \sigma \partial^\mu \sigma - m_\sigma^2 \sigma^2) + \frac{1}{2} (\partial_\mu \sigma^* \partial^\mu \sigma^* - m_{\sigma^*}^2 \sigma^{*2}) \\ &\quad - \frac{1}{4} \omega_{\mu\nu} \omega^{\mu\nu} + \frac{1}{2} m_\omega^2 \omega_\mu \omega^\mu - \frac{1}{4} \phi_{\mu\nu} \phi^{\mu\nu} + \frac{1}{2} m_\phi^2 \phi_\mu \phi^\mu \\ &\quad - \frac{1}{4} \boldsymbol{\rho}_{\mu\nu} \cdot \boldsymbol{\rho}^{\mu\nu} + \frac{1}{2} m_\rho^2 \boldsymbol{\rho}_\mu \cdot \boldsymbol{\rho}^\mu + \mathcal{L}_M^{NL}, \end{aligned} \quad (5.39)$$

with the nonlinear terms the contain meson self interactions are

$$\begin{aligned}
\mathcal{L}_M^{NL} = & -\frac{\kappa_3 g_{\sigma N} m_\sigma^2}{6m_N} \sigma^3 - \frac{\kappa_4 g_{\sigma N}^2 m_\sigma^2}{24m_N^2} \sigma^4 + \frac{\zeta_0 g_{\omega N}^2}{24} (\omega_\mu \omega^\mu)^2 \\
& + \frac{\eta_1 g_{\sigma N} m_\omega^2}{2m_N} \sigma \omega_\mu \omega^\mu + \frac{\eta_2 g_{\sigma N}^2 m_\omega^2}{4m_N^2} \sigma^2 \omega_\mu \omega^\mu \\
& + \frac{\eta_\rho g_{\sigma N} m_\rho^2}{2m_N} \sigma \boldsymbol{\rho}_\mu \cdot \boldsymbol{\rho}^\mu + \frac{\eta_{1\rho} g_{\sigma N} m_\rho^2}{4m_N^2} \sigma^2 \boldsymbol{\rho}_\mu \cdot \boldsymbol{\rho}^\mu \\
& + \frac{\eta_{2\rho} g_{\omega N} m_\rho^2}{4m_N^2} \omega_\mu \omega^\mu \boldsymbol{\rho}_\nu \cdot \boldsymbol{\rho}^\nu.
\end{aligned} \tag{5.40}$$

The mesons are coupled to baryons in Eq. (5.38) and coupled to themselves in Eq. (5.39). In Eq. (5.40), it includes the RMF nonlinear σ and ω mesons self-interaction and cross interactions between σ , ω , and ρ mesons. In the RMF models, $g_{\sigma B}$, κ_3 , η_1 , etc. are coupling constants and parameters of the model. They are determined numerically by fitting the model's predictions to experimental data from nuclear matter and finite nuclei. The obtained values from the fitting process depend on the observables and their weights. The RMF parameter sets are sets of these explicit values. In this work, we use the RMF parameter sets whose values can be seen in Refs.[34, 92, 93, 94].

The investigations regarding the contribution of the nucleon sector in EoS are well-established because, in this sector, the RMF parameter constraints are relatively tight. The binding energies and EoS, i.e., pressure as a function of the ratio of nucleon density over the saturation density, in the cases of symmetric nuclear matter (SNM) and pure neutron matter (PNM) are shown in Figs. 5.1 and 5.2. These are from employing parameters sets called G3 [34], BSP [88, 92, 91], TM1e [93], and FSUH [94]. The curves from these parameter sets are compared to the results from experimental data [95, 96] and the predictions from the chiral effective field theory [97, 98]. In general, all parameter sets are quite compatible with the experimental data, but we note that the results at low densities from G3 are more compatible with the chiral effective field theory calculations than other parameter sets. Also note the disadvantage of the RMF parameter sets used here, i.e., from the upper panel of Fig. 5.1, we see that all RMF parameter sets prediction on the binding energy are incompatible with the FOPI data. This is clearly an alarming issue, although from the upper panel of Fig. 5.2 the RMF parameter sets prediction on the EoS is not that bad. Despite these drawbacks, we still use the G3 parameter set to study the NS properties.

It is a known fact that the hyperons and other exotic particles' coupling constants are experimentally difficult to constrain. Therefore, the contribution of the hyperons sector in the EoS is uncertain. On the other hand, when hyperons and other exotic particles are included, they tend to soften the EoS in the NS core. However, for an NS with a huge

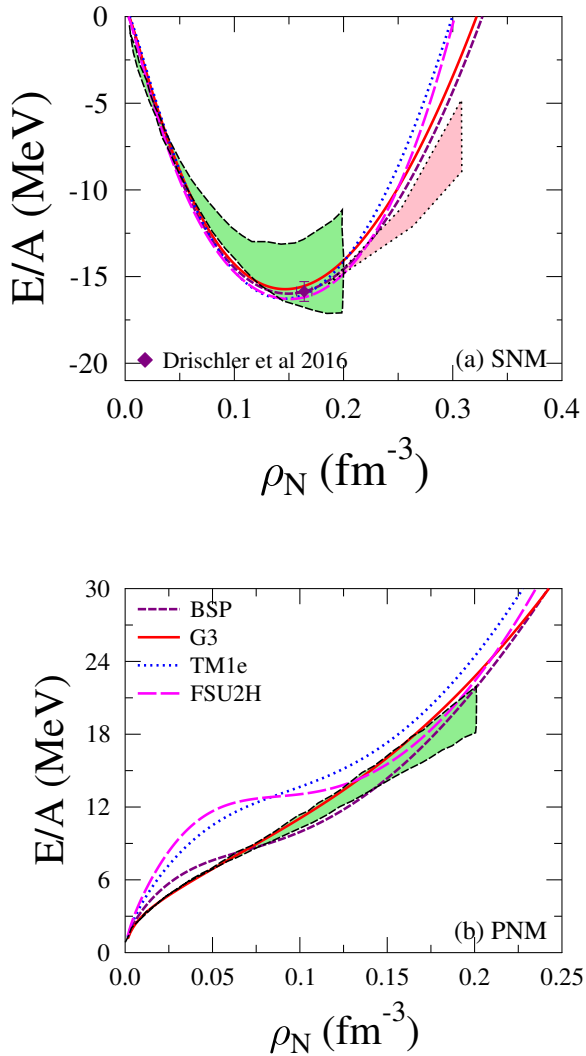


Figure 5.1: Here, we show the binding energy on SNM (a) and PNM (b) cases from G3, BSP, TM1e, and FSUH RMF parameter sets. The light green shaded area is from chiral effective theory [97], while the pink shaded area is a constraint imposed by the SNM binding energy, which is extracted from FOPI experimental data [95]. In addition, the SNM binding energy at saturation value from Refs. [97] is also shown with a purple diamond.

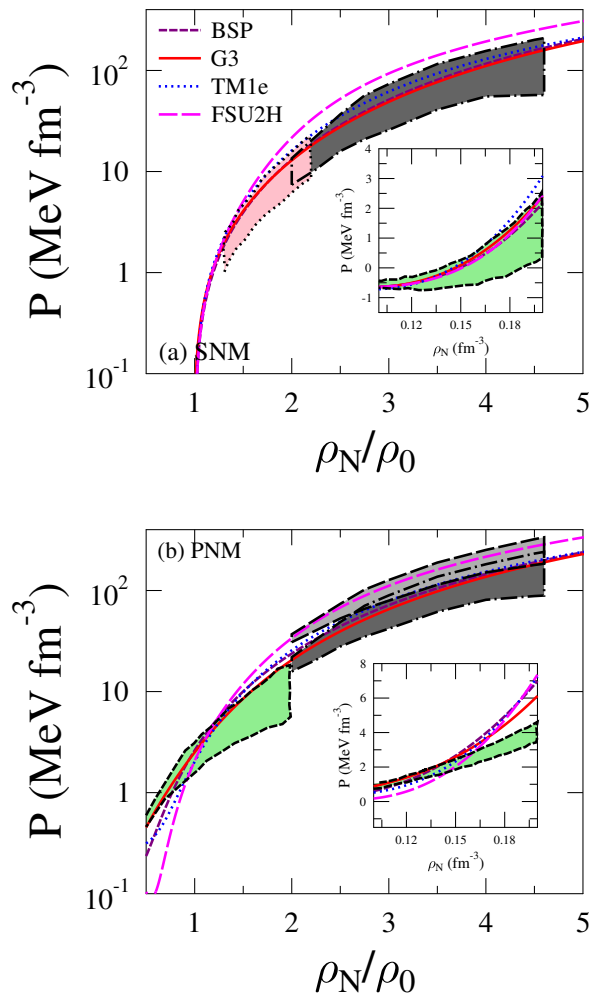


Figure 5.2: Here, the EoS is shown as the pressure as a function of the ratio nucleon density to saturation density (ρ_N/ρ_0) in the cases of SNM and PNM, which are shown in panels (a) and (b) respectively. The curves are calculated using G3, BSP, TM1e, and FSUH parameter sets. The gray shaded areas are extracted from the heavy-ion experimental data [96]. The pink shaded area in (a) is extracted from the FOPI experimental data [95]. The green shaded areas in panels (a) and (b) are the theoretical binding energy at low densities in the case of PNM, which is obtained from the chiral effective field theory calculations [97, 98].

mass that is larger than $2.0M_{\odot}$, it is obvious that the density in its core is larger than $2\rho_0$. If it is true, then hyperons should exist in the said NS core.¹ Hence, to include hyperon's contributions, we take SU(3) prescription and potential depths' experimental value at the saturation density of nuclear matter to determine the hyperon coupling constants, while neglecting the contribution from other exotics. Why we do this is that SU(3) prescription produces a stiffer EoS relative to the one from SU(6) [88].

We use the inner and outer crust EoSs based on the Hartree-Fock Thomas-Fermi model following Miyatsu *et al.* [99] to describe the NS's crusts. The drawback of this method is that there is an uncertainty that should be paid attention to.² For the detailed discussion about this uncertainty, please see Ref. [88] and the references therein.

The β -stability is assumed to happen in the NS matter. Hence, the charge neutrality from lepton and baryon charges, the baryon density conservation, and the potential chemical balancing can be used to determine the compositions of the mesons, baryons, and leptons in an NS. Here, to generate the EoSs, we also use another constraint from restricting the speed of sound at high densities $v_s \leq c/\sqrt{3}$, with c is the speed of light. To see the recent progress of speed of sound constraints on NS discussions, please see Ref. [100] and the references therein.

In Fig. 5.3, we show the EoSs and their speed of sound from matter without hyperon (G3 WoutH), with hyperon (G3 WH), and with the constraint for the speed of sound (G3 WoutHSS and G3 WHSS). In correspond to that, in Fig. 5.4, we show the mass-radius (M-R) curves from TOV GR. From Fig. 5.3, we observe that G3 WoutH is more compatible with the recent EoS constraints [80, 57, 58], and the stiffness of the corresponding EoSs is increased by the speed of sound's restriction. However, the effect for all G3 WoutHSS, WHSS, WoutH, and WH are insufficient to reach the constraint from GW170817 at high densities.

In Fig. 5.4, we can see the impacts of the hyperons and the speed of sound's constraint on M-R curves within TOV GR. All maximum masses from each EoS are in agreement with radius constraints for their NS with canonical mass ($1.4 M_{\odot}$) from Refs [57, 58]. However, hyperons' contribution on G3 WH EoS lowers the NS maximum mass significantly below the mass constraint of $2.0 M_{\odot}$. It can be seen that using the speed of sound requirement (G3 WHSS) increases the NS maximum mass. However, it is still less than

¹There is this problem called *hyperon puzzle* which states that the maximum mass from including hyperons in the calculation is always smaller than the one obtained without hyperons and other exotics. For the related discussions on the hyperon puzzle, please see, e.g, Ref. [94] and the references therein.

²The most evident problem that we see in our calculation is that the calculations in the NS core have a different scale of units (for illustration, km compared to mm) than in the NS crust. This makes the produced tabulated data—the energy density and the pressure—quite difficult to fit into a polynomial function. Hence, we use a piecewise function consisting of fitted polynomial functions from each sector, i.e., the inner core, outer core, inner crust, and outer crust. On the junctions between each function, we often had “gaps” that are hard to smoothen.

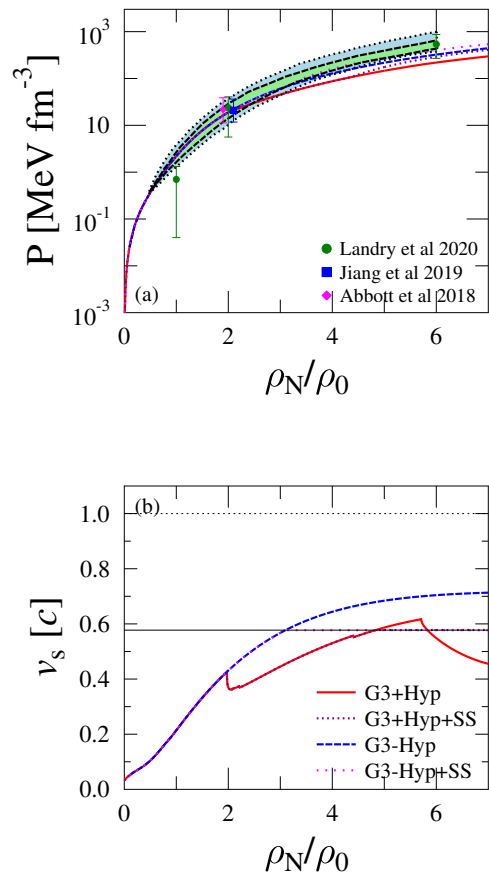


Figure 5.3: These EoSs are calculated using the G3 parameter set. The EoS without and with hyperon is denoted here by G3-Hyp and G3+Hyp, respectively. The “+SS” denotes the use of the speed of sound’s constraint ($v_s \leq c/\sqrt{3}$). In panel (a), pressure is shown as a function of the ratio of ρ_N to ρ_0 . In panel (b), the speed of sound is shown as the function of ρ_N to ρ_0 . For comparison, some data are given as follow: the light blue and light green shaded area are from GW170817 [80], the data points for particular densities are taken from GW170817 [80], a recent non-parametric analysis [57], and the joint of PSR J0030+0451, GW170817, and the nuclear data analysis [58].

the mass constraints from $2.0 M_{\odot}$ pulsars.

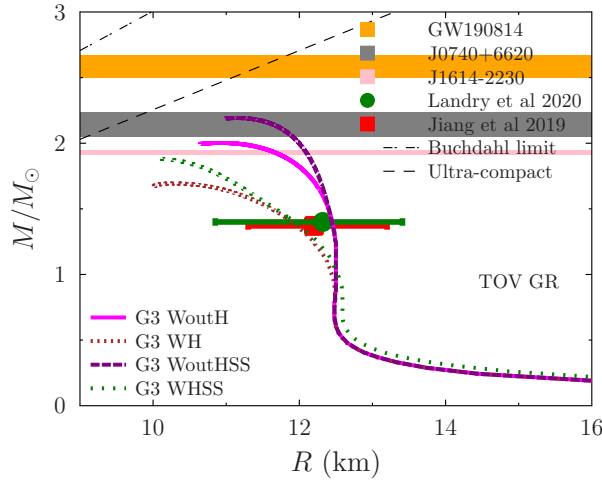


Figure 5.4: The M-R curves are calculated using the TOV GR framework. These are from using the G3 parameter set without hyperon (WoutH), with hyperon (WH), and the ones with additional speed of sound constraint (WoutHSS and WHSS). They are compared with the data from the GW190814 event [6], Landry *et al.* 2020 [57], and Jiang *et al.* 2019 [58]. We also show the results PSR J1614-2230 analysis [71, 72, 73] and PSR J0740+6620 analysis [73, 7]. The ultra-compact limit and Buchdahl limit lines are also shown.

Now, if the $2.6 M_{\odot}$ secondary object detected in GW190814 is a non-rotating NS, then, at least in GR theory, it has a different EoS than ours here. This is because all the maximum masses predicted by all EoSs used in this work are less than $2.6 M_{\odot}$. Recent investigations [8, 61] show that the $2.6 M_{\odot}$ constraint and the canonical $1.4 M_{\odot}$ NS radius constraints can be simultaneously satisfied using particular Big Apple RMF EoS if the hyperons are excluded in the NS matter. This Big Apple EoS is also compatible with finite nuclei and nuclear matter constraints, but it is not compatible with ones from heavy-ion collision constraints [96]. Hence, the author of Ref. [8] concluded that the $2.6 M_{\odot}$ secondary object is unlikely to be an NS within GR.

To this end, it is worth mentioning that EiBI, with acceptable EoS, can have NS maximum larger than $2 M_{\odot}$ without reaching the Buchdahl limit [33]. However, the radius also increases. Therefore in Chapter 7, we will systematically investigate, within the EiBI theory, the tension between the relatively small recent radius and the considerably high maximum mass constraints.

CHAPTER 6

ULTRA-COMPACT OBJECT FROM SEMI-CLASSICAL GRAVITY

In this chapter, we present the first part of our work. The following passage is from our paper published in Ref. [101].

6.1 A Short Introduction to The Semi-classical Gravity

Semi-classical gravity (SCGrav) is one of the earliest investigations to reconcile quantum field theory and GR. Its discoveries are the BH entropy, BH temperature, and Unruh effect (see monograph [45] and [46]). In this theory, the vacuum in a general space-time is generally different from the usual one in Minkowski space-time. It is caused by the Bogolyubov transformation, which says that a vacuum state in the coordinate system X^μ is different from another vacuum state in another coordinate system x^μ though the two coordinate systems are related by a coordinate transformation $x^\mu \rightarrow X^\mu(x^\alpha)$. This problem can be solved because it turns out that the stress tensor $T_{\mu\nu}$ is indifferent to one's choice of coordinate system. Even though there are infinities inside the components of the stress tensor, people had identified which infinities describe the real physical system, and the result is the Hadamard vacuum state. The Hadamard vacuum is a quantum state whose infinities in the two-point function are the same as the infinities from the one in Minkowskian space-time. Another state exists, e.g., the Unruh vacuum, which describes the vacuum around a Schwarzschild BH. This is the reason why people usually use the Unruh state to study the formation of a BH. The studies of n -point functions are related to regularization of these infinities in the stress tensor's expectation value ($\langle \hat{T}_{\mu\nu} \rangle$). Hence, the matter part in the EFE is quantum but the geometrical part is still classic

$$G_{\mu\nu} = \frac{8\pi G}{c^4} \langle \hat{T}_{\mu\nu} \rangle.$$

Note that in SCGrav, this modified EFE is for the vacuum case, which means that the right-hand side came from quantizing the vacuum. For it to be physical, the stress tensor's expectation value should satisfy Wald's renormalization axioms (see page 89 of [47]). From now, we shall use the natural unit $c = 1$ convention.

It is known that the renormalization methods can only be applied in some specific cases [102]. In conformal field theory, these methods give rise to an anomaly called the

trace anomaly [45], which is still unsolvable. The role of the cosmological constant is also nontrivial [103], hence in this theory, one cannot treat this constant as a free parameter.

Since we shall investigate the Boulware vacuum in the next sections, we shall briefly discuss this and compare it to the Unruh vacuum. The Boulware vacuum is a quantum state of the exterior of any massive body and it is singular at the horizon. The Unruh vacuum is the quantum state of a gravitational collapse and at large distances, it features Hawking radiation [104, 105]. In general, these two vacuums are inequivalent. A detailed discussion about the relationship between both vacuums can be seen in Ref. [106]. A study had investigated the dynamical evolution of a collapsed star within semi-classical gravity [107]. It found that in some cases, the trapping horizon is not formed and new collapsed horizonless objects could exist. Since these objects have no horizon, there is no confrontation between the information paradox and the run-away endpoint problem. It also found that both vacuums can locally describe the same exterior region as long as there is no horizon. If the horizon exists, then the Boulware vacuum is no longer valid and the Unruh vacuum is used instead. Please see the technical details of this matter in Ref. [107]. Another study by Ho and Matsuo [108] has shown that if a compact object has no singularity nor horizons, then its exterior can be described by the Boulware vacuum as long as it is in a stationary state. Furthermore, Ho and Matsuo have shown by nonperturbative analysis of the semiclassical Einstein equation in another paper [109] that it is possible to consider the Boulware vacuum for any compact object. These results [108, 109] is in contrast to the common view that Boulware vacuum becomes unphysical if the compact object's radius is smaller than the Schwarzschild radius since the stress tensor is divergent at the Schwarzschild radius. In this work, we study the horizonless compact object in SCGrav and its radius is larger than the Schwarzschild radius. Therefore, choosing a Boulware vacuum is relatively safe.

Recently, Carballo-Rubio [5] proposed a new type of TOV-like equation from semi-classical gravity theory. The solutions obey the usual boundary conditions, i.e., zero pressure at the surface of the star. They arise from one of two possible pressure equations $p'(r)$. One of them has a negative sign which corresponds to the usual TOV equation at a weak limit and the other has a positive sign which is identified as a nontrivial combination of the black stars and gravastars. This calculation is done by defining a relation between pressure p , mass m , and energy density ρ by a constant $\lambda > 1$. This trick makes the EoS unique. The pressure equation p' with the negative sign had been analyzed by Ho and Matsuo [108]. They show that by using constant energy density and without making the pressure goes to infinity, the Buchdahl limit can be violated.

In this work, we study much further the pressure equation p' with the negative sign. The writing is organized as follows. In Section 6.2, we revisit the models (Refs. [5]

and [108]) briefly. In Section 6.3, we study the model given the assumption of non-negative pressure and energy density, and we employ a simple linear EoS. We then look at the deviation from the case of TOV in GR. In Section 6.4 part B, the numerical results are discussed. The numerical schemes are discussed in length in Section 6.5. This is crucial to justify our results in the following sections since both Refs. [5] and [108] use integration from surface to center (denoted as backward integration), whereas we do the opposite (denoted as forward integration). Finally in Section 6.6, our work is summarized.

6.2 Theory of a Compact Star in Semi-classical Gravity

In this section, we follow Ref. [5]. We start by using the renormalized stress-energy tensor (RSET) $\langle \hat{T}_{\mu\nu} \rangle$ in the following modified EFE

$$G_{\mu\nu} = 8\pi G T_{\mu\nu} + 96\pi^2 l_p^2 \langle \hat{T}_{\mu\nu} \rangle, \quad (6.1)$$

where the constant l_p is the *renormalized Planck length* describing the quantum vacuum polarization of $N \gg 1$ matter fields. This constant is related to the Planck length $L_{\text{Pl}} = \sqrt{\hbar G/c^3}$ (in SI units) by the following relation:

$$l_p = \sqrt{\frac{N}{12\pi}} L_{\text{Pl}}.$$

The constant l_p is treated as an arbitrarily adjustable parameter.

To explain where the new term came from, we discuss the modified EFE above in its original form

$$G^{\mu\nu} = 8\pi G \left(T_{\mu\nu} + \hbar c N \langle \hat{T}_{\mu\nu} \rangle \right) + \mathcal{H}_{\mu\nu}.$$

These new terms came from two possible theories, i.e.,

1. from $\mathcal{O}(1/N)$ contributions with respect to the term proportional to $\hbar N \langle \hat{T}_{\mu\nu} \rangle$, which might be related to more loops in the Feynman diagrams that may include gravitons, or
2. from adding $\hbar^{n-1} G^{n-2} \mathcal{R}^n$ ($n \geq 2$) in the Einstein-Hilbert Lagrangian, where \mathcal{R} some kind of curvature scalars, e.g., $R_{\mu\nu} g^{\mu\nu}$, $R_{\mu\nu} R^{\mu\nu}$, and $R_{\mu\nu\alpha\beta} R^{\mu\nu\alpha\beta}$.

This is valid if the curvature remains small enough. We also ignore $\mathcal{H}_{\mu\nu}$ because we think the leading term $\langle T_{\mu\nu} \rangle$ is already small and thus $\mathcal{H}_{\mu\nu}$ should be smaller. Carballo-Rubio had proven that $\mathcal{H}_{\mu\nu} = 0$ is justified.

Next we use a similar scheme to derive the usual TOV equation, starting with the static

and spherically symmetric space-time

$$ds^2 = g_{\mu\nu} dx^\mu dx^\nu = ds_{(2)}^2 + r^2(d\theta^2 + \sin^2 \theta d\varphi^2), \quad (6.2)$$

$$ds_{(2)}^2 = -e^{\nu(r)} dt^2 + \frac{dr^2}{1 - 2Gm(r)/r}. \quad (6.3)$$

This metric has a time symmetry so it has a timelike Killing vector $\xi^\mu = \delta_t^\mu$. Next, we use a perfect fluid with isotropic pressure as the stress tensor

$$T^{\mu\nu} = (\rho + p)u^\mu u^\nu + pg^{\mu\nu}, \quad (6.4)$$

with u^μ is the normalized timelike 4-velocity of the fluid ($u^\mu u_\mu = -1$). It is usual to choose the fluid to be standing still, i.e., only u^0 is nonzero. $g^{\mu\nu}$ is the inverse of the metric.

The RSET is calculated using the s -wave Polyakov approximation (see Ref. [110] page 216)

$$\langle \hat{T}_{\mu\nu} \rangle = \frac{\delta_\mu^a \delta_\nu^b}{4\pi r^2} \langle \hat{T}_{ab}^{(2)} \rangle. \quad (6.5)$$

The a and b indices denote the coordinates in $ds_{(2)}^2$, so the other tensor $\langle \hat{T}_{ab}^{(2)} \rangle = \langle 0 | \hat{T}_{ab}^{(2)} | 0 \rangle$ is calculated in a space-time with metric $ds_{(2)}^2$. In this model, we use the Boulware vacuum state $|0\rangle$, which is associated with the Killing vector mentioned before. The Killing covector is then just $\xi_\mu = -e^\nu \delta_{\mu t}$. To obtain $\langle \hat{T}_{ab}^{(2)} \rangle$, people usually employ null coordinate (u, r) , calculate $\langle \hat{T}_{ab}^{(2)} \rangle$, and then transform back to (t, r) coordinate. On the other hand, it was shown in Ref. [111] that we can use a shortcut, which is still equivalent to the usual method. This shorcut is

$$\langle \hat{T}_{ab}^{(2)} \rangle = \frac{1}{48\pi} \left(R^{(2)} g_{ab} + A_{ab} - \frac{1}{2} g_{ab} A \right), \quad (6.6)$$

where $R^{(2)}$ is the Ricci scalar from metric $ds_{(2)}^2$, and

$$A_{ab} = \frac{4}{|\xi|} \nabla_a \nabla_b |\xi|, \quad (6.7)$$

with $|\xi| = e^{\nu/2}$.

Hence, from $\nabla_\mu T^{\mu\nu} = 0$, one obtains the usual equation

$$-p' - \frac{(p + \rho)}{2} \nu' = 0, \quad (6.8)$$

with $f' = df/dr$, and from the modified EFE (Eq. (6.1)), one obtain

$$\frac{\nu'}{r} - \frac{2Gm}{r^3(1-2Gm/r)} = \frac{8\pi Gp}{1-2Gm/r} - \frac{l_P^2}{4} \left(\frac{\nu'}{r}\right)^2, \quad (6.9)$$

$$\begin{aligned} \frac{2Gm'}{r^2} &= 8\pi G\rho + \frac{l_P^2}{r^2} \left[\left(1 - \frac{2Gm}{r}\right) (\nu'' + (\nu')^2) \right. \\ &\quad \left. - \left(\frac{Gm'}{r} - \frac{Gm}{r^2}\right) \nu' - \frac{3}{4} \left(1 - \frac{2Gm}{r}\right) (\nu')^2 \right]. \end{aligned} \quad (6.10)$$

The reason why $\nabla_\mu \langle T^{\mu\nu} \rangle = 0$ should be satisfied (see the Wald's axioms in Ref. [47]) is due to the mathematical consequence of Eq. (6.1), i.e.,

$$\nabla_\mu G^{\mu\nu} = 8\pi G \left(\nabla_\mu T^{\mu\nu} + \hbar c N \nabla_\mu \langle \hat{T}^{\mu\nu} \rangle \right).$$

The left-hand side goes to zero because of the contracted Bianchi identity. Then right-hand side should also be zero. Since it is common to use conservation equation $\nabla_\mu T^{\mu\nu} = 0$ so $\nabla_\mu \langle T^{\mu\nu} \rangle = 0$.

From Eq. (6.9), there are two roots:

$$\nu' = -\frac{2r}{l_P^2} \left(1 \pm \sqrt{1 + \frac{l_P^2}{r^2} \frac{2Gm}{r} \frac{(1 + 4\pi r^3 p/m)}{(1 - 2Gm/r)}} \right). \quad (6.11)$$

These roots lead to two different expressions for both p' and m' . The negative (positive, resp.) sign on the right-hand side corresponds to what we call as the *negative (positive)* branches. In $l_p \rightarrow 0$ limit, the negative branch becomes the TOV equation in GR while the positive branch does not. Next, we focus on this negative branch in the rest of this chapter.

6.3 Analysing the Negative Branch

The following passage is our argument why we choose the negative branch. We study the negative branch from the model given the non-negative pressure p and energy density ρ assumption. Here we define

$$X = \frac{2Gm}{r} \frac{(1 + 4\pi r^3 p/m)}{(1 - 2Gm/r)}, \quad (6.12)$$

for simplicity. Then, we have

$$p' = \frac{(p + \rho)r}{l_P^2} \left(1 + k \sqrt{1 + \frac{l_P^2}{r^2} X} \right) \quad (6.13)$$

where $k = \pm 1$ is used to contain the positive-negative sign. We investigate this equation in three cases: (a) $\frac{l_p^2}{r^2}X < 1$, (b) $\frac{l_p^2}{r^2}X > 1$ and (c) $\frac{l_p^2}{r^2}X = 1$. Notice that $X > 0$ because $2Gm/r < 1$.

Consider the case (a). Using binomial expansion with respect to small $\frac{l_p^2}{r^2}X$, and calculating to only the first leading order, we obtain

$$p' = \begin{cases} \frac{\rho+p}{2} \left(\frac{4r}{l_p^2 X} + \frac{X}{r} \right), & k = +1, \\ -\frac{\rho+p}{2} \frac{X}{r}, & k = -1. \end{cases} \quad (6.14)$$

Because of the nonzero pressure at the star's center and the pressure going to zero at the surface at $r = R$, we need $p' < 0$, at least in some parts in the domain $0 < r < R$. This is satisfied by $k = -1$ but not by $k = +1$. Notice that when $k = -1$, it is just the TOV equation. Next consider the case (b). Using binomial expansion again, this leads to

$$p' = k \frac{(\rho + p)\sqrt{X}}{l_p}. \quad (6.15)$$

The condition $p' < 0$ then eliminates $k = +1$. Lastly, consider the case (c). The binomial expansion then leads us to

$$p' = \frac{(p + \rho)r}{l_P^2} \left(1 + k\sqrt{2} \right). \quad (6.16)$$

Again from the condition $p' < 0$, we should choose $k = -1$. Hence from all the three cases above, we only use the negative branch so that the boundary conditions $p(0) = p_c > 0$ and $p(R) = 0$ are satisfied.

Now we investigate Eq. (6.10). It is clear that m' is located on both left and right hand side. Our choice

$$p' = \frac{(p + \rho)r}{l_P^2} \left(1 - \sqrt{1 + \frac{l_p^2}{r^2}X} \right), \quad (6.17)$$

then gives us the following

$$m' = 4\pi\rho r^2 \left(\frac{1 + \sum_{i=1}^7 A_i}{1 + \sum_{i=1}^4 B_i} \right). \quad (6.18)$$

The terms in the numerator inside the round bracket are

$$A_1 = \frac{3l_p^2 p}{\rho r^2 \sqrt{1 + \frac{l_p^2}{r^2} X}}, \quad (6.19)$$

$$A_2 = -\frac{3l_p^2 m(1 + 4\pi r^3 p/m)}{4\pi \rho r^5 \sqrt{1 + \frac{l_p^2}{r^2} X}}, \quad (6.20)$$

$$A_3 = -\frac{Gl_p^2 m^2 (1 + 4\pi r^3 p/m)}{2\pi \rho r^6 (1 - 2Gm/r) \sqrt{1 + \frac{l_p^2}{r^2} X}}, \quad (6.21)$$

$$A_4 = -\frac{m \left(1 - \sqrt{1 + \frac{l_p^2}{r^2} X}\right)}{4\pi \rho r^3}, \quad (6.22)$$

$$A_5 = -\frac{(1 - 2Gm/r) \left(1 - \sqrt{1 + \frac{l_p^2}{r^2} X}\right)}{4\pi G \rho r^2}, \quad (6.23)$$

$$A_6 = \frac{(1 - 2Gm/r) \left(1 - \sqrt{1 + \frac{l_p^2}{r^2} X}\right)^2}{8\pi G \rho l_p^2}, \quad (6.24)$$

$$A_7 = \frac{l_p^2}{\rho r \sqrt{1 + \frac{l_p^2}{r^2} X}} p'. \quad (6.25)$$

The terms in the denominator inside the round bracket are

$$B_1 = \frac{4\pi l_p^2 p r}{m \sqrt{1 + \frac{l_p^2}{r^2} X}}, \quad (6.26)$$

$$B_2 = -\frac{l_p^2 (1 + 4\pi r^3 p/m)}{r^2 \sqrt{1 + \frac{l_p^2}{r^2} X}}, \quad (6.27)$$

$$B_3 = -\frac{2G l_p^2 m (1 + 4\pi r^3 p/m)}{r^3 (1 - 2Gm/r) \sqrt{1 + \frac{l_p^2}{r^2} X}}, \quad (6.28)$$

$$B_4 = -\left(1 - \sqrt{1 + \frac{l_p^2}{r^2} X}\right). \quad (6.29)$$

m' is lengthy and complicated. But, it is common to use the boundary conditions $m(0) = 0$ and $m(R) = M > 0$, so that $m' > 0$. Hence, we need to be careful on fixing the constants and the data of both pressure and mass near the center.

Before integrating numerically, let us investigate both p' and m' at the limit $l_p \rightarrow 0$. If

we Taylor expand p' with respect to small l_p , we obtain

$$p' = -\frac{G(m + 4\pi r^3 p)(\rho + p)}{r(r - 2Gm)} + \frac{G^2 l_p^2 (m + 4\pi r^3 p)^2 (\rho + p)}{2r^3(r - 2Gm)^2} + \mathcal{O}(l_p^3). \quad (6.30)$$

If we Taylor expand A_i and B_i with respect to small l_p , we obtain

$$A_1 = \frac{l_p^2}{r^2} \frac{3p}{\rho} + \mathcal{O}(l_p^3) > 0, \quad (6.31)$$

$$A_2 = -\frac{l_p^2}{r^2} \frac{3m(1 + 4\pi r^3 p/m)}{4\pi r^3 \rho} + \mathcal{O}(l_p^3) < 0, \quad (6.32)$$

$$A_3 = -\frac{l_p^2}{r^2} \frac{Gm^2(1 + 4\pi r^3 p/m)}{2\pi r^4 \rho(1 - 2Gm/r)} + \mathcal{O}(l_p^3) < 0, \quad (6.33)$$

$$A_4 = \frac{l_p^2}{r^2} \frac{Gm^2(1 + 4\pi r^3 p/m)}{4\pi r^4 \rho(1 - 2Gm/r)} + \mathcal{O}(l_p^3) > 0, \quad (6.34)$$

$$A_5 = \frac{l_p^2}{r^2} \frac{m(1 + 4\pi r^3 p/m)}{4\pi r^3 \rho} + \mathcal{O}(l_p^3) > 0, \quad (6.35)$$

$$A_6 = \frac{l_p^2}{r^2} \frac{Gm^2(1 + 4\pi r^3 p/m)^2}{8\pi r^4 \rho(1 - 2Gm/r)} + \mathcal{O}(l_p^3) > 0, \quad (6.36)$$

$$A_7 = -\frac{l_p^2}{r^2} \frac{Gm(1 + p/\rho)(1 + 4\pi r^3 p/m)}{r(1 - 2Gm/r)} + \mathcal{O}(l_p^3) < 0, \quad (6.37)$$

and

$$B_1 = \frac{l_p^2}{r^2} \frac{4\pi r^3 p}{m} + \mathcal{O}(l_p^3) > 0, \quad (6.38)$$

$$B_2 = -\frac{l_p^2}{r^2} \left(1 + \frac{4\pi r^3 p}{m}\right) + \mathcal{O}(l_p^3) < 0, \quad (6.39)$$

$$B_3 = -\frac{l_p^2}{r^2} \frac{2Gm(1 + 4\pi r^3 p/m)}{r(1 - 2Gm/r)} + \mathcal{O}(l_p^3) < 0, \quad (6.40)$$

$$B_4 = \frac{l_p^2}{r^2} \frac{Gm(1 + 4\pi r^3 p/m)}{r(1 - 2Gm/r)} + \mathcal{O}(l_p^3) > 0. \quad (6.41)$$

Since all $(Gm/r) \sim 0$, $(r^3 p/m) \sim 0$, $(r^3 \rho/m) \sim 0$, and $(p/\rho) \neq \infty$ as $r \rightarrow 0$, no singularity occur on each A_i and B_i at $r = r_c \sim 0$ as long as $r_c > l_p$. Substituting all A_i

and B_i into m' , we obtain

$$\begin{aligned} \sum_{i=1}^7 A_i &= \frac{l_p^2}{r^2} \left[\frac{3p}{\rho} - 2 \frac{m(1+4\pi r^3 p/m)}{4\pi r^3 \rho} - \frac{Gm^2(1+4\pi r^3 p/m)}{4\pi r^4 \rho(1-2Gm/r)} \right. \\ &\quad \left. + \frac{Gm^2(1+4\pi r^3 p/m)^2}{8\pi r^4 \rho(1-2Gm/r)} - \frac{Gm(1+p/\rho)(1+4\pi r^3 p/m)}{r(1-2Gm/r)} \right] + \mathcal{O}(l_p^3), \end{aligned} \quad (6.42)$$

$$\sum_{i=1}^4 B_i = \frac{l_p^2}{r^2} \left[-1 - \frac{Gm(1+4\pi r^3 p/m)}{r(1-2Gm/r)} \right] + \mathcal{O}(l_p^3). \quad (6.43)$$

The conditions on the surface of the object are $p = 0$, $\rho = \rho_0$, $r = R$ and $m = M$. So at the surface, we have

$$p'(R) = -\frac{GM\rho_0}{R^2(1-2GM/R)} + \frac{G^2 l_p^2 M^2 \rho_0}{2R^5(1-2GM/R)^2} + \mathcal{O}(l_p^3) \quad (6.44)$$

and

$$\begin{aligned} \sum_{i=1}^7 A_i &= \frac{l_p^2}{R^2} \left[-2 \frac{M}{4\pi R^3 \rho_0} - \frac{GM^2}{4\pi R^4 \rho_0 (1-2GM/R)} \right. \\ &\quad \left. + \frac{GM^2}{8\pi R^4 \rho_0 (1-2GM/R)} - \frac{GM}{R(1-2GM/R)} \right] + \mathcal{O}(l_p^3), \end{aligned} \quad (6.45)$$

$$\sum_{i=1}^4 B_i = \frac{l_p^2}{R^2} \left[-1 - \frac{GM}{R(1-2GM/R)} \right] + \mathcal{O}(l_p^3). \quad (6.46)$$

It is easy to see that $m'(R)$ is finite if $\rho_0 \neq 0$, although in the case of TOV GR, $\rho_0 = 0$ corresponds to no solution. It seems that the changes of both R and M might be significant if the value of ρ_0 goes to zero.

Now we investigate the region near the center. The subscript c will denote the value at the center. At $r = r_c \sim 0$, we have

$$\begin{aligned} \sum_{i=1}^7 A_i &= \frac{l_p^2}{r_c^2} \left[\frac{3p_c}{\rho_c} - 2 \frac{(1+3p_c/\rho_c)}{3} - \frac{Gm_c^2(1+3p_c/\rho_c)}{4\pi r_c^4 \rho_c (1-2Gm_c/r_c)} \right. \\ &\quad \left. + \frac{Gm_c^2(1+3p_c/\rho_c)^2}{8\pi r_c^4 \rho_c (1-2Gm_c/r_c)} - \frac{Gm_c(1+p_c/\rho_c)(1+3p_c/\rho_c)}{r_c(1-2Gm_c/r_c)} \right] + \mathcal{O}(l_p^3) \\ &= \frac{l_p^2}{r_c^2} \left[\frac{p_c}{\rho_c} - \frac{2}{3} \right] + \mathcal{O}(r_c^2), \end{aligned} \quad (6.47)$$

$$\sum_{i=1}^4 B_i = \frac{l_p^2}{r_c^2} \left[-1 - \frac{Gm_c(1+3p_c/\rho_c)}{r_c(1-2Gm_c/r_c)} \right] + \mathcal{O}(l_p^3) = -\frac{l_p^2}{r_c^2} + \mathcal{O}(r_c^2). \quad (6.48)$$

We use the usual expression for mass $m_c = (4/3)\pi\rho_c r_c^3$ in the second equality. After substituting into p' and m' , we have

$$p'(r_c) \sim -\frac{4}{3}\pi G r_c (\rho_c + p_c)(\rho_c + 3p_c) + \frac{8}{9}\pi^2 G^2 l_p^2 r_c (\rho_c + p_c)(\rho_c + 3p_c)^2 \quad (6.49)$$

and

$$m'(r_c) \sim 4\pi r_c^2 \rho_c \left(\frac{1 + (l_p/r_c)^2 (3p_c/\rho_c - 2/3)}{1 - (l_p/r_c)^2} \right). \quad (6.50)$$

From the above expressions, $m'(r_c)$ is singular at $r_c = l_p$.

For now, let us set $r_c = \alpha l_p$ where $\alpha > 0$ and $\alpha \neq 1$. Then, Eq. (6.49) can be reexpressed as follows

$$p'(r_c) \simeq -\frac{4}{3}\pi G \rho_c^2 \left(1 + \frac{p_c}{\rho_c} \right) \left(1 + 3\frac{p_c}{\rho_c} \right) \alpha l_p \left[1 - \frac{2}{3}\pi G \rho_c \left(1 + 3\frac{p_c}{\rho_c} \right) l_p^2 \right]. \quad (6.51)$$

Since we demand that $p_c > 0$, then $p'(0) < 0$, which implies

$$l_p < \sqrt{\frac{3}{2\pi G(\rho_c + 3p_c)}}, \text{ or equivalently, } N < \frac{18}{L_{\text{Pl}}^2 G(\rho_c + 3p_c)}. \quad (6.52)$$

Hence, both p_c and the EoS affect the upper bound of l_p and the strong energy condition should be satisfied due to the square root in Eq. (6.52).

Now we look at m' . Using the same approximation as for p' , Eq. (6.50) becomes

$$m'(r_c) \sim 4\pi r_c^2 \rho_c \left[1 - \frac{3p_c/\rho_c + 1/3}{1 - \alpha^2} \right]. \quad (6.53)$$

Since in the limit of TOV GR, the mass should grow from center to surface ($m' > 0$). In the case of $\alpha > 1$, $m'(r_c) > 0$ is trivially satisfied. On the other hand in the case of $\alpha < 1$ and if the second term inside the square bracket is less than unity, $m'(r_c) > 0$ can happen. This implies

$$3p_c < (2/3 - \alpha^2)\rho_c. \quad (6.54)$$

In the case of $\alpha = \sqrt{2/3}$, then $p_c < 0$. This is in contradiction to our assumptions that $p > 0$ and $\rho > 0$ inside the star. In the case of $\alpha > \sqrt{2/3}$, then

$$\rho_c < -\left(\frac{3p_c}{\alpha^2 - 2/3} \right) < 0. \quad (6.55)$$

This expression is also in contradiction to our assumptions. Lastly, in the case of $\alpha <$

$\sqrt{2/3}$, then

$$\rho_c > \left(\frac{3p_c}{2/3 - \alpha^2} \right) > 4.5p_c, \quad (6.56)$$

which implies $dp/d\rho = w < 2/9$, which means that the squared speed of sound is lower than the upper bound from both QCD ($w \leq 1/3$) and causality ($w \leq 1$) [112]. This, in consequence, leads to lower compactness, according to Ref. [53], which stated that by a linear equation of state (EoS) $\rho = p/w + \rho_0$ and using TOV GR, the produced maximum compactness is

$$\left(\frac{2GM}{R} \right)_{\max} \sim \frac{8}{9 \left(\frac{0.51w+0.77}{w(w+4.18)} + 1 \right)}. \quad (6.57)$$

The expression on the right-hand side is a monotonically increasing function of w , but the compactness $2GM/R$ cannot go beyond the Buchdahl limit $2GM/R = 8/9$. Also notice that this condition of $m'(r)$ applies only at $r = r_c$, so it may not be true for $r > r_c$. But, since the equation of state is unchanging from any regions of r , this condition should hold even when $r \gg r_c$.

For a moment, let us consider negative m_c , which is possible according to Ref [113], so that the case of $\alpha < 1$ can be investigated. Then, we can see from Eq. (6.43) that $m'(r)$ at $\alpha = 1$ has no singularity anymore. If we demand $\sum_i B_i > 0$ then we can obtain

$$m_c < \frac{\rho_c r_c}{G\rho_c - 3Gp_c} \equiv m_{c,max}. \quad (6.58)$$

From assumption $m_c < 0$, we can obtain another restriction for the EoS, i.e.,

$$w > 1/3. \quad (6.59)$$

Notice that $m_{c,max} \rightarrow 0$ if r_c is sufficiently small, so we can use the limit from negative value $m_c \rightarrow 0^-$. In this limit, Eq. (6.30) becomes $p'(r_c) < 0$, thus the pressure decreases from p_c . Eq. (6.42) becomes

$$\sum_i A_i \sim \alpha^{-2} \left[\frac{p_c}{\rho_c} - \frac{2}{3} \right]. \quad (6.60)$$

Since we want $\sum_i B_i > 0$ and $m'(r) > 0$, then

$$w > 2/3. \quad (6.61)$$

Recall that these came from considering the limit of $m_c \rightarrow 0^-$. On the other hand, in the

limit of $m_c \rightarrow -\infty$, from Eq. (6.30) we have

$$0 > m_c > -4\pi r_c^3 p_c \equiv m_{c,min}, \quad (6.62)$$

which set the minimum value of m_c . Again, if r_c is sufficiently small, $m_{c,min} \rightarrow 0$. Hence, for the case of $m_c < 0$, we obtain $w > 2/3$ and $m_{c,min} < m_c < m_{c,max}$ that restricts w and m_c .

Since the restriction of $m_c < 0$ is tight if r_c very small, we do not use the $m_c < 0$ case in the following sections and rather use $m_c = 4\pi r_c^3 \rho_c / 3$.

6.4 Numerical Results

The following linear EoS

$$\rho(p) = p/w + \rho_0 \quad (6.63)$$

is used in this study. The constant ρ_0 define the energy density at the surface that act like a surface tension. $\rho_0 \neq 0$ because no solution exists for $\rho_0 = 0$. Also, ρ_0 cannot be negative, or it will violate weak energy condition [53]. The constant w , defined as $w = dp/d\rho$, is the speed of sound squared from thermodynamics and Newtonian mechanics. w is restricted to at least two conditions [112]:

1. $0 < w \leq 1$ from causality, and
2. $0 < w \leq 1/3$ from QCD.

Hence, we shall choose $1/3 \leq w \leq 1$ and $\alpha > 1$ because we want the largest compactness possible from the model.

We need to fix suitable value for l_p , α , ρ_0 , and p_c carefully such that all boundary conditions are satisfied before integrating p' and m' numerically. The units we use here follows Ref. [89], which is called “NS” units. In this units, r is in metres, both p and ρ are in MeV/fm³, and m is in the solar mass M_\odot , which has unit MeV m³/fm³. Here we use the compactness defined as $C = GM/R$ and ρ_0 related to the MIT bag constant B by $\rho_0 = 4B$ [54].

The upper bound of l_p can now be estimated. Since it is usual to have p_c and ρ_0 around $\sim 10^3$ MeV/fm³, then by Eq. (6.52), we obtain $l_p \lesssim 10$ km, which is trivial since neutron stars usually has $R \sim 10$ km. This is equivalent to $N < 10^{79}$. By this, the absolute value of RSET should satisfy

$$|\langle T_{\mu\nu} \rangle| < \frac{|T_{\mu\nu}|}{3.162 \times 10^{52} \text{ kg m}^3 \text{ s}^{-2}}. \quad (6.64)$$

This is in SI units, where $\hbar c = 3.162 \times 10^{-27} \text{ kg m}^3 \text{ s}^{-2}$.

It is also interesting to see that by

$$p' = -\frac{(p + \rho)X}{r \left(1 + \sqrt{1 + (l_p/r)^2 X}\right)}, \quad (6.65)$$

which is equivalent to Eq. (6.17), the numerical calculation is much more smooth. This is because the smallness of l_p often make computers cannot detect the second term in the square root of Eq. (6.17), which then make $p' = 0$ in some regions of r . We can evade this problem if we use Eq. (6.65).

In the following numerical results, we shall show that the contribution of l_p does not affect the maximum mass significantly. This can be seen in Fig. 6.1, which are profiles from variation of w . There w does increase the mass and the radius, but this can also be obtained from the standard TOV equation in GR.

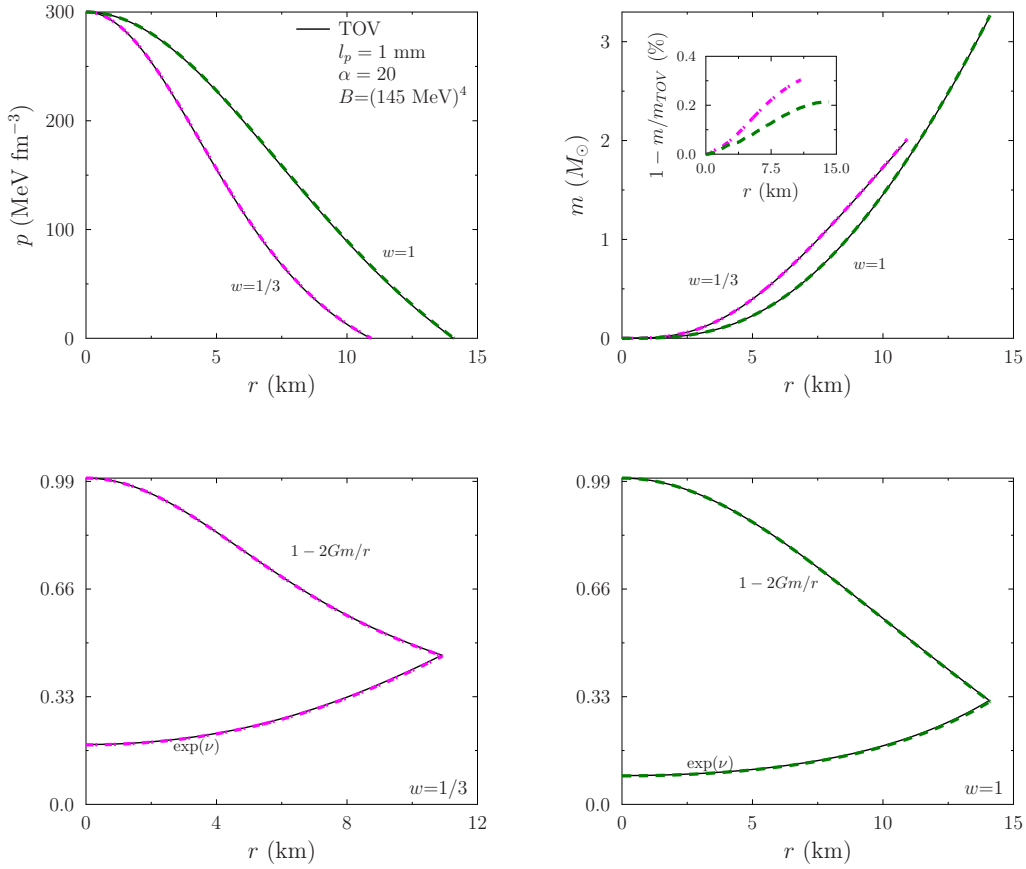


Figure 6.1: These are some profiles of p and m in the upper panels from setting $l_p = 1 \text{ mm}$ and $\alpha = 20$. Here we vary w . $\exp(\nu)$ and $1 - 2Gm/r$ are shown in the lower panels.

Similar profiles also arise from varying B , α and l_p . In Figs. 6.2, 6.3, 6.4 and 6.5,

variations of w , B , α and l_p , respectively, are used to produce the M-R curves. It is clear that the semi-classical correction does not affect the M-R relation compared to TOV GR.

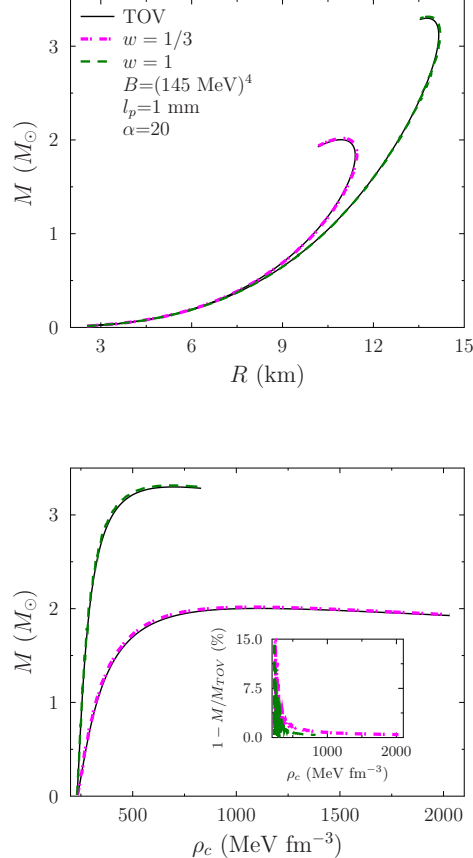


Figure 6.2: Here are the M-R curves from variations of w .

We tried using $\alpha < 1$, but we failed to find any numerical solution that satisfies the boundary conditions on both the center and the surface. Even though the mass profile increases a little in the beginning, the mass always goes to a negative value later on. It is intriguing that for the similar case in Ref. [108] (they use constant energy density) their integration method breaks down at $r = l_p$. They integrate the equations from the surface to the center. In the next section, we show that it is consistent with our results, which is from integrating the equations from the center to the surface.

Moreover, although we have a similar aspect compared to Ref. [108], our results are different from theirs since they use $m_c < 0$ while we use $m_c = 0$. This negative m_c , because they integrate from the surface to the center, is not an input anymore. Our $m_c = 0$ case here gives only slightly larger compactness than the Buchdahl bound, but their results from negative m_c can give compactness very near the black hole limit. For details about this, see the following section.

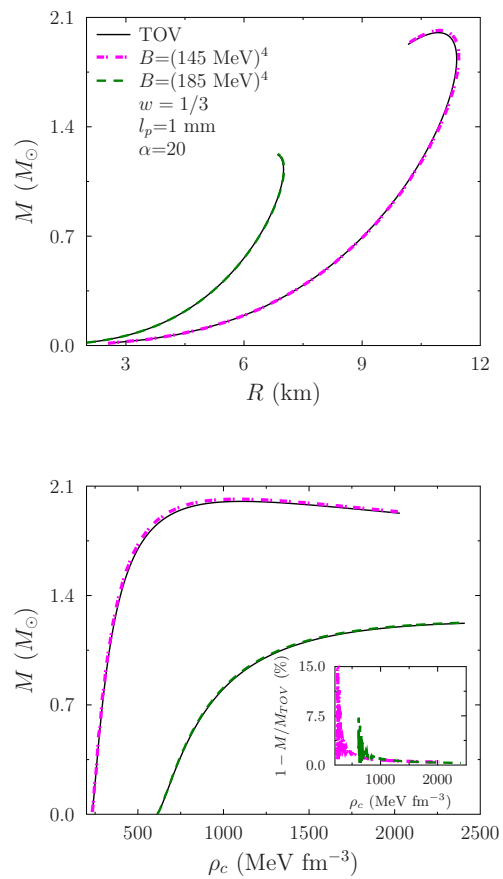


Figure 6.3: Here are the M-R curves from variations of B . If B is decreased, it produces higher mass and larger radius.

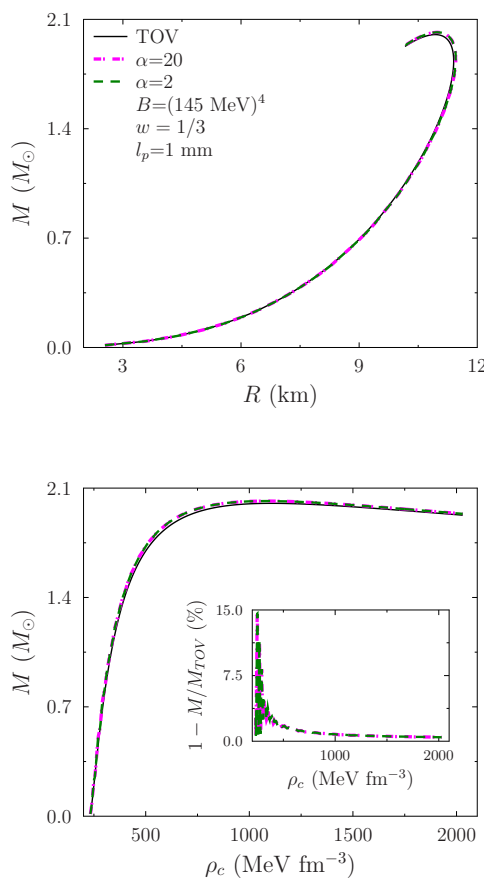


Figure 6.4: Here are the M-R curves from variations of α .

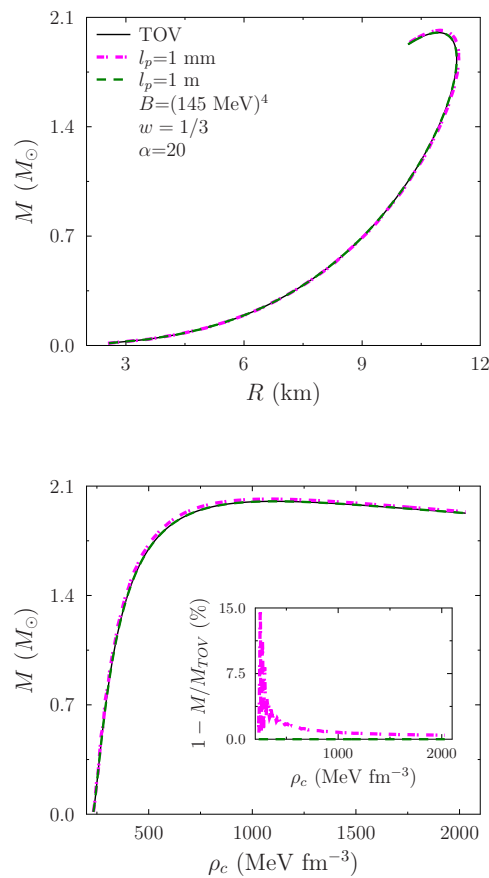


Figure 6.5: Here are the M-R curves from variations of l_p .

6.5 Numerical Verification

This passage is a part of our first work which had been published in PRD (Ref. [101]).

Here, we explain the integration schemes used in this chapter. We call the schemes used here as *forward* integration and *backward* integration, respectively, to denote the integration from the center of the star to its surface and vice versa. One can do either forward integration or backward integration for the standard TOV equation and the result will be the same. Yet, it is not true anymore for the positive branch we discussed before, which does not become the standard TOV equation in the limit $l_p \rightarrow 0$.

We shall discuss in detail both schemes in reproducing the solutions, by numerical calculation, in

1. the negative branch obtained previously by Ho and Matsuo [108] in the case of constant energy density ρ , and
2. the positive branch obtained previously by Carballo-Rubio [5] using constant λ trick.

We emphasize these schemes because we use forward integration in the previous sections, but both Refs. [5] and [108] use backward integration. We shall show that we get consistent results from both schemes for the negative branch, but inconsistent for the positive branch.

6.5.1 Numerical solutions from negative branch

Suppose we use the tortoise coordinate r_* , rather than r , hence g_{rr} is redefined by

$$g_{rr} = C(r)/F^2(r), \quad (6.66)$$

$$C(r) = e^{\nu(r)}, \quad (6.67)$$

and the constants are renamed by $\alpha = l_p^2$ and $\kappa = 8\pi G$. These definitions are going to be used only in this subsection. Then the Eqs. (6.9) and (6.10) become

$$\begin{aligned} 0 &= -\frac{1}{8r^2C(r)^2} \left[-3\alpha F(r)^2 C'(r)^2 + 4rC(r)^2 F(r)F'(r) \right. \\ &\quad + 2C(r)F(r) (\alpha C'(r)F'(r) + F(r) (\alpha C''(r) - 2rC'(r))) \\ &\quad \left. + 2\kappa r^2 C(r)^3 (p + \rho) \right], \end{aligned} \quad (6.68)$$

$$\begin{aligned} 0 &= \frac{1}{4r^2C(r)^2} \left[\alpha F(r)^2 C'(r)^2 - \alpha C(r)F(r) (F(r)C''(r) + C'(r)F'(r)) \right. \\ &\quad \left. - 2C(r)^2 F(r) (rF'(r) + F(r)) + C(r)^3 (2 - \kappa r^2(\rho - p)) \right]. \end{aligned} \quad (6.69)$$

These are equivalent to Eqs. (5.7) and (5.8) in Ref. [108]. To avoid confusion, we use ρ and ν to denote energy density and metric function, respectively, and m is still used as the mass function. (In Ref. [108] the authors use m and ρ to denote energy density and metric function, respectively.)

Choosing the energy density to be constant $\rho = \rho_0$, then from Eq. (6.8), we obtain

$$p(r) = -\rho_0 + p_0 e^{-\nu(r)/2}. \quad (6.70)$$

Here $p_0 = \rho_0 \sqrt{1 - 2GM/R}$ (with $M = m(R)$) to satisfy $p(R) = 0$.

The equations above are still evaluated in terms of r . Since we want to integrate these equations in terms of the tortoise radius r_* , we define

$$r_* = \int \frac{dr}{F(r)}. \quad (6.71)$$

Then Eqs. (6.68) and (6.69) become differential equations for $r(r_*)$ and $\nu(r_*)$, respectively,

$$\begin{aligned} 0 &= -\frac{1}{8r(r_*)^2} [2 \{\alpha\nu''(r_*) - 2r(r_*)\nu'(r_*)r'(r_*)\} \\ &\quad + 4r(r_*)r''(r_*) + 2\kappa r(r_*)^2 p_0 e^{\nu(r_*)/2} - \alpha[\nu'(r_*)]^2], \end{aligned} \quad (6.72)$$

$$\begin{aligned} 0 &= \frac{1}{4r(r_*)^2} [-\alpha\nu''(r_*) - 2(r(r_*)r''(r_*) + [r'(r_*)]^2) \\ &\quad + e^{\nu(r_*)}[2 - \kappa r(r_*)^2(2\rho_0 - p_0 e^{-\nu(r_*)/2})]]. \end{aligned} \quad (6.73)$$

If Eq. (6.72) is subtracted by Eq. (6.73), the result is a quadratic equation for $\eta'(r_*)$. Its roots correspond to the negative and positive branch. Because, in this subsection, we focus only on the negative branch we choose one of the two roots, i.e.,

$$\nu'(r_*) = -\frac{2}{\alpha} \left(r(r_*)r'(r_*) - \sqrt{Y} \right), \quad (6.74)$$

with

$$Y = r(r_*)^2 \left(\alpha\kappa p_0 e^{\frac{\nu(r_*)}{2}} + r'(r_*)^2 - \alpha\kappa\rho_0 e^{\nu(r_*)} \right) + \alpha (e^{\nu(r_*)} - r'(r_*)^2). \quad (6.75)$$

This form becomes the standard TOV equation in the limit $\alpha \rightarrow 0$. This choice then give

us $\nu''(r_*)$, which implies

$$\begin{aligned} r''(r_*) &= \frac{1}{4(\alpha - r(r_*)^2)r'(r_*)} \left[\kappa r(r_*)^2 e^{\frac{\nu(r_*)}{2}} \left(2\rho_0 e^{\frac{\nu(r_*)}{2}} - p_0 \right) \right. \\ &\quad \times \left(2\sqrt{Y} - \alpha\nu'(r_*) \right) - \left(2\sqrt{Y} - \alpha\nu'(r_*) \right) 2e^{\nu(r_*)} \\ &\quad \left. + 4r(r_*)r'(r_*) \left(\alpha\kappa p_0 e^{\frac{\nu(r_*)}{2}} + r'(r_*)^2 - \alpha\kappa\rho_0 e^{\nu(r_*)} \right) \right]. \end{aligned} \quad (6.76)$$

This came from adding Eq. (6.72) and Eq. (6.73).

Thus, we have $\nu(r_*)$ as a first order ordinary differential equation (ODE) while $r(r_*)$ is a second order ODE. These ODEs have parameters: M , $R_* = r_*(R)$, ρ_0 , and two coupling constants: α and κ . Because we do the backward integration, the initial conditions at $r_* = R_*$ are as follows:

$$R_* = R + 2GM \ln(R/2GM - 1), \quad (6.77)$$

$$\nu(R_*) = \ln(\sqrt{1 - 2GM/R}), \quad (6.78)$$

$$r(R_*) = R, \quad (6.79)$$

$$r'(R_*) = 1 - 2GM/R. \quad (6.80)$$

We follow the recipe in Ref. [108] to fix the three input parameters R , M , and ρ_0 : (1) fix M first, then (2) fix R such that $R > 2GM$, lastly (3) explore the values of ρ_0 .

For every ρ_0 value, we have different value of shooting parameter $k = 2GM/R$, with $0 < k < 1$. k is carefully chosen so that at the center the slope of $p(r_*)$ is not steep ($|p'(r_* \rightarrow -\infty)| < \infty$). These steps are done due to the following reason. When we integrate the equation in the opposite direction (forward integration), we can get the same curves as the TOV equation in the limit of zero α . This can be done if $|p'(r_*)| < \infty$ because by doing so, the pressure does not increase or decrease too rapidly. Second, in the TOV GR system, $p'(r = 0) \sim 0$ so the negative branch, for sufficiently small α , should also has this property. We assume that r_* is linear to r in the region near $r = 0$ so that $p'(r_* = 0) \sim 0$, which implies $|p'(r \rightarrow 0)| < \infty$. [Of course, this assumption is generally not true, as was shown in Ref. [108]. But, this assumption is true in the case of regular geometry discussed in Ref. [108]. See subsection 6.5.3 for more details.]

Now we calculate the ODEs by backward integration and recalculate using forward integration. The results from comparing these two schemes are shown in Fig. 6.6. We see that the results from forward integration and backward integration are the same. Indeed in the limit of $r_* \rightarrow -\infty$, the pressure does not go to the Planck scale for the macroscopic size of R .

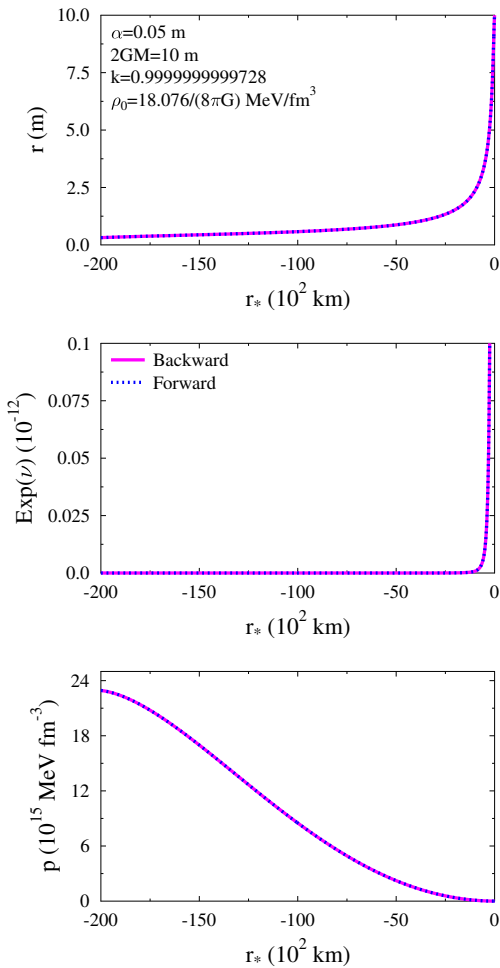


Figure 6.6: Here are the backward and forward integration results on the negative branch. Here $k = 2GM/R$ is the shooting parameter which is chosen so that $p'(r_* = 0) \sim 0$. $\text{Exp}(\nu)$ goes really close to zero but never reach zero as $r_* \rightarrow -\infty$.

6.5.2 Forward and backward integration solutions from positive branch

Carballo-Rubio, in Ref. [5], had shown that the positive branch has exact solutions. These solutions behaves very similar to a mixture of gravastars and black stars. While energy density is still positive valued

$$\rho(r) = \frac{1 + \mathcal{O}(l_p^2/r^2)}{8\pi Gr^2 R^2} \left[R^2 + r^2 e^{\frac{(\lambda+1)(r^2-R^2)}{l_p^2}} \right], \quad (6.81)$$

with $\lambda > 1$ a constant, the pressure is negative

$$p = \frac{-1 + \mathcal{O}(l_p^2/r^2)}{8\pi Gr^2 R^2} \left[R^2 - r^2 e^{\frac{(\lambda+1)(r^2-R^2)}{l_p^2}} \right]. \quad (6.82)$$

Moreover, they satisfy weak, dominant, and null energy conditions, while violating the strong energy condition. This last condition is assumed unnecessary since it is violated by the Casimir energy phenomenon.

The important trick to derive Eqs. (6.82)-(6.81) is the introduction of $\lambda > 1$, which is a constant and defined as

$$\lambda \equiv \sqrt{1 + \frac{l_p^2}{r^2} \frac{2Gm}{r} \frac{(1 + 4\pi r^3 p/m)}{(1 - 2Gm/r)}}. \quad (6.83)$$

This constant implies a fixed form of EoS and mass profile

$$\rho = -p + \frac{l_p^2}{(\lambda+1)r} p', \quad (6.84)$$

$$m = \frac{r^3 (-8\pi G l_p^2 p + \lambda^2 - 1)}{2G (l_p^2 + (\lambda^2 - 1) r^2)}. \quad (6.85)$$

Since $p(r=R)=0$, we have the compactness

$$2C = \frac{2GM}{R} = \frac{1}{(l_p^2/[R^2(\lambda^2-1)]+1)}, \quad (6.86)$$

with $M = m(R)$. The solution for the metric function is

$$\nu(r) = \nu(R) + \frac{(\lambda+1)(R^2-r^2)}{l_p^2}, \quad (6.87)$$

with $\nu(R) = \ln(1 - 2GM/R + \mathcal{O}(l_p^2/R^2))$. Arbitrary compactness can be reach since it

depends on λ . The system is also stable by curvature and boundary conditions arguments.

To reproduce the analytic solutions by numerical schemes, we need the equation for the pressure. After some algebra, we obtain

$$p'(r) = g(r) + p(r)h(r), \quad (6.88)$$

$$g(r) = \frac{(\lambda + 1)^2 (l_p^4 + (\lambda - 2)l_p^2 r^2 - (\lambda^2 - 1)r^4)}{4\pi G l_p^2 r (l_p^2 - (\lambda + 1)r^2) (l_p^2 + (\lambda^2 - 1)r^2)}, \quad (6.89)$$

$$h(r) = \frac{2(\lambda + 1)r ((2\lambda + 1)l_p^4 + (\lambda^3 + \lambda^2 - 2\lambda - 2)l_p^2 r^2 - (\lambda - 1)(\lambda + 1)^2 r^4)}{l_p^2 (l_p^2 - (\lambda + 1)r^2) (l_p^2 + (\lambda^2 - 1)r^2)}. \quad (6.90)$$

We integrate this equation by backward integration starting from $r = R$ and $p(R) = 0$. Since this is a first-order ODE, R is related to M . Hence, unlike in the previous subsection, there is no shooting parameter k . Notice that $g(r)$ has singularity at $r = 0$, so we expect uncontrolled behavior of p near $r = 0$. Then, from the result of backward integration, we numerically integrate it again by forward integration.

The result from backward integration is shown in top panel of Fig. 6.7. It is clear that it violates $|p'(r \rightarrow 0)| < \infty$ as $r \rightarrow 0$. The numerical result from backward integration perfectly fits the analytic solution Eq. (6.82)

Then, for the forward integration, we tried to use the smallest possible $r = r_c \sim 0$ as the initial position and its corresponding $p(r_c)$ from the data from backward integration. The resulting curve is shown in the middle panel, while the comparison in Log plot is in the bottom panel. The results from backward and forward integration are different. The real and imaginary words in the legends denote the real and imaginary part of $\log(p/p_c)$. The pressure p/p_c from forward integration suddenly goes to zero at $r = r_f$ much earlier than R from the backward integration. It is easily seen using the Log plot since when $p/p_c < 0$, $\log(p/p_c) \in \mathbb{C}$. In Fig. 6.7, we obtain that $r_f \sim 5$ m while $R = 10$ km. We do not know how to remedy this yet.

6.5.3 Comparison of our numerical results with the density for regular geometry part of Ho-Matsu model

In this subsection, we discuss the validity of our numerical calculation by comparing the result of section 6.1.3 in Ref. [108] called “density for regular geometry”. We numerically calculate them using backward and forward integrations to check the consistency of the numerical calculation from both our equations and the equations in Ref. [108] restricted only in the interior of the star, which means that the geometry is regular for $0 \leq r \leq R$, and pressure is both finite and positive valued. As a disclaimer, we do not investigate

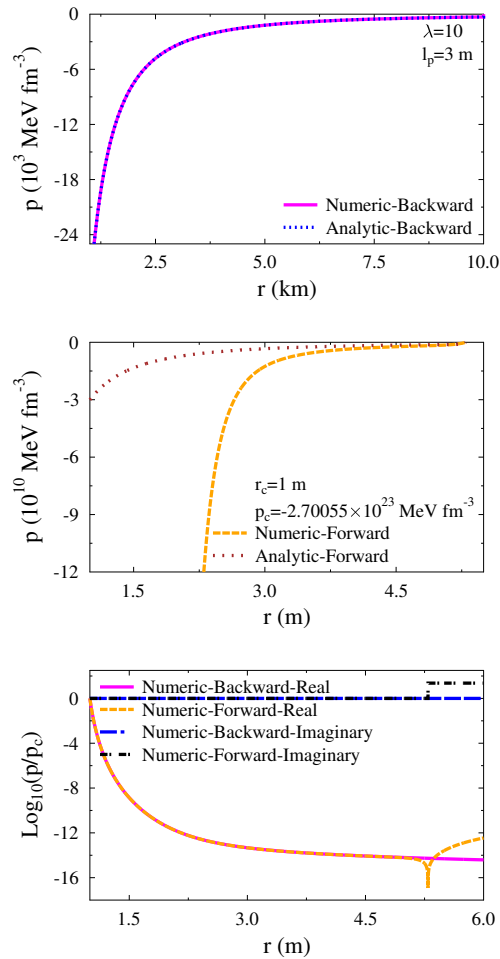


Figure 6.7: These are the profiles of pressure in the positive branch from backward integration (top panel), forward integration (middle panel), and the comparison between them (bottom panel). We calculate first by backward integration, then the result is used for forward integration. In the most bottom panel, we show the real and imaginary part of $\log(p/p_c)$ since, for the forward integration, $p/p_c = 0$ at $r = r_f \sim 5 \text{ m}$ is much smaller than $R = 10 \text{ km}$. It is easier to see since $\log(p/p_c) \in \mathbb{C}$ when $p/p_c < 0$.

the cases of too small density and too large density from the Ho-Matsu model. This is because in the cases of too small density and too large density, $r_*(r)$ is not a bijective map, i.e., when r is increased, r_* is not monotonically increasing.

We had reproduced some relatively similar plots compared with Fig. 14 and Fig. 15 of Ref. [108]. These are shown in Fig. 6.6. The trend of the plots satisfies the condition discussed in section 6.1.3 of Ref. [108]. However, we are unable to reproduce exactly the quantitative result as shown in Fig. 14 and Fig. 15 of Ref. [108], because the authors of Ref. [108] did not specify the units they are using. We only guess the initial data until we obtain similar behavior for both $r(r_*)$ and $\nu(r_*)$, i.e., both R and ρ_0 are suitably chosen (with $2GM$ fixed) such that $p(r_*)$ decreases monotonically as r_* increases. It turns out that this method gives us r that is increasing monotonically as r_* increases. This aspect is similar to the ones in Ref. [108], so in principle, we can replace r with r_* and vice versa. All functions of r_* in Fig. 6.6 are shown as functions of r in Fig. 6.8. There, the numerical calculation result by integrating the equations (6.74)-(6.76) from center to surface are shown. We compare it with the usual TOV equation in GR. Note that p becomes very steep as r goes to zero since r , as a function of r_* , drops really quick in that area (r near zero). Also, note that m_c (mass near the center) is both large in magnitude and negative valued. We suspect that this negative and large magnitude m_c may be the reason why the compactness can be very close to the black hole limit ($2GM/R = 1$). However, this value is outside the range from our lower and upper bound ($m_{c,min}$ and $m_{c,max}$ from Eq. (6.62) and Eq. (6.58)), which is $-10^{-3}M_\odot \lesssim m_c \lesssim -10^{-7}M_\odot$. Therefore, it seems that our analytical estimation for the upper and lower bound of negative m_c may not be justified for constant energy density EoS.

We also observe that the system should have very large density ρ_0 and central pressure p_c to obtain large compactness. We estimate that, in our units, $\rho_0 \sim 10^{12} \text{ MeV fm}^{-3}$, which is about nine orders of magnitude larger than the bag constants B that we used in the previous section. From Fig. 6.8, notice that $p_c \sim 10^{16} \text{ MeV fm}^{-3}$, which is larger than the energy density. If we input ρ_0 and p_c around this estimation, but now with $m_c = 0$, into our equations (6.18)-(6.29) and integrate them from $r = \alpha l_p$ to $r = R$, then the compactness is less than when $m_c < 0$. It is shown in Fig. 6.9, where the compactness is slightly above the Buchdahl limit (BL) $2GM/R = 8/9$. Note that r_* is also monotonically increasing as r increases.

From our previous results, we hypothesize that a very high uniform density and central pressure can give us a star with compactness beyond BL. To test this, we vary w , B , and p_c and calculate similar profiles as Fig. 6.9. The results are compiled in Table 6.1. The variations are blue-colored, and if the resulting compactness violates BL, it is red-colored. We vary w , p_c , and B in the top, middle, and bottom three rows, respectively. We can see

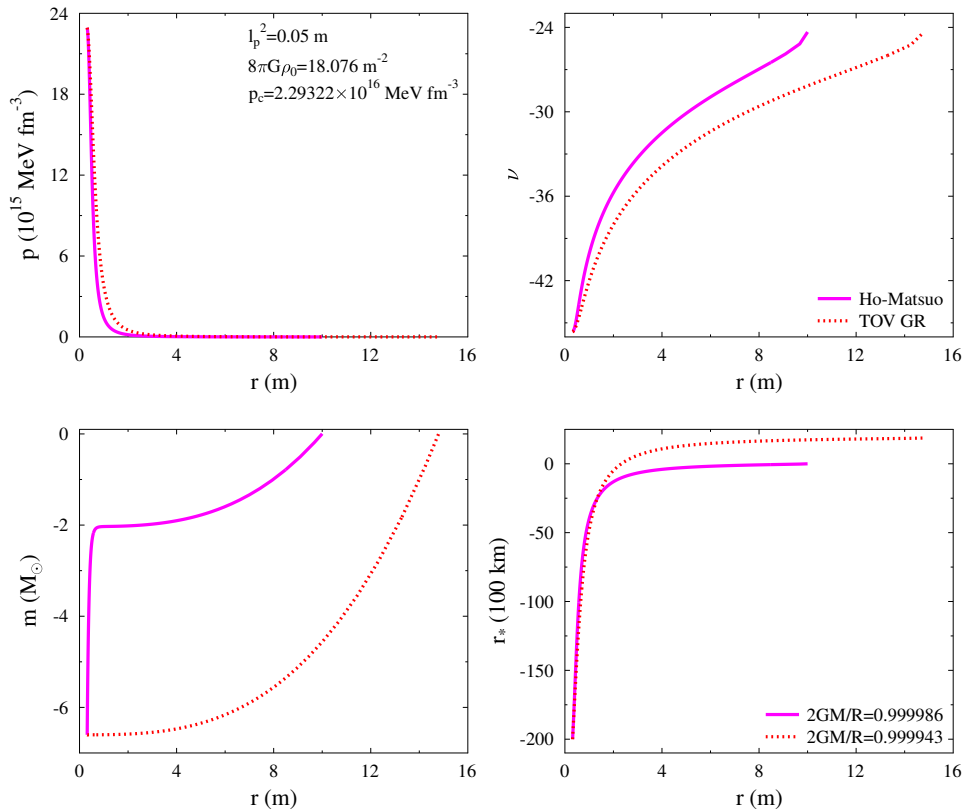


Figure 6.8: In these plots, the dashed line is from the TOV GR system, but the solid line is the same as in Fig. 6.6. Both results are integrated from center to surface. Because in SCGrav system r is restricted to $r > l_p$, p then will never go to infinity. But in TOV GR, r can be arbitrarily close to zero, so p will eventually go to infinity. Notice also that the mass at the center (m_c) is negative.

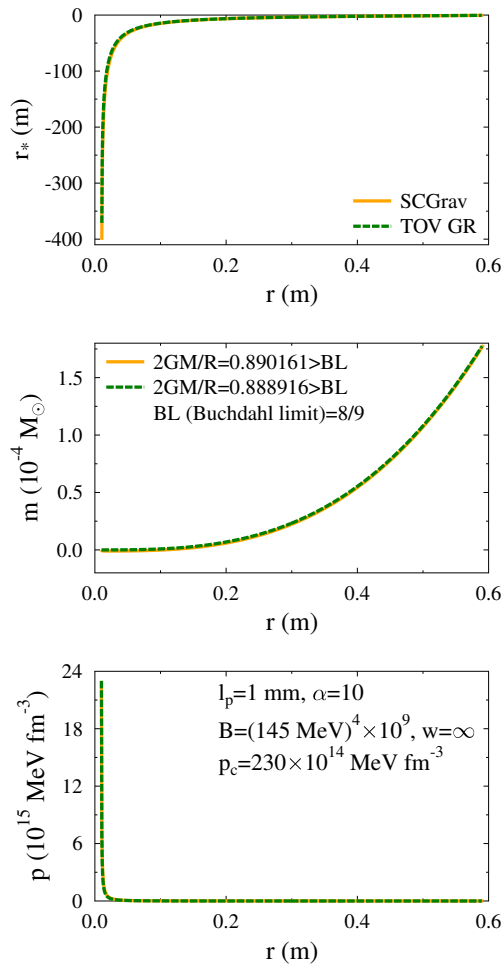


Figure 6.9: Here we use linear EoS with $1/w = 0$, $B \sim 10^{12} \text{ MeV fm}^{-3}$, and $p_c \sim 10^{16} \text{ MeV fm}^{-3}$ and $m_c = 0$. The compactness is less than black hole limit, unlike Fig. 6.8, although slightly larger than Buchdahl limit (BL).

that if w increases, then the compactness is increased. To obtain compactness over BL, however, B and p_c should be increased up to at least eight and thirteen orders of magnitude larger, respectively, than B and p_c in the upper three rows. [The entries with bold fonts are from Fig. 6.9.] We compare the resulting compactness from SCGrav with the result from TOV GR and find that the compactness is quite close to SCGrav. Of course, the results from TOV GR will have infinite pressure as $r \rightarrow 0$, if the compactness violates the Buchdahl limit. This is not the case for the SCGrav model since r is restricted to $r > l_p > 0$.

Table 6.1: Here we show the effect from variations of w , B , and p_c , with $m_c = 0$, into compactness in our semiclassical model (SCGrav) using constant density EoS. The resulting compactness is compared to the TOV GR system counterparts.

$l_p(\text{m})$	α	$p_c(\text{MeV fm}^{-3})$	w	$B(\text{MeV}^4)$	$2GM/R(\text{SCGrav})$	$2GM/R(\text{TOV GR})$
0.001	10	230	1/3	$(145)^4$	0.531671 < BL	0.528683 < BL
0.001	10	230	1	$(145)^4$	0.662569 < BL	0.658682 < BL
0.001	10	230	∞	$(145)^4$	0.754262 < BL	0.74993 < BL
0.001	10	230×10^{12}	∞	$(145)^4 \times 10^9$	0.888742 < BL	0.888769 < BL
0.001	10	230×10^{13}	∞	$(145)^4 \times 10^9$	0.888961 > BL	0.888902 > BL
0.001	10	230×10^{14}	∞	$(145)^4 \times 10^9$	0.890161 > BL	0.888916 > BL
0.001	10	230×10^{14}	∞	$(145)^4 \times 10^8$	0.889297 > BL	0.888892 > BL
0.001	10	230×10^{14}	∞	$(145)^4 \times 10^7$	0.889019 > BL	0.888889 = BL
0.001	10	230×10^{14}	∞	$(145)^4 \times 10^6$	0.88893 > BL	0.888889 = BL

6.6 Conclusions

In this first part of our work, we investigate SCGrav proposed by Carballo-Rubio in Ref. [5]. Characterized by the positive-negative sign in p' , the model has two different sets of equations. This happened because the EFE for metric solution ν' ((6.11)) has two roots and p' is related to ν' by Eq. (6.8). Each is called the negative branch and the positive branch. The positive branch and the negative branch, respectively, were discussed by [5] and by Ref. [108]. Here, we further investigate the negative branch by employing linear EoS $\rho = p/w + \rho_0$ with $w = 1/3$ and $w = 1$, respectively.

Here, we find that the choice of r_c affects the range of l_p . The reason is as follows. Because $m'(r)$ is a lot more complicated than the usual TOV equation (see Eqs.(6.18)-(6.29)), $m'(r)$ has terms that can make $m'(r) < 0$, which may imply negative $m(r \gg r_c)$ if at the center $m(r_c) = m_c \sim 0$. Both l_p and r_c affect these terms in $m'(r)$, because $m'(r_c)$ is singular when $l_p = r_c$.

To analyze $m'(r)$ around $l_p = r_c$, we fix $r_c = \alpha l_p$ with $\alpha \neq 1$. We also demand $m'(r) > 0$ for $0 < r < R$ because it is usual to expect the increase of mass as r increases,

at least in TOV GR case. We found, with some approximations, that $0 < \alpha < \sqrt{2/3}$. This result demands a restricted set of EoS because the speed of sound squared $w = dP/d\rho$ should satisfy $w < 2/9$. This implies less compactness GM/R than the results from $w = 1/3$ and $w = 1$. Thus, we are not discussing the case of $w < 2/9$. For the case of $\sqrt{2/3} \leq \alpha < 1$, this implies either $p_c < 0$ or $\rho_c < 0$. This contradicts our nonnegative pressure and energy density. For the case of $\alpha > 1$, we can use any EoS. Hence, our results, which demands $\alpha > 0$, does agree with Ref. [108], i.e., their integration breaks down at region $r \leq l_p$.

The parameter l_p has an upper bound dependent on the central pressure p_c . By doing some approximations, we found that $l_p < 10$ km from the dimensional analysis. This upper bound is in the same order of magnitude as the radius of known NSs. This upper bound also us $N < 10^{79}$, which implies that l_p can be huge compared to the Planck length.

Using variations of w , B , α , and l_p , our numerical results show that the M-R relations are indistinguishable if compared to TOV GR. Thus, the parameter l_p has no significant effect compared to TOV GR, even though l_p is not in the limit $l_p \rightarrow L_{\text{Pl}}$.

The compactness can reach the ultra-compact range if we adjust both w and B suitably. But, this can also be achieved in TOV GR. Moreover, the Buchdahl limit could be violated using constant energy density (or $w = \infty$), according to the authors in Ref. [108]. Yet, to overcome the Buchdhal limit, it requires two ingredients. First, both the central pressure p_c and the energy density ρ , which should be constant, require very large values. This makes the compactness overcome the Buchdhal limit just a little bit. Second, the central mass m_c should be negative. This makes the compactness much higher. However, the first criterion is unphysical, yet the second criterion is a possible solution for TOV GR. The lower bound m_c now becomes unclear. As far as we know, no study had considered calculating the TOV equation from the center to the surface using negative m_c . We left determining the range of m_c into future research.

In conclusion, the solutions from the modified TOV equation from the negative branch of SCGrav are no different than the solutions of the TOV equation from GR. Instead, new physics may come from its positive branch, which preliminary results are already shown by Carballo-Rubio himself in Ref. [5].

This page intentionally left blank

CHAPTER 7

MOMENT OF INERTIA AND TIDAL DEFORMATION IN EDDINGTON-INSPIRED BORN INFELD THEORY OF GRAVITY

In this chapter, we present the second part of our work. The following passage is from our paper [114].

7.1 Introduction

In this section, we explain the reasons why we investigate the predictions for NS properties using the EiBI gravity theory.

The Eddington-inspired Born-Infeld (EiBI) gravity is an interesting theory because of its features compared to those of General Relativity (GR) [28, 29, 30, 31, 115, 32, 116, 117, 118]. The EiBI theory, proposed by Banados and Ferreira [29], is a combination of Palatini formalism and a gravitational version of the Born-Infeld electrodynamic theory. The reviews of the EiBI gravity and its applications can be found in Refs. [119, 120]. From the astrophysical point of view, the EiBI gravity is interesting because it can increase the maximum mass of a nonrotating compact object by increasing its nonlinearity parameter κ [33, 121, 122]. The other parameter in EiBI gravity, λ , corresponds to the cosmological constant Λ_c by $\lambda = \kappa\Lambda_c + 1$. People usually set $\lambda = 1$ in most cases. However, the problem with $\lambda = 1$ is that the radius also increases when the mass increases, and vice versa.

We need to note that, in the case of $\lambda = 1$, the moment of inertia of a type of compact star, whose matter is described by FPS EoS, was discussed in Ref. [31]. Furthermore, the authors of Ref. [31] showed that, if $\kappa > 0$, there always exists regular solution for compact stars and the corresponding maximum compactness is $GM/R \sim 0.3$, which is quite independent from κ . Also, there exists the collapse constraint, i.e., if the requirement $\kappa\Delta < 0$ is satisfied, with Δ is given as

$$\Delta = (p_c\kappa - 3\kappa\rho_c - 4)(1 + \kappa\rho_c) - \kappa(1 - \kappa p_c)(p_c + \rho_c)\frac{d\rho(p_c)}{dp_c},$$

then the compact stars exist. Here, p_c and ρ_c are, respectively, the star's central pressure and central density. This expression means that if the EoS obeys the thermodynamic relation, which implies $\rho = \rho(p)$, then the onset region of the star's stability in EiBI theory depends only on P_c and κ .

Concerned with the star's stability in EiBI theory with $\lambda = 1$, the authors of Ref. [123] showed that the standard results of stellar stability in GR also hold in EiBI, only up to the fundamental mode frequency. This means that for a sequence of stars with the same EoS, the fundamental mode ω^2 passes through zero at central density, whose value corresponds to the maximum-mass configuration. For higher-order, though, they depend on κ . This in turn implies that the stellar models with central densities less than the corresponding critical points are stable.

For the case of $\kappa < 0$, the EiBI theory shows singularities in the EoS and the Ricci scalar from the physical metric associated with the phase transition matter [124]. This happens because the discontinuity in energy density appears around the transition region. Furthermore, authors in Refs. [125, 127, 128, 129] had discussed the appearance of curvature singularities at the surface of compact stars with polytropic EoS in EiBI theory. However, as far as we know, there is no discussion regarding tidal deformation within EiBI theory in the literature up to now, except for Ref. [126] which uses apparent formulation to calculate the tidal deformation equations and they set $\lambda = 1$. Concerned with some recent NS observational results, we think that comparing the NS in EiBI theory with the recent NS constraints [57, 58, 82, 83, 84, 85] has not yet been done.

We also expect that setting λ away from unity might increase (or decrease) the maximum mass while also decreasing (or increasing) its radius. Thus, it can achieve relatively larger compactness, given suitable values of κ and λ . Since the cosmological constant Λ_c is related to λ by $\lambda = \kappa\Lambda_c + 1$, therefore, in the next sections, we investigate the role of κ and Λ_c to the mass, the radius, the moment of inertia, and the tidal deformation of NS in EiBI theory in more detail. Moreover, we relate our results with the question of the tension between nuclear physics and the prediction of NS properties. Specifically, we discuss the possibility of whether the second object with mass $2.6M_\odot$ in the GW190814 event is static or slowly rotating NS. Here we use a quite recent G3 RMF parameter set from Ref. [34]. The representations of the EoS will also include contributions from hyperons and restriction to the speed of sound at high densities. The reason is discussed in Section 5.2.

The main reason why we use EiBI theory is that it has a nice property that the exterior solution (for a spherically symmetric system without an electric nor magnetic source) is the same as general relativity (GR). This in turn makes the cosmological constant in EiBI the same as the one in GR. This is crucial to simplifying the calculations to obtain the equations of motions and their boundary conditions for both the moment of inertia and tidal deformation.

7.2 The Eddington-inspired Born-Infeld Theory of Gravity

Here, we review the EiBI theory and discuss the calculations of its moment of inertia and the tidal deformation. We start by reviewing the equations following Refs. [32, 33]. The EiBI theory has the following equations of motions:

$$q^{\mu\nu} = \tau (\lambda g^{\mu\nu} - 8\pi G\kappa T^{\mu\nu}(\mathbf{g})), \quad (7.1)$$

$$q_{\mu\nu} = g_{\mu\nu} + \kappa R_{\mu\nu}(\mathbf{q}), \quad (7.2)$$

where $\tau = \sqrt{g}/\sqrt{q}$, $q = -\det(q_{\mu\nu})$, $g = -\det(g_{\mu\nu})$. It is common to use $\tau = \sqrt{\det(g_{\sigma\nu})\det(q^{\mu\sigma})} = [\det(\lambda\delta_\nu^\mu - 8\pi G\kappa T_\nu^\mu)]^{-1/2}$, because $1/q = \det(q^{\mu\nu})$. The constants λ and κ are the parameters of EiBI. Note that these are different from functions $\bar{\lambda}(r)$ and $\tilde{\kappa}(r)$ which we shall define later. Also note that κ has dimension (length)² and λ is dimensionless. The cosmological constant Λ_c is related to λ by this relation:

$$\lambda = \kappa\Lambda_c + 1. \quad (7.3)$$

The arguments in $R_{\mu\nu}$ and $T^{\mu\nu}$ are different since to raise or lower the tensor indices, each tensor uses a different metric. The apparent metric $q_{\mu\nu}$ is used by $R_{\mu\nu}$ while the physical metric $g_{\mu\nu}$ is used by $T_{\mu\nu}$. Those two equations of motions above came from the EiBI action

$$S = \frac{1}{8\pi G\kappa} \int_{(\mathcal{M}, \mathbf{g})} d^4x \left[\sqrt{-\det(g_{\mu\nu} + \kappa R_{\mu\nu}(\Gamma))} - \lambda \sqrt{-\det(g_{\mu\nu})} \right], \quad (7.4)$$

where Palatini formalism has been used to the Ricci tensor $R_{\mu\nu}$. The formalism means that the Ricci tensor is dependent on a connection $\Gamma_{\beta\gamma}^\alpha(\mathbf{q})$, but this connection is dependent on the apparent metric, i.e.,

$$\Gamma_{\beta\gamma}^\alpha = \frac{1}{2} q^{\alpha\sigma} (\partial_\gamma q_{\beta\sigma} + \partial_\beta q_{\gamma\sigma} - \partial_\sigma q_{\beta\gamma}). \quad (7.5)$$

One can rearrange these equation into the form similar to the usual Einstein field equation (EFE), which became

$$R_\nu^\mu(\mathbf{q}) - \frac{1}{2} R_\sigma^\sigma \delta_\nu^\mu(\mathbf{q}) = 8\pi G T_{\text{eff}\,\nu}^\mu(\mathbf{g}), \quad (7.6)$$

$$T_{\text{eff}\,\nu}^\mu(\mathbf{g}) = \tau T_\nu^\mu(\mathbf{g}) - \left[\frac{\tau T_\sigma^\sigma(\mathbf{g})}{2} + \frac{1 - \tau\lambda}{8\pi G\kappa} \right] \delta_\nu^\mu. \quad (7.7)$$

From knowing this and for brevity, we will write the Ricci tensor $R_{\mu\nu}$ dan the stress tensor $T_{\mu\nu}$ without their arguments.

7.2.1 Vacuum solution

Since we will discuss the effect of nonzero cosmological constant Λ_c to the compact stars in EiBI theory, the vacuum solution (without electric nor magnetic charge) needs to be mentioned. This will be crucial for our metric ansatz in the presence of an ideal isotropic fluid so that we can obtain suitable equations of motion and their boundary conditions. Suppose that we use static and spherically symmetric metric on both metrics

$$\mathbf{q} = q_{\mu\nu}dx^\mu dx^\nu = -C^2(r)dt^2 + D^2(r)dr^2 + r^2[d\theta^2 + \sin^2\theta d\varphi^2], \quad (7.8)$$

$$\mathbf{g} = g_{\mu\nu}dx^\mu dx^\nu = -A^2(r)dt^2 + B^2(r)dr^2 + F^2(r)[d\theta^2 + \sin^2\theta d\varphi^2], \quad (7.9)$$

given no matter present $T_\nu^\mu = 0$. From Eq. (7.1) we have these metric relations

$$F^2 = r^2/\lambda, \quad (7.10)$$

$$A^2 = C^2/\lambda, \quad (7.11)$$

$$B^2 = D^2/\lambda. \quad (7.12)$$

Substituting these into Eq. (7.2), then we can obtain

$$C'' = \frac{DC - D^3C + rCD' + rDC' + r^2D'C'}{r^2D}, \quad (7.13)$$

$$\frac{C'}{C} = -\frac{1}{r} + \left(\frac{1}{r} - \frac{r}{\kappa} + \frac{r}{\kappa\lambda}\right)D^2 + \frac{D'}{D}, \quad (7.14)$$

$$\frac{D'}{D} = \frac{1}{2r} + \left(-\frac{1}{2r} + \frac{r}{2\kappa} - \frac{r}{2\kappa\lambda}\right)D^2, \quad (7.15)$$

where $f' = df/dr$. The solutions from these equations are

$$C^2 = D^{-2} = 1 - \frac{2GM}{r} - \frac{\Lambda_c r^2}{3\lambda}. \quad (7.16)$$

We can see that the apparent metric in the presence of no matter indicates a de-Sitter space with an “apparent” cosmological constant Λ_c/λ .

7.2.2 Moment of Inertia

Now, to calculate the moment of inertia, we follow the Hartle-Thorne method. We start by setting the apparent and physical metric in these forms:

$$\begin{aligned} q = q_{\mu\nu} dx^\mu dx^\nu &= -e^{\beta(r)} dt^2 + e^{\alpha(r)} dr^2 + r^2 [d\theta^2 + \sin^2 \theta (d\varphi - \omega(r)dt)^2] \\ &\quad + \mathcal{O}(\Omega^2), \end{aligned} \quad (7.17)$$

$$\begin{aligned} g = g_{\mu\nu} dx^\mu dx^\nu &= -e^{\nu(r)} dt^2 + e^{\bar{\lambda}(r)} dr^2 + d(r) [d\theta^2 + \sin^2 \theta (d\varphi - v(r)dt)^2] \\ &\quad + \mathcal{O}(\Omega^2). \end{aligned} \quad (7.18)$$

The apparent metric follows the Hartle-Thorne metric [130] and its generalization is used in the physical metric. Both describe a spherically symmetric massive body with radius R with apparent (physical, resp.) angular velocity ω (v) goes to Ω (Ω_{phy}) as $r \rightarrow R$. Here we use slow rotating approximation, i.e., if Ω_k is defined as Kepler angular velocity, which is the mass-shedding limit of any massive star, it is assumed that $\Omega/\Omega_k \ll 1$ and $\Omega_{\text{phy}}/\Omega_k \ll 1$. From the vacuum solution, we see that the physical metric has its 2-sphere with radius $\sqrt{d(r)}$, which coincides with r at the exterior region $r \geq R$.

The massive body is modeled by an ideal fluid with isotropic pressure

$$T_\nu^\mu = [\epsilon + p] u^\mu u_\nu + p \delta_\nu^\mu, \quad (7.19)$$

$$u^t = [-(g_{tt} + 2\Omega_{\text{phy}} g_{t\varphi} + \Omega_{\text{phy}}^2 g_{\varphi\varphi})]^{-1/2}, \quad (7.20)$$

$$u^\varphi = \Omega_{\text{phy}} u^t, \quad u^r = u^\theta = 0. \quad (7.21)$$

The explicit expression of the components of the physical stress tensor are

$$T_t^t = -\epsilon, \quad T_r^r = T_\theta^\theta = T_\varphi^\varphi = p, \quad (7.22)$$

$$T_\varphi^\varphi = (\epsilon + p)(\Omega_{\text{phy}} - v)e^{-\nu} d \sin^2 \theta, \quad (7.23)$$

$$T_t^\varphi = -(\epsilon + p)\Omega_{\text{phy}}. \quad (7.24)$$

These are obtained after neglecting $\mathcal{O}(\Omega_{\text{phy}})$. From these, then τ is

$$\tau = 1/(ab^3), \quad (7.25)$$

$$a = \sqrt{\lambda + 8\pi G\kappa\epsilon}, \quad (7.26)$$

$$b = \sqrt{\lambda - 8\pi G\kappa p}. \quad (7.27)$$

From Eq. (7.1), we have these relations

$$e^\nu = e^\beta a/b^3, \quad e^{\bar{\lambda}} = e^\alpha/(ab), \quad d = r^2/(ab). \quad (7.28)$$

Now, we assume that the effective stress tensor also has similar form as the physical stress tensor, but to differentiate with the previous stress tensor, we add additional subscript “eff”. Their nonzero components are

$$T_{\text{eff } t}^t = -\epsilon_{\text{eff}}, \quad (7.29)$$

$$T_{\text{eff } r}^r = p_{\text{eff}} = T_{\text{eff } \theta}^\theta = T_{\text{eff } \varphi}^\varphi, \quad (7.30)$$

$$T_{\text{eff } \varphi}^t = (\epsilon_{\text{eff}} + p_{\text{eff}})(\Omega - \omega)e^{-\beta(r)}r^2 \sin^2 \theta. \quad (7.31)$$

Then we obtain these relations from the equations above, $T_{\text{eff } \varphi}^t = T_\varphi^t/ab^3$, and $T_{\text{eff } t}^t = T_t^t/abc^2$:

$$\epsilon_{\text{eff}} = \frac{a^2 - 3b^2 + 2ab^3}{16\pi G\kappa ab^3}, \quad (7.32)$$

$$p_{\text{eff}} = \frac{a^2 + b^2 - 2ab^3}{16\pi G\kappa ab^3}, \quad (7.33)$$

$$(\Omega - \omega) = (\Omega_{\text{phy}} - v)\frac{b^2}{a^2}, \quad (7.34)$$

$$\Omega = \Omega_{\text{phy}}. \quad (7.35)$$

The last equation is in agreement with the boundary condition, i.e., $(\Omega - \omega) \sim (\Omega_{\text{phy}} - v)$ as $r \rightarrow R$.

The nonzero components of the Ricci tensor $R_{\mu\nu}(\mathbf{q})$ can be obtained straightforwardly. If we define the mass $m(r)$ inside one of the metric function by

$$e^{-\alpha} = 1 - \frac{2Gm(r)}{r} - \frac{\Lambda_c r^2}{3\lambda}, \quad (7.36)$$

then with some algebraic calculations one can obtain

$$m'(r) = \frac{r^2}{4G\kappa} \left(\frac{2}{\lambda} - \frac{3}{ab} + \frac{a}{b^3} \right), \quad (7.37)$$

$$\beta'(r) = -2p'(r) \left[2\pi G\kappa \left(\frac{3}{b^2} + \frac{1}{a^2} \frac{d\epsilon}{dp} \right) + \frac{1}{\epsilon + p} \right], \quad (7.38)$$

$$\begin{aligned} p'(r) &= -\frac{1}{4\pi G\kappa} \left[\frac{r}{2\kappa} \left(\frac{1}{ab} + \frac{a}{b^3} - 2 \right) + \frac{2Gm}{r^2} + \frac{\Lambda_c r}{3\lambda} \right] \\ &\times \left(\frac{4}{a^2 - b^2} + \frac{3}{b^2} + \frac{1}{a^2} \frac{d\epsilon}{dp} \right)^{-1} \left(1 - \frac{2Gm(r)}{r} - \frac{\Lambda_c r^2}{3\lambda} \right)^{-1}. \end{aligned} \quad (7.39)$$

Eqs. (7.37) and (7.38) are from tt and rr components of the EFE, respectively. Eq. (7.39) came from the Bianchi identity $\nabla_\mu T_{\text{eff } r}^\mu = 0$. The boundary conditions are $m(0) = 0$, $m(R) = M$, $p(R) = 0$, $\beta(R) = \ln(1 - 2GM/R - \Lambda_c R^2/(3\lambda))$. One can see that the equation of motions are invariant to $\beta \rightarrow \beta + k$ (k a constant), so we can obtain the

correct $\beta(r)$ from arbitrary starting value of $\beta(0) = \beta_{0,\text{old}}$. After running the code, we obtain $\beta_R = \beta(R)$. This can be used to obtain the correct initial value $\beta(0) = \beta_{0,\text{new}}$ by

$$\beta_{0,\text{new}} = \beta_{0,\text{old}} - [\beta_R - \ln(1 - 2GM/R - \Lambda_c R^2/(3\lambda))]. \quad (7.40)$$

Then by running the program again, the correct profile of $\beta(r)$ will be obtained.

To obtain the moment of inertia, we need the equation of motion for ω . It is in principle can be derived from the $t\varphi$ component of the EFE. We use the following formula [130]

$$R_\varphi^t = \frac{1}{\sqrt{-\det(q_{\alpha\beta})}} \partial_\mu \left(\sqrt{-\det(q_{\alpha\beta})} \Gamma_{\nu\varphi}^\mu q^{t\nu} \right), \quad (7.41)$$

to calculate the geometry part. From Eq. (7.41) and ignoring $\mathcal{O}(\omega^2)$ terms, one obtains this component explicitly:

$$R_\varphi^t = -\frac{e^{-(\beta+\alpha)/2}}{2r^2 \sin \theta} \partial_r (e^{-(\beta+\alpha)/2} r^4 \sin^3 \theta \partial_r \omega). \quad (7.42)$$

From before, we have $T_{\text{eff}\varphi}^t = (\epsilon_{\text{eff}} + p_{\text{eff}})(\Omega - \omega)e^{-\beta(r)}r^2 \sin^2 \theta$. Defining $\tilde{\omega} = (\Omega - \omega)/\Omega$, then $R_\varphi^t/(8\pi G) = T_{\text{eff}\varphi}^t$ becomes

$$\partial_r (e^{-(\beta+\alpha)/2} r^4 \partial_r \tilde{\omega}) = 16\pi G r^4 (\epsilon_{\text{eff}} + p_{\text{eff}}) e^{(\alpha-\beta)/2} \tilde{\omega}. \quad (7.43)$$

The boundary condition to calculate moment of inertia I is as follows. The right hand side in the equation above will vanish in the exterior region $r \geq R$, thus

$$\tilde{\omega}(r \geq R) = 1 - \frac{2GI}{r^3}, \quad (7.44)$$

Then by rearranging Eq. (7.43), one arrives at

$$\tilde{\omega}'(r) = \frac{6e^{\beta/2}}{r^4(1 - 2Gm/r - \Lambda_c r^2/(3\lambda))^{1/2}} \tilde{\kappa}, \quad (7.45)$$

$$\tilde{\kappa}'(r) = \frac{8\pi G r^4}{3} \frac{(\epsilon_{\text{eff}} + p_{\text{eff}}) e^{-\beta/2}}{(1 - 2Gm/r - \Lambda_c r^2/(3\lambda))^{1/2}} \tilde{\omega}, \quad (7.46)$$

This form is neat because the boundary conditions are $\tilde{\omega}(R) = 1 - 2GI/R^3$, $\tilde{\kappa}(R) = GI$. Since the boundary condition at the center is unknown, let us pay attention that Eqs. (7.45) and (7.46) are invariant from $\tilde{\omega}(r) \rightarrow \zeta \tilde{\omega}(r)$ and $\tilde{\kappa}(r) \rightarrow \zeta \tilde{\kappa}(r)$. Suppose that we run the code from initial values $\tilde{\omega}(0) = \tilde{\omega}_0$ and $\tilde{\kappa}(0) = \tilde{\kappa}_0$. Then the result can be written as $\tilde{\omega}(R) = (1 - 2GI/R^3)/\zeta$ and $\tilde{\kappa}(R) = GI/\zeta$, with ζ a constant. To satisfy the boundary conditions, we rename the previous initial values by a new ones, i.e., $\tilde{\omega}(0) = \tilde{\omega}_0 \zeta$ and

$\tilde{\kappa}(0) = \tilde{\kappa}_0 \zeta$ with

$$\zeta = \frac{1}{\tilde{\omega}(R) + 2\tilde{\kappa}(R)/R^3}. \quad (7.47)$$

since we already obtain the moment of inertia I from $\tilde{\kappa}(R)$ by $I = \tilde{\kappa}(R)\zeta/G$, recalculating from these new initial values is unnecessary, although to confirm that, one can check it by running the code again. Now, following the logic in Refs. [31, 30], from the boundary conditions, then we have $v(R) = \omega(R) = 2I\Omega/R^2$. Thus, I is the physical moment of inertia.

Here, we briefly describe the numerical procedure for the moment of inertia I as follows. We use a *FORTRAN77* code with Runge-Kutta 4th order algorithm. First, we calculate all $p'(r)$, $m'(r)$ and $\nu'(r)$ (Eqs. (7.37)-(7.39)). We run the code from the center $r = r_c \sim 0$ up to $r = R$ where the pressure become zero $p(R) = 0$. The initial data at the center are $p(r_c) = p_c$, $m(r_c) = 0$ and $\beta(r_c) = 0$. At this point, we obtain R , $m(R) = M$ and $\beta(R) = \beta_R$. Since in general, $\beta(R) \neq \ln(1 - 2GM/R - \Lambda_c R^2/(3\lambda))$, we recalculate the equations $p'(r)$, $m'(r)$ and $\nu'(r)$ by replacing the initial value $\beta(r_c) = \beta_{0,\text{new}}$ using Eq. (7.40). Second, we calculate all $p'(r)$, $m'(r)$, $\nu'(r)$, $\tilde{\omega}'(r)$ and $\tilde{\kappa}'(r)$ from $r = r_c$ to $r = R$. From inputs $p(r_c) = p_c$, $m(r_c) = 0$, $\beta(r_c) = \beta(r_c)_\text{new}$ and $\tilde{\omega}(r_c) = \tilde{\kappa}(r_c) = 0$, we obtain $\tilde{\omega}(R)$ and $\tilde{\kappa}(R)$. The moment of inertia I is then calculated by $I = \tilde{\kappa}(R)\zeta/G$ with ζ from Eq. (7.47).

7.2.3 Tidal Deformation

Here we describe the theory of tidal perturbation, only the electric type, in the EiBI gravity. We follow the method illustrated in Refs. [132, 133]. We start with the Regge-Wheeler metric [131]. The perturbed metrics are

$$g_{\mu\nu} = \eta_{\mu\nu} + h_{\mu\nu}, \quad (7.48)$$

$$q_{\mu\nu} = \zeta_{\mu\nu} + f_{\mu\nu}, \quad (7.49)$$

with

$$h_{\mu\nu} = \begin{pmatrix} -H_0 e^\nu & H_1 & 0 & 0 \\ H_1 & H_2 e^{\bar{\lambda}} & 0 & 0 \\ 0 & 0 & K r^2 & 0 \\ 0 & 0 & 0 & K r^2 \sin^2 \theta \end{pmatrix} Y_{lm}(\theta, \phi), \quad (7.50)$$

$$f_{\mu\nu} = \begin{pmatrix} -F_0 e^\nu & F_1 & 0 & 0 \\ F_1 & F_2 e^{\bar{\lambda}} & 0 & 0 \\ 0 & 0 & \bar{G} r^2 & 0 \\ 0 & 0 & 0 & \bar{G} r^2 \sin^2 \theta \end{pmatrix} Y_{lm}(\theta, \phi), \quad (7.51)$$

while the unperturbed part is

$$\eta_{\mu\nu} dx^\mu dx^\nu = -e^{\nu(r)} dt^2 + e^{\bar{\lambda}(r)} dr^2 + d(r) d\Omega^2, \quad (7.52)$$

$$\zeta_{\mu\nu} dx^\mu dx^\nu = -e^{\beta(r)} dt^2 + e^{\alpha(r)} dr^2 + r^2 d\Omega^2, \quad (7.53)$$

with $d\Omega^2$ is the surface element of a 2-sphere. Here, H_0 , H_1 , H_2 , K , F_0 , F_1 , F_2 , and \bar{G} are functions of r .

7.2.3.1 The vacuum case

To determine the Love number, which is calculated at region far from the star, we investigate the vacuum case first ($T_\nu^\mu = 0$). From Eq. (7.1), one obtains

$$d = r^2/\lambda, \quad e^\nu = e^\beta/\lambda, \quad e^{\bar{\lambda}} = e^\alpha/\lambda, \quad (7.54)$$

$$H_0 = -H_2 = H, \quad F_0 = -F_2 = F, \quad (7.55)$$

$$H = F, \quad K = \bar{G}/\lambda. \quad (7.56)$$

From evaluating Eq. (7.2) order by order through some algebra, one can obtain the following equations:

$$e^\beta = e^{-\alpha} = 1 - \frac{2GM}{r} - \frac{\Lambda_c r^2}{3\lambda}, \quad (7.57)$$

$$F_1 \propto e^{(\alpha-\beta)/2}, \quad (7.58)$$

$$H_1 = F_1 \left(\frac{1}{\lambda} - \frac{l(l+1)\kappa}{2r^2} \right), \quad (7.59)$$

$$\begin{aligned} F'' + 2e^\alpha \left(\frac{1}{r} - \frac{\Lambda_c r}{\lambda} \right) F' - 2 \left(\frac{1}{r^2} - e^\alpha \frac{\Lambda_c}{\lambda} \right) F + e^\alpha \frac{(l-1)(l+2)}{r^2} G \\ = 0. \end{aligned} \quad (7.60)$$

Then after more algebraic manipulations, the last line above becomes

$$F'' + \left[\frac{1}{r} + e^\alpha \left(\frac{1}{r} - \frac{\Lambda_c r}{\lambda} \right) \right] F' - \left[e^a \left(\frac{l(l+1)}{r^2} + \frac{2\Lambda_c}{\lambda} \right) + \beta'^2 \right] F = 0. \quad (7.61)$$

Now we come to the tricky part. To calculate the tidal deformation, the calculation is done at $r \rightarrow \infty$, which is not satisfied by de Sitter space-time. To remedy this shortcoming, we assume that $|\Lambda_c|$ is sufficiently small such that $|G^2 M^2 \Lambda_c / \lambda| < 1$ hence F can be expressed as

$$F(x) = \sum_{i=0}^{\infty} F_i(x) \varepsilon^i, \quad \varepsilon = \frac{G^2 M^2 \Lambda_c}{\lambda}, \quad x = \frac{r}{GM} - 1. \quad (7.62)$$

We assume that the series converges rapidly, so consider the terms only up to the first order:

$$F(x) = F_0(x) + \varepsilon F_1(x). \quad (7.63)$$

From $\Lambda_c = 0$ we have the usual solution is known to have the form including the associated Legendre polynomial of the second kind Q_l^2 and the first kind P_l^2 :

$$F_0(x) = C_{1,l} Q_l^2(x) + C_{2,l} P_l^2(x). \quad (7.64)$$

The constants $C_{1,l}$ and $C_{2,l}$ will be determined later. Substitute this into Eq. (7.61) we obtain the equations fo F_1 :

$$(1-x^2) \left(\frac{d^2 F_1(x)}{dx^2} + D(x) \right) - 2x \frac{dF_1(x)}{dx} + \left(l(l+1) - \frac{4}{1-x^2} \right) F_1(x) = 0, \quad (7.65)$$

with

$$D(x) = -\frac{1}{3} \left(\frac{x+1}{x-1} \right)^2 \left[2(x-2) \frac{dF_0(x)}{dx} + \left(l(l+1) - \frac{6x^2 - 20x + 22}{1-x^2} \right) F_0(x) \right]. \quad (7.66)$$

The next step is we solve this (with $l = 2, 3, 4$) case by case. In general, we obtain that the solution has the following form:

$$F_1(x) = C_{3,l} Q_l^2(x) + C_{4,l} P_l^2(x) + C_{2,l} S_l^2(x) + C_{1,l} T_l^2(x) \quad (7.67)$$

with

$$S_l^2(x) = \frac{f_{1,l}(x)}{x^2 - 1} + (x^2 - 1)f_{2,l}(x), \quad (7.68)$$

$$\begin{aligned} T_l^2(x) &= \frac{f_{3,l}(x)}{(x+1)(x-1)^2} + \frac{f_{4,l}(x)}{x+1} \ln(x-1) \\ &\quad + f_{5,l}(x) \left(\frac{x+1}{x-1} \right) \ln(x+1) + (x^2 - 1)f_{6,l}(x). \end{aligned} \quad (7.69)$$

For $l = 2$, we have

$$f_{1,2} = \frac{8x^6}{7} + 6x^5 - \frac{x^4}{7} - \frac{59x^3}{4} - \frac{46x^2}{7} + \frac{21x}{4} + 1, \quad (7.70)$$

$$f_{2,2} = \frac{3}{56}(113 \log(x-1) + 15 \log(x+1)), \quad (7.71)$$

$$f_{3,2} = -\frac{8x^6}{7} + \frac{389x^5}{56} + \frac{2057x^4}{168} - \frac{1987x^3}{84} - \frac{1469x^2}{84} + \frac{1357x}{56} + \frac{235}{56}, \quad (7.72)$$

$$f_{4,2} = -\frac{4x^5}{7} - \frac{25x^4}{7} - \frac{17x^3}{14} + \frac{171x^2}{14} + \frac{153x}{14} - \frac{25}{14}, \quad (7.73)$$

$$f_{5,2} = \frac{4x^4}{7} + \frac{13x^3}{7} - \frac{93x^2}{14} + \frac{34x}{7} - \frac{25}{14}, \quad (7.74)$$

$$f_{6,2} = \frac{1}{7}(-24) \left(2\text{Li}_2\left(\frac{1-x}{2}\right) + \ln\left(\frac{x+1}{4}\right) \ln(x-1) \right). \quad (7.75)$$

For $l = 3$, we have

$$f_{1,3} = \frac{20x^7}{3} + 40x^6 - \frac{20x^5}{7} - \frac{375x^4}{4} - \frac{220x^3}{7} + \frac{185x^2}{4} + 20x, \quad (7.76)$$

$$f_{2,3} = \frac{25}{56}x(127 \log(x-1) + \log(x+1)), \quad (7.77)$$

$$\begin{aligned} f_{3,3} &= -\frac{20x^7}{3} + \frac{8195x^6}{168} + \frac{5225x^5}{72} - \frac{35845x^4}{252} - \frac{9977x^3}{84} + \frac{7305x^2}{56} \\ &\quad + \frac{8941x}{168} - 32, \end{aligned} \quad (7.78)$$

$$f_{4,3} = -\frac{10x^6}{3} - \frac{70x^5}{3} - \frac{925x^4}{42} + \frac{3425x^3}{42} + \frac{195x^2}{2} - \frac{845x}{42} - \frac{635}{21}, \quad (7.79)$$

$$f_{5,3} = \frac{10x^5}{3} + \frac{40x^4}{3} - \frac{1315x^3}{42} + \frac{20x^2}{7} + \frac{135x}{14} + \frac{5}{21}, \quad (7.80)$$

$$f_{6,3} = \frac{1}{7}(-200)x \left(2\text{Li}_2\left(\frac{1-x}{2}\right) + \ln\left(\frac{x+1}{4}\right) \ln(x-1) \right). \quad (7.81)$$

For $l = 4$, we have

$$\begin{aligned} f_{1,4} &= \frac{595x^8}{22} + 175x^7 - \frac{277315x^6}{4928} - \frac{14305x^5}{32} - \frac{202325x^4}{4928} + \frac{14405x^3}{48} \\ &\quad + \frac{342515x^2}{4928} - \frac{1225x}{32} - \frac{615}{64}, \end{aligned} \quad (7.82)$$

$$f_{2,4} = \frac{25(7x^2 - 1)(7613 \log(x - 1) + 67 \log(x + 1))}{4928}, \quad (7.83)$$

$$\begin{aligned} f_{3,4} &= -\frac{595x^8}{22} + \frac{1159715x^7}{6336} + \frac{14823115x^6}{44352} - \frac{8024815x^5}{14784} - \frac{3123931x^4}{4928} \\ &\quad + \frac{7841513x^3}{14784} + \frac{169207x^2}{448} - \frac{7430627x}{44352} - \frac{2160637}{44352}, \end{aligned} \quad (7.84)$$

$$\begin{aligned} f_{4,4} &= -\frac{595x^7}{44} - \frac{4445x^6}{44} - \frac{38235x^5}{308} + \frac{113875x^4}{308} + \frac{154025x^3}{308} - \frac{42865x^2}{308} \\ &\quad - \frac{6715x}{28} - \frac{3735}{308}, \end{aligned} \quad (7.85)$$

$$\begin{aligned} f_{5,4} &= \frac{595x^6}{44} + \frac{665x^5}{11} - \frac{34285x^4}{308} - \frac{4540x^3}{77} + \frac{30455x^2}{308} + \frac{535x}{77} \\ &\quad - \frac{3735}{308}, \end{aligned} \quad (7.86)$$

$$f_{6,4} = \frac{1}{77}(-1500)(7x^2 - 1) \left(2\text{Li}_2\left(\frac{1-x}{2}\right) + \ln\left(\frac{x+1}{4}\right) \ln(x-1) \right). \quad (7.87)$$

$\text{Li}_n(z)$ is the polylogarithm function.

Next we need to obtain $C_{1,l}$, $C_{2,l}$, $C_{3,l}$, and $C_{4,l}$. It turns out that the general results have the following pattern

$$C_{i,l} = A_{i,l} + \lambda_l B_{i,l}, \quad (i = 1, \dots, 4). \quad (7.88)$$

The constants $A_{n,l}$ and $B_{n,l}$ ($n = 1, \dots, 4$) has the following pattern: $A_{i,l} \propto \mathcal{E}_m(GM)^l$ and $B_{i,l} \propto \mathcal{E}_m(GM)^{-l-1}$ ($i = 1, 2, 3, 4$), where \mathcal{E}_m is related to the static external quadrupolar tidal field, which is produced by an external gravitational potential. If subjected to this gravitational potential, then the star is responding by its own quadrupole moment, which is recorded by λ_l . Then, λ_l is related to the Love number k_l .

To obtain λ_l and getting rid of \mathcal{E}_m , we define $y(R) = RF'(R)/F(R)$ and $C = GM/R$. We substitute

$$F(x) = (C_{1,l} + \varepsilon C_{3,l})Q_l^2(x) + (C_{2,l} + \varepsilon C_{4,l})P_l^2(x) + \varepsilon C_{2,l}S_l^2(x) + \varepsilon C_{1,l}T_l^2(x) \quad (7.89)$$

into y , then through another long calculations, we obtain

$$\lambda_l = -\frac{(A_{1,l} + \varepsilon A_{3,l})Q^*(R) + (A_{2,l} + \varepsilon A_{4,l})P^*(R) + \varepsilon(A_{1,l}T^*(R) + A_{2,l}S^*(R))}{(B_{1,l} + \varepsilon B_{3,l})Q^*(R) + (B_{2,l} + \varepsilon B_{4,l})P^*(R) + \varepsilon(B_{1,l}T^*(R) + B_{2,l}S^*(R))}, \quad (7.90)$$

where

$$Q^*(R) = yQ_l^2(C) + C[dQ_l^2(C)/dC], \quad (7.91)$$

$$P^*(R) = yP_l^2(C) + C[dP_l^2(C)/dC], \quad (7.92)$$

$$T^*(R) = yT_l^2(C) + C[dT_l^2(C)/dC], \quad (7.93)$$

$$S^*(R) = yS_l^2(C) + C[dS_l^2(C)/dC]. \quad (7.94)$$

Then, we can obtain the Love number by this relation:

$$k_l = \frac{(2l-1)!!}{2R^{2l+1}} \lambda_l. \quad (7.95)$$

Notice that since $\lambda_l \propto a_{i,l}/b_{i,l} \propto (GM)^{2l+1}$, then $\lambda_l R^{-2l-1} \propto C^{2l+1}$, which then allows us to we redefine k_l with

$$k_l = -\frac{(2l-1)!!}{2} \frac{(a_{1,l} + \varepsilon a_{3,l})Q^*(R) + (a_{2,l} + \varepsilon a_{4,l})P^*(R) + \varepsilon(a_{1,l}T^*(R) + a_{2,l}S^*(R))}{(b_{1,l} + \varepsilon b_{3,l})Q^*(R) + (b_{2,l} + \varepsilon b_{4,l})P^*(R) + \varepsilon(b_{1,l}T^*(R) + b_{2,l}S^*(R))}, \quad (7.96)$$

with $a_{i,l}$ and $b_{i,l}$ as functions of C . Note that the reason we use Eq. (7.96) is because this form is more easy to write in the *FORTRAN77* code than Eq. (7.90). In their explicit form, the constants are shown below:

$$a_{1,2} = 0, \quad b_{1,2} = \frac{15}{8} \frac{1}{C^3}, \quad (7.97)$$

$$a_{2,2} = \frac{1}{3}C^2, \quad b_{2,2} = 0, \quad (7.98)$$

$$a_{3,2} = \frac{113}{84}C^2, \quad b_{3,2} = \frac{1787}{392} \frac{1}{C^3}, \quad (7.99)$$

$$a_{4,2} = \frac{13}{9}C^2, \quad b_{4,2} = -\left(\frac{5\pi^2}{7} + \frac{3305}{448} + \frac{15\ln^2(2)}{7}\right) \frac{1}{C^3}, \quad (7.100)$$

$$a_{1,3} = 0, \quad b_{1,3} = \frac{35}{8} \frac{1}{C^4}, \quad (7.101)$$

$$a_{2,3} = \frac{1}{45} C^3, \quad b_{2,3} = 0, \quad (7.102)$$

$$a_{3,3} = \frac{127}{756} C^3, \quad b_{3,3} = \frac{24805}{1512} \frac{1}{C^4}, \quad (7.103)$$

$$a_{4,3} = \frac{158}{945} C^3, \quad b_{4,3} = - \left(\frac{25\pi^2}{9} + \frac{13795}{576} + \frac{25 \ln^2(2)}{3} \right) \frac{1}{C^4}, \quad (7.104)$$

$$a_{1,4} = 0, \quad b_{1,4} = \frac{735}{64} \frac{1}{C^5}, \quad (7.105)$$

$$a_{2,4} = \frac{1}{630} C^4, \quad b_{2,4} = 0, \quad (7.106)$$

$$a_{3,4} = \frac{7613}{465696} C^4, \quad b_{3,4} = \frac{469685}{5808} \frac{1}{C^5}, \quad (7.107)$$

$$a_{4,4} = \frac{200077}{10866240} C^4, \quad b_{4,4} = - \left(\frac{875\pi^2}{88} + \frac{14680085}{202752} + \frac{2625 \ln^2(2)}{88} \right) \frac{1}{C^5}. \quad (7.108)$$

7.2.3.2 The Non-vacuum case

One can see that to obtain the Love number, Eq. (7.96) needs $y(R)$, $M = m(R)$, and $r = R$ as input. So we need the equations of $y(r)$ in the interior. The metric is still the same but now we use ideal fluid in the stress tensor, rather than the empty space. We define the perturbed stress tensor as follows

$$T_\nu^\mu = T_0^\mu{}_\nu + \delta T_\nu^\mu, \quad (7.109)$$

with $T_0^\mu{}_\nu$ is the usual ideal fluid and

$$\delta T_\nu^\mu = \text{diag} \left(-\frac{d\epsilon}{dp}, 1, 1, 1 \right) \delta p Y_{lm}(\theta, \phi). \quad (7.110)$$

Then, from Eq. 7.1, we obtain the relations between the metric functions:

$$d = r^2/(ab), \quad e^\nu = e^\beta a/b^3, \quad e^\lambda = e^\alpha/(ab), \quad (7.111)$$

$$H_0 = H, \quad H_2 = -Ha^2/b^2, \quad F_0 = -F_2 = F. \quad (7.112)$$

One can evaluate Eq. (7.2) order by order and use mathematical identities of the

spherical harmonics $Y_{lm}(\theta, \phi)$, which gives the following equations:

$$H = \frac{16\pi G\kappa\delta p}{b^2 - a^2}, \quad (7.113)$$

$$K = \frac{\bar{G}}{ab} + \frac{4\pi G\kappa}{ab} \left(\frac{1}{b^2} - \frac{1}{a^2} \frac{d\epsilon}{dp} \right) \delta p, \quad (7.114)$$

$$F = 4\pi G\kappa \left(\frac{4}{b^2 - a^2} - \frac{3}{b^2} - \frac{1}{a^2} \frac{d\epsilon}{dp} \right) \delta p \quad (7.115)$$

Eliminating δp , we have

$$H = \frac{4}{a^2 - b^2} \left(\frac{4}{a^2 - b^2} + \frac{3}{b^2} + \frac{1}{a^2} \frac{d\epsilon}{dp} \right)^{-1} F, \quad (7.116)$$

$$F_1 = C_0 e^{(\alpha-\beta)/2}, \quad (7.117)$$

$$H_1 = F_1 \left(\frac{a}{b^3} - \frac{l(l+1)\kappa}{2r^2} \right). \quad (7.118)$$

Lastly, after lots of calculations, we have

$$\begin{aligned} F'' &+ e^\alpha \left(\frac{2}{r} + \frac{r}{2\kappa} \left(-4 + \frac{a}{b^3} + \frac{3}{ab} \right) \right) F' - \left(\frac{2}{r^2} - \frac{e^\alpha}{\kappa} \left(2 - \frac{3a}{b^3} + \frac{1}{ab} \right) \right) F \\ &+ e^\alpha \left(\frac{(l-1)(l+2)}{r^2} - \frac{2}{ab\kappa} \right) \bar{G} + K \left(\frac{2e^\alpha}{\kappa} \right) = 0. \end{aligned} \quad (7.119)$$

After some more algebraic manipulation, this becomes

$$F'' + f(r)F' + g(r)F = 0, \quad (7.120)$$

with

$$f(r) = \frac{re^{\alpha(r)}}{\kappa} \left(\frac{1}{ab} - 1 \right) + \frac{e^{\alpha(r)}}{r} + \frac{1}{r}, \quad (7.121)$$

$$\begin{aligned} g(r) &= \frac{2e^\alpha}{\kappa} \frac{a}{b^3} \left(2 - \frac{4}{(a^2 - b^2)} \left(\frac{4}{a^2 - b^2} + \frac{1}{a^2} \frac{d\epsilon}{dp} + \frac{3}{b^2} \right)^{-1} \right) \\ &- \left(\frac{l(l+1)e^\alpha}{r^2} + \frac{2e^\alpha}{\kappa} + \beta'(r)^2 \right). \end{aligned} \quad (7.122)$$

Defining $y(r) = rF'(r)/F(r)$, we thus obtain the first order equation

$$y'(r) = -f(r)y(r) - rg(r) - \frac{y(r)^2}{r} + \frac{y(r)}{r}. \quad (7.123)$$

The boundary condition is $y(0) = l$. Since $|k_4| \ll |k_3| \ll |k_2|$, it is also a usual practice

to only evaluate k_2 (using Eq. (7.96)) as the so-called dimensionless tidal deformability:

$$\Lambda = \frac{2k_2}{3C^5}, \quad (7.124)$$

with $C = GM/R$.

The numerical scheme for the tidal calculation is as follows. First, we calculate $p'(r)$, $m'(r)$ and $y'(r)$ (resp., Eqs. (7.37), (7.39) and (7.123)) using the Runge-Kutta 4th order algorithm using our *FORTRAN77* code. We run the code from $r = r_c \rightarrow 0$, after inputting the initial values $p(r_c) = p_c$, $m(r_c) = 0$ and $y(r_c) = l$, to $r = R$ where $p(R) = 0$. At this point, we obtain R , $m(R) = M$ and $y(R)$. These three numbers are substituted into Eq. (7.96) to calculate k_l .

7.3 Numerical Results and Discussions

In this section, we show the numerical results by employing the EoS calculated from RMF theory with the G3 parameter set. We include hyperons contribution and the speed of sound constrain in the EoS (denoted by WHSS). This speed of sound constraint is just forcing it to obey $v_s \leq c/\sqrt{3}$ at high densities. This constraint came from QCD. Here, we mainly use WHSS because (1) we suspect that hyperon matter exists in heavy NSs with mass $M \gtrsim 2.0M_\odot$, and (2) the speed of sound constraint stiffens the matter and thus increases the maximum mass. We also sometimes compare the results with those from EoS without hyperon (WoutHSS). Furthermore, to restrict the range of κ and Λ_c , we compare the results with the known observational analysis data.

The role of κ to adjust the mass and radius of NS had been studied in Ref. [33]. However, in this work, we use different EoSs, which are also more refined, and more recent constraints of NS properties are also used. After that, we show the impact of Λ_c on the mass-radius (M-R) relation, the moment of inertia I , and the Love number Λ to see its tidal deformability.

First, we consider the standard case $\Lambda_c = 0$ (or $\lambda = 1$). In Fig. 7.1, we show the M-R relation. The results from G3 WHSS EoS and G3 WoutHSS EoS are presented in panel (a) and panel (b), respectively. From Fig. 7.1, we see that the M and R of NS increase simultaneously if we increase the κ value. This impact is significant independent of the type of EoS used. Observe that the $2.1M_\odot$ mass constraint from PSR J0740+6620 (grey band) can be easily reached by the maximum mass while also still satisfying the radius constraint from NSs with a mass around $1.4M_\odot$ [57, 58]. Observe also that, due to its softer EoS, G3 WHSS EoS needs a larger value of κ to reach $2.6M_\odot$ mass constraint from GW190814 (orange band), which in turn does not satisfy the radius constraint (Refs. [57, 58]).

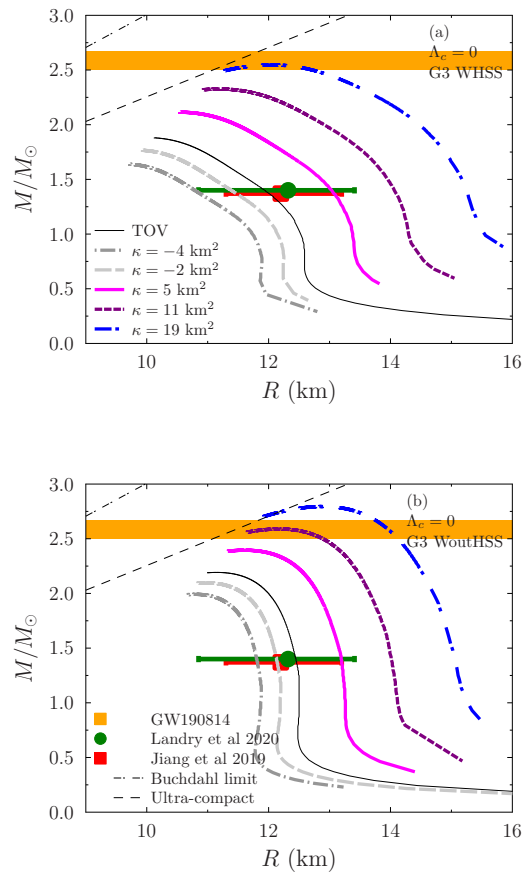


Figure 7.1: From varying κ with $\Lambda_c = 0$, the M-R relation result is shown here. We use G3 EoS with hyperon and sound of speed constraint (WHSS) in panel (a). On the other hand, we use no hyperon but still with the sound of speed constraint (WoutHSS) in panel (b). Observe that by increasing κ , both M and R will increase. We find that κ can have a negative value and the solutions exist if $\kappa > -5 \text{ km}^2$, which is similar to Ref. [33].

We include a realistic case of $\Lambda_c = 2.08 \times 10^{-52} \text{ m}^{-2}$, which came from the observed cosmological constant in Refs. [134, 135, 136, 137]

$$\rho_{\Lambda_c} = \frac{\Lambda_c}{8\pi G} \sim 10^{-8} \frac{\text{erg}}{\text{cm}^3}. \quad (7.125)$$

We use this value as the upper bound for Λ_c in this realistic case. This choice is safe from an unphysical phenomenon due to the following reason. Consider $|\Lambda_c| \geq 10^{-22} \text{ m}^{-2}$, $\lambda = 1$, $M = 1M_\odot$ and $r = 1 \text{ AU}$ in Eq. (7.36), then the term with Λ_c will dominate, hence Newtonian gravity breaks down in the solar system. We can see that the results are almost indistinguishable if compared to the results from $\Lambda_c = 0$, because of the smallness of the observed Λ_c value. In Figs. 7.2-7.4, we vary κ value and show the resulting M-R relation, moment inertia, and tidal deformation. It is evident that our results, when κ is much larger than 5 km^2 , are not in good agreement with observation data from canonical mass NSs ($1.4M_\odot$). Due to our choice of EoS, it is evident that the $2.1M_\odot$ mass constraint can be reached when $\kappa \approx 5 \text{ km}^2$. Hence, we conclude that the NS properties predicted by EiBI theory is compatible with the recent observational constraints from Refs. [57, 58, 73, 7, 82, 83] if we choose a physically save Λ_c value in the range of $0 \leq \Lambda_c \leq 2.08 \times 10^{-52} \text{ m}^{-2}$ and $\kappa \approx 5 \text{ km}^2$. (In fact, this result is valid for $|\Lambda_c| < 10^{-22} \text{ m}^{-2}$, since λ is still very close to unity when $\kappa \sim 10^8 \text{ m}^2$.)

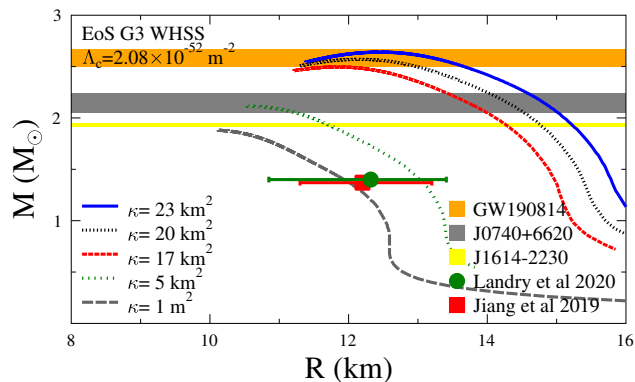


Figure 7.2: Here are the M-R relations from G3 WHSS EoS with κ variations and $\Lambda_c = 2.08 \times 10^{-52} \text{ m}^{-2}$. These are compared to the data from Landry et al 2020 [57], Jiang et al 2019 [58], the pulsar-binary systems (PSRs) J1614-2230 [71, 72, 73], J0740+6620 [73, 7], and the GW190814 data [6].

Looking at this, there is one tempting question for us: is it possible to reach maximum mass around $2.6M_\odot$ while also keeping the results still in agreement with the $1.4M_\odot$ NS radius constraint from observation data? It turns out that we can do this, but with the cost of the unphysical value of Λ_c , i.e., it is negative and its absolute value is much larger than the observed value ($2.08 \times 10^{-22} \text{ m}^{-2}$). Hence, we name this case as an unrealistic case.

The reasons are as follows. Increasing the absolute value of Λ_c shifts the position of

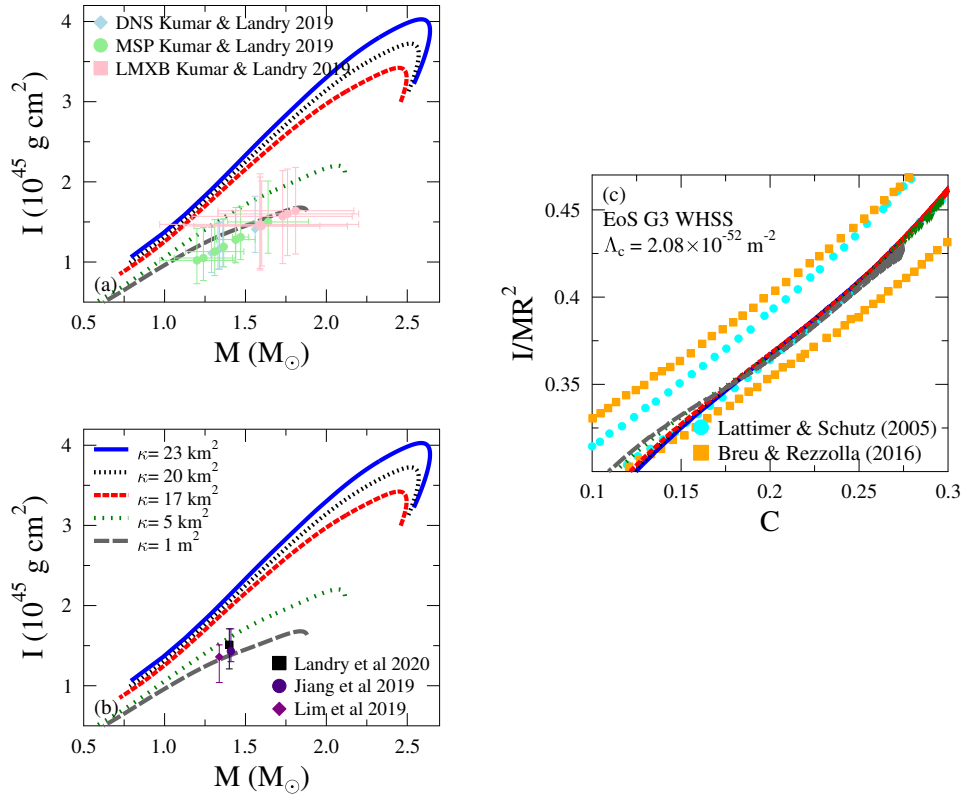


Figure 7.3: These are the moment of inertia I from G3 WHSS EoS with κ variations and $\Lambda_c = 2.08 \times 10^{-52} \text{ m}^{-2}$. In panel (a), we compare them with data from Kumar & Landry 2019 [82], where the specific method used there are labelled as DNS, MSP, and LMXB. In panel (b), we use data from Landry et al 2020 [57], Jiang et al 2019 [58], and Lim et al 2019 [83]. In panel (c), we compare I/MR^2 with the upper and lower bound data from Lattimer & Schutz 2005 [84] and Breu & Rezzolla 2016 [85].

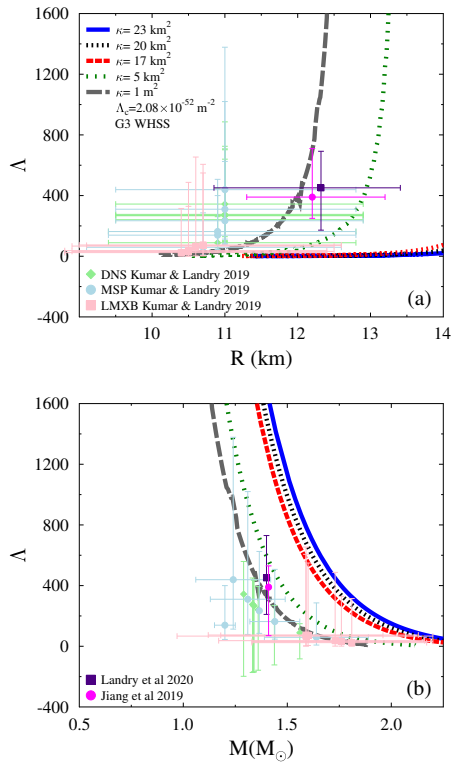


Figure 7.4: These are the calculated Love number Λ from G3 WHSS EoS with κ variations and $\Lambda_c = 2.08 \times 10^{-52} \text{ m}^{-2}$. In panel (a), we compare them with data from Kumar-Landry 2019 [82]. In panel (b), we compare them with data from Landry et al 2020 [57] and Jiang et al 2019 [58].

the 'tail' to the left (right, resp.), when $\Lambda_c < 0$ ($\Lambda_c > 0$). What we mean by the tail is the part of the M-R curve that corresponds to the smaller central pressure and, for the case of $\Lambda_c = 0$, the tail is positioned at the lower right. In Fig. 7.5, the results from variations of Λ_c are shown for the cases of different κ ($\kappa = 1 \text{ m}^2$ and $\kappa = 5 \text{ km}^2$) and different EoSs (WHSS and WoutHSS). It is clear that variations of Λ_c impact the radius greater than from variations of κ , except for the neighborhood of the maximum mass. A positive (negative, resp.) value of Λ_c tends to increase (decrease) the radius.

We compare two different EoSs (G3 WHSS in the upper panels and G3 WoutHSS in the lower panels) in Fig. 7.5. When we increase Λ_c , both R and M increase, and vice-versa. From the plots, we can see that for $\kappa = 1 \text{ m}^2$ and $\kappa = 5 \text{ km}^2$, the range of Λ_c can be constrained with the $2.0M_\odot$ mass constraint and $1.4M_\odot$ mass and radius constraints from observations [57, 58, 71, 72, 73, 7]. The range of Λ_c for $\kappa = 1 \text{ m}^2$ is wider i.e., $-10^{-7} < \Lambda_c/(\text{m}^{-2}) < 10^{-8}$, than that of $\kappa = 5 \text{ km}^2$, i.e., $-10^{-9} \leq \Lambda_c/(\text{m}^{-2}) \leq 10^{-10}$. Then, by increasing κ value and decreasing Λ_c value, it is possible to have a relatively large maximum mass with relatively small radius. However, for the larger the κ value, the narrower the range of Λ_c value becomes.

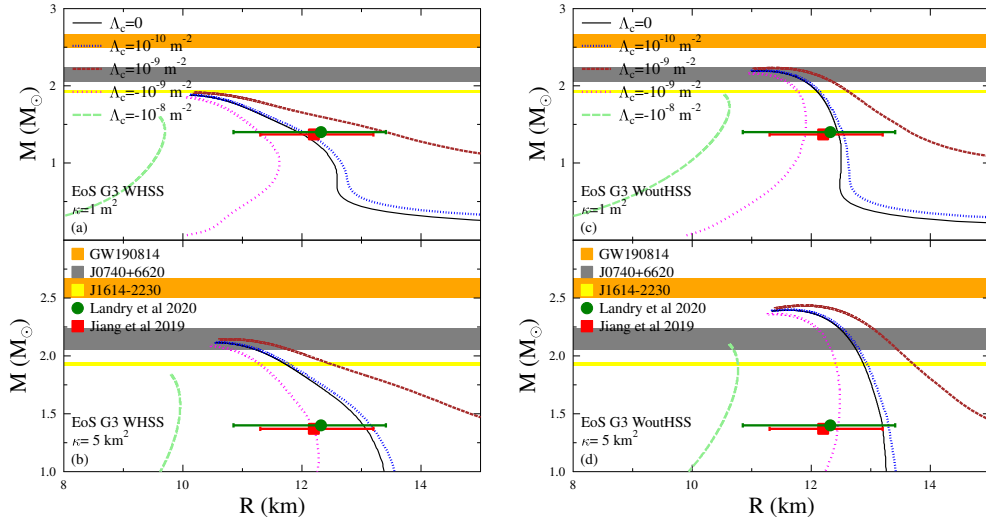


Figure 7.5: Here, we show the M-R relation by variations of Λ_c . We use small κ ($\kappa = 1 \text{ m}^2$) and large κ ($\kappa = 5 \text{ km}^2$), respectively, in panels (a) and (b). They are also from using G3 WHSS EoS. The panels (c) and (d) contain the same thing but differ in the EoS, which is WoutHSS.

Thus, we can obtain the M-R curves that satisfy both the $2.6M_\odot$ mass constraint and the radius constraint for $1.4M_\odot$ NS from observations simultaneously. For G3 WHSS and G3 WoutHSS EoSs, we set $\kappa = 26 \text{ km}^2$ and $\kappa = 13 \text{ km}^2$, respectively, and use an unavoidably large and negative Λ_c . Yet, the range of Λ_c is narrow, i.e., $\Lambda_c = -(2.4 - 3.2) \times 10^{-9} \text{ m}^{-2}$. These results are shown in Fig. 7.6. Note that when $\Lambda_c \geq 0$, both canonical mass radii and maximum mass constraints cannot be satisfied simultaneously.

The results from G3 WHSS EoS yield more significant radius shifting by varying Λ_c than that of G3 WoutHSS EoS because usually, the equations used λ rather than Λ_c .

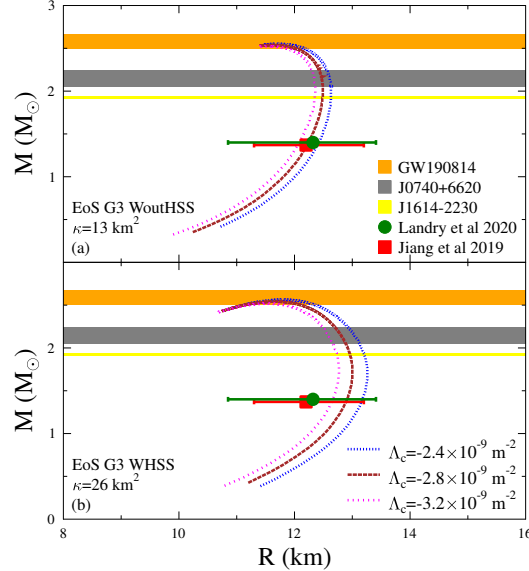


Figure 7.6: These are M-R curves from different EoSs [G3 WoutHSS in panel (a) and WoutHSS in panel (b)]. These curves satisfy both the data from Landry *et al.* and Jiang *et al.* and the mass constraint from the GW190814 data.

We show the sensitivity of κ and Λ_c variations in Fig. 7.7. There, the M-R curves satisfy both the radius constraint for canonical mass NSs from observations [57, 58] and the $2.6M_\odot$ mass constraint from GW190814 [6]. The range of variations of both parameters is narrow. It is evident from the lower panel of Fig. 7.7 that in this region the radius is quite sensitive to Λ_c variation.

For completeness, we show the impact of κ variation on the moment of inertia and the Love number in Figs. 7.8 and 7.9, respectively. We do not show the results from varying Λ_c value because the results are similar to varying κ . We can see that moment of inertia and Love number are not too sensitive with variations of κ and the results are quite compatible with the NS's tidal deformability observations from Refs. [82, 57, 58, 79, 80, 6].

To this end, we must consider the later results very carefully. The $2.6M_\odot$ mass constraint and the canonical NS $R_{1.4M_\odot}$ radius constraint, which is $11 \text{ km} \lesssim R_{1.4M_\odot} \lesssim 13 \text{ km}$, can only be satisfied by EiBI gravity if the cosmological constant satisfies: (1) $\Lambda_c < 0$ and (2) $|\Lambda_c|$ is unphysically large. We know, however, that our universe has a positive and tiny cosmological constant [134, 135, 136, 137]. Therefore, we conclude that the $2.6M_\odot$ object observed in GW190814 event [6] is not likely an NS within the EiBI theory.

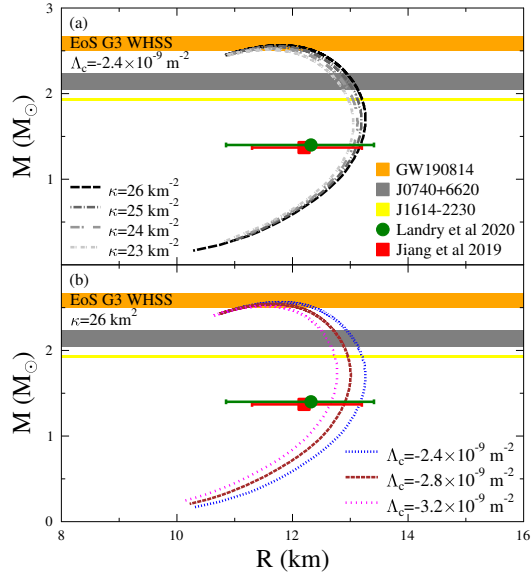


Figure 7.7: These are M-R relations from G3 WHSS with variations of κ in panel (a) and variation of Λ_c in panel (b). These parameters' values are chosen so that they satisfy the data from Landry *et al.* and Jiang *et al.*, while simultaneously maintain their maximum mass at the range provided by the GW190814 data.

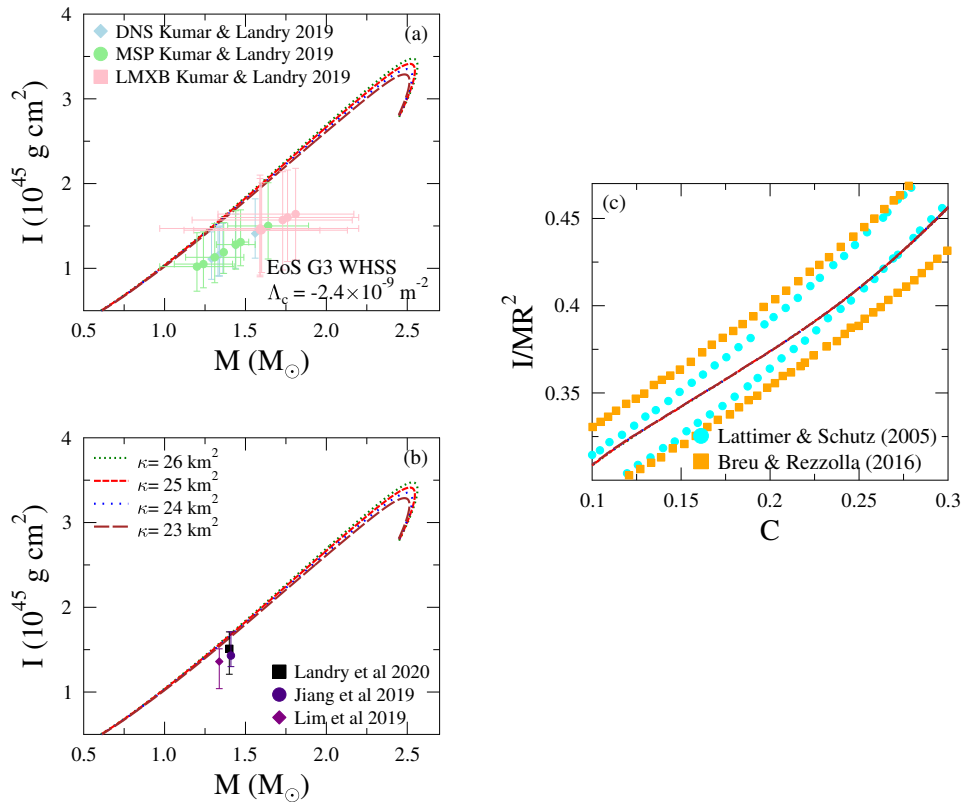


Figure 7.8: Moment of inertia within EiBI obtained from G3 WHSS EoS with variations of κ and very large and negative Λ_c .

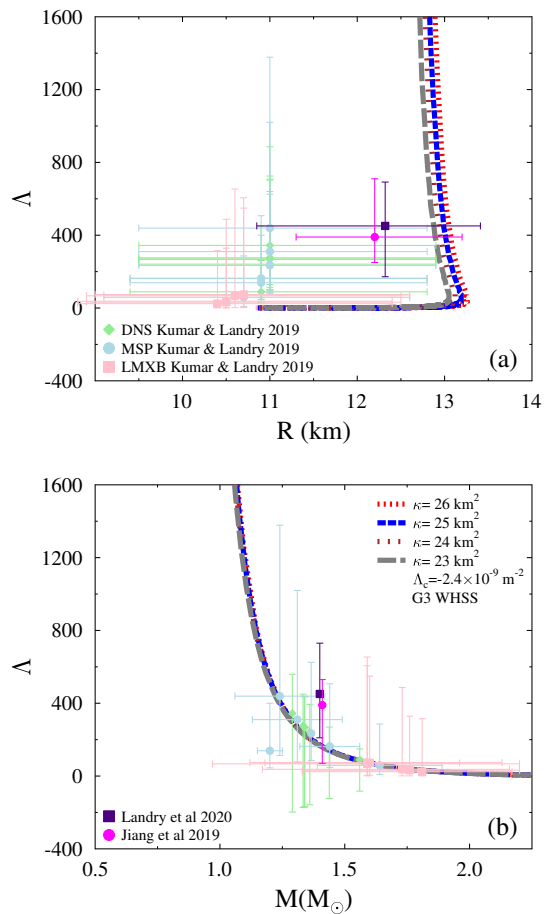


Figure 7.9: The tidal deformation with κ varied and negative with very large value of Λ_c .

7.4 Conclusions

Motivated by the question of whether the $2.6M_{\odot}$ mysterious object observed in the GW190814 event could be an NS or not, here we investigate the role of parameter κ and Λ_c from EiBI gravity on the mass-radius relation, the moment of inertia, and the tidal deformability of an NS. The EoS in the core of NS is calculated using the RMF model using the G3 parameter set [34]. To determine the hyperon coupling constants, we use the SU(3) prescription and the hyperon potential depths [94]. In the inner and outer crusts, we use the EoS from Miyatsu *et al.* [99]. We also employ a constraint on the speed of sound in the NS matter such that to not exceed $c/\sqrt{3}$ at high densities. The predictions from the G3 parameter set are shown to be compatible with the experimental nuclear matter data and the NS-related properties, including the nuclear matter EoS at intermediate density.

We have shown that the NS mass M depends significantly on the value of κ . For $\kappa > 0$, the NS maximum mass increases when the κ value increases. For $\kappa < 0$, the NS maximum mass decreases when $|\kappa|$ value increases. On the other hand, the value of Λ_c affects the NS radius R . For $\Lambda_c > 0$, the NS radius tends to increase when Λ_c value increases. For $\Lambda_c < 0$, the NS radius tends to decrease when $|\Lambda_c|$ value increases.

We have also found for G3 with hyperon and speed of sound treatment at high densities (G3 WHSS), $\kappa \approx 5 \text{ km}^2$ and Λ_c value $\leq 2.08 \times 10^{-52} \text{ m}^{-2}$, which is the cosmological constant from observations, then the mass-radius relation satisfies both the NS $M \sim 2.0M_{\odot}$ and canonical mass-radius observation constraints [57, 58, 71, 72, 73, 7]. If we use EoS without hyperons but still use the speed of sound constraint (G3 WoutHSS), then the constraints can be satisfied even with a much smaller κ value.

We have also found that the G3 WHSS and G3 WoutHSS EoSs can both satisfy the $2.6M_{\odot}$ mass requirement and recent observation analysis [82, 57, 58, 79, 80, 6] simultaneously. However, the κ value is relatively large and the Λ_c value is unphysically large and negative. This unphysical aspect means that at the range of the solar system, Newtonian gravity breaks down.

Hence, if the EiBI gravity is the description of our universe and the accepted value of the physical cosmological constant value is very small and positive, then the $2.6M_{\odot}$ object observed in GW190814 event [6] is not likely an NS.

This page intentionally left blank

CHAPTER 8

CONCLUSIONS

In this chapter, we present our conclusions from the first and second parts of our work shown in chapters 6 and 7.

8.1 First part

In this first part of our work, we discuss the SCGrav much further and conclude with the following.

We use linear EoS that corresponds to UCO. Then the structure of the Eqs. (6.17)-(6.29) constraints the range of both α and w at the center. It turns out that the results are not significantly different from the usual TOV GR system. Thus, it is similar to the conclusion in Ref. [53] which says that UCOs from a linear equation of state in the Carballo-Rubio model's negative branch is unable to generate gravitational echoes if the speed of sound is $c/\sqrt{3}$. This speed of sound's upper bound came from QCD. Above this, i.e. the speed of sound is c which is from causality condition, a UCO can be produced, hence there is a gravitational echo from these objects. But then, these UCOs are not generated from adjusting the parameters from the semi-classical theory.

On the other hand, the positive branch is still open for more numerical analysis. We expect that, in this branch, the quantum effect from the semi-classical terms is significant for ECO.

The numerical verification is also discussed. Although most of it discusses the reproduction of the results from the literature, these are crucial since numerical treatment for the positive branch is not the same as the negative branch. We found that the equations from the negative branch can be integrated and give the same results regardless of the starting point of integration, i.e., one can integrate from the center of the star to its surface or from surface to center. The former is called forward integration and the latter is called backward integration. On the other hand, the equations from the positive branch can give a different result if we compare the results from the forward integration and backward integration.

Another interesting aspect discussed in the numerical verification is that for the negative branch, choosing negative central mass m_c and $\rho = \text{constant}$ can give compactness very near the black hole limit. This is larger than our results which from zero m_c , which only gives us compactness slightly larger than the Buchdahl bound, even though we also

set $\rho = \text{constant}$. Moreover, the value of ρ and p_c are also too huge, i.e., at least about a million times larger than the usual values from NS. Thus the possibility of something that violates the Buchdahl limit is pretty low to have its matter content similar to the usual matter that we know in NS.

8.2 Second part

In the second part of our work, we discussed the role of cosmological constant Λ_c in the EiBI gravity. The NS core EoS is calculated using the RMF model with the G3 parameter set [34] for both excluding and including hyperons contributions and the speed of sound is constrained to not exceeding $c/\sqrt{3}$ at high densities, denoted by WoutHSS and WHSS.

We find that if we use the observed data $\Lambda_c = 2.08 \times 10^{-52} \text{ m}^{-2}$ as an upper bound, then only $2.1M_\odot$ constraint can be reached if $\kappa \simeq 5 \text{ km}^2$ and G3 WHSS EoS is used. Using G3 WoutHSS EoS will give us a slightly higher maximum mass. The $2.1M_\odot$ constraint from the GW190814 event cannot be reached if the radius constraint for canonical mass $1.4M_\odot$ NSs from observations should also be satisfied. This radius constraint is crucial so that the moment of inertia and tidal deformation results are also in agreement with data from observations.

We also find that using $|\Lambda_c|$ larger than this value can give us an interesting but unphysical result. The G3 WHSS (with hyperons) and G3 WoutHSS (without hyperons) EoSs can satisfy the $2.6M_\odot$ constraint and the canonical mass-radius observation constraints, simultaneously, only if the κ value is relatively large ($\kappa = 13 \text{ km}^2$ for G3 WoutHSS EoS and $\kappa = 26 \text{ km}^2$ for G3 WHSS EoS) and the absolute Λ_c value is too large ($|\Lambda_c| \lesssim 10^{-9} \text{ m}^{-2}$) while its sign is negative. From these choices, the moment of inertia and the tidal deformability predictions from them is still compatible with recent observation analysis results.

Since the accepted value of the cosmological constant is positive and very small ($\Lambda_c = 2.08 \times 10^{-52} \text{ m}^{-2}$), we conclude that—according to the EoSs used here—the second object with mass $2.6M_\odot$ observed in GW190814 event [6] is not likely to be a static nor slowly-rotating NS.

REFERENCES

- [1] B. P. Abbott *et al.* [LIGO collab.] “Multi-messenger Observations of a Binary Neutron Star Merger,” *Astrophys. J. Lett.* **848**, no.2, L12 (2017) [arXiv:1710.05833 [astro-ph.HE]].
- [2] V. Cardoso and P. Pani, “Testing the nature of dark compact objects: a status report,” *Living Rev. Rel.* **22**, no.1, 4 (2019) [arXiv:1904.05363 [gr-qc]].
- [3] P. O. Mazur and E. Mottola, “Gravitational condensate stars: An alternative to black holes,” [arXiv:gr-qc/0109035 [gr-qc]].
- [4] P. O. Mazur and E. Mottola, “Gravitational vacuum condensate stars,” *Proc. Nat. Acad. Sci.* **101**, 9545-9550 (2004) [arXiv:gr-qc/0407075 [gr-qc]].
- [5] R. Carballo-Rubio, “Stellar equilibrium in semiclassical gravity,” *Phys. Rev. Lett.* **120**, no.6, 061102 (2018) [arXiv:1706.05379 [gr-qc]].
- [6] R. Abbott *et al.* [LIGO Scientific and Virgo], “GW190814: Gravitational Waves from the Coalescence of a 23 Solar Mass Black Hole with a 2.6 Solar Mass Compact Object,” *Astrophys. J. Lett.* **896**, no.2, L44 (2020) [arXiv:2006.12611 [astro-ph.HE]].
- [7] H. T. Cromartie *et al.* [NANOGrav], “Relativistic Shapiro delay measurements of an extremely massive millisecond pulsar,” *Nature Astron.* **4**, no.1, 72-76 (2019) [arXiv:1904.06759 [astro-ph.HE]].
- [8] F. J. Fattoyev, C. J. Horowitz, J. Piekarewicz and B. Reed, “GW190814: Impact of a 2.6 solar mass neutron star on the nucleonic equations of state,” *Phys. Rev. C* **102**, no.6, 065805 (2020) [arXiv:2007.03799 [nucl-th]].
- [9] A. Nathanael, E. R. Most and L. Rezzolla, “GW170817 and GW190814: tension on the maximum mass,” [arXiv:2101.01735 [astro-ph.HE]].
- [10] J. J. Li, A. Sedrakian and F. Weber, “Rapidly rotating Δ -resonance-admixed hypernuclear compact stars,” *Phys. Lett. B* **810**, 135812 (2020) [arXiv:2010.02901 [astro-ph.HE]].

- [11] N. B. Zhang and B. A. Li, “GW190814’s Secondary Component with Mass 2.50–2.67 M_{\odot} as a Superfast Pulsar,” *Astrophys. J.* **902**, no.1, 38 (2020) [arXiv:2007.02513 [astro-ph.HE]].
- [12] E. R. Most, L. J. Papenfort, L. R. Weih and L. Rezzolla, “A lower bound on the maximum mass if the secondary in GW190814 was once a rapidly spinning neutron star,” *Mon. Not. Roy. Astron. Soc.* **499**, no.1, L82-L86 (2020) [arXiv:2006.14601 [astro-ph.HE]].
- [13] X. Zhou, A. Li and B. A. Li, “ R -mode Stability of GW190814’s Secondary Component as a Supermassive and Superfast Pulsar,” [arXiv:2011.11934 [astro-ph.HE]].
- [14] B. Biswas, R. Nandi, P. Char, S. Bose and N. Stergioulas, “GW190814: On the properties of the secondary component of the binary,” [arXiv:2010.02090 [astro-ph.HE]].
- [15] S. H. Yang, C. M. Pi, X. P. Zheng and F. Weber, “Constraints from compact star observations on non-Newtonian gravity in strange stars based on a density dependent quark mass model,” [arXiv:2101.11192 [astro-ph.HE]].
- [16] I. A. Rather, U. Rahaman, M. Imran, H. C. Das, A. A. Usmani and S. K. Patra, “Rotating Neutron stars with Quark cores,” [arXiv:2102.04067 [nucl-th]].
- [17] Z. Roupas, G. Panotopoulos and I. Lopes, “QCD color superconductivity in compact stars: color-flavor locked quark star candidate for the gravitational-wave signal GW190814,” [arXiv:2010.11020 [astro-ph.HE]].
- [18] A. Sedrakian, F. Weber and J. J. Li, “Confronting GW190814 with hyperonization in dense matter and hypernuclear compact stars,” *Phys. Rev. D* **102**, no.4, 041301 (2020) [arXiv:2007.09683 [astro-ph.HE]].
- [19] Z. Cao, L. W. Chen, P. C. Chu and Y. Zhou, “GW190814: Circumstantial Evidence for Up-Down Quark Star,” [arXiv:2009.00942 [astro-ph.HE]].
- [20] I. Bombaci, A. Drago, D. Logoteta, G. Pagliara and I. Vidana, “Was GW190814 a black hole – strange quark star system?,” [arXiv:2010.01509 [nucl-th]].
- [21] C. Zhang and R. B. Mann, “Unified Interacting Quark Matter and its Astrophysical Implications,” [arXiv:2009.07182 [astro-ph.HE]].
- [22] K. Zhang and F. L. Lin, “Constraint on hybrid stars with gravitational wave events,” *Universe* **6**, no.12, 231 (2020) [arXiv:2011.05104 [astro-ph.HE]].

- [23] I. A. Rather, A. A. Usmani and S. K. Patra, “Hadron-Quark phase transition in the context of GW190814,” [arXiv:2011.14077 [nucl-th]].
- [24] B. J. Barros, Z. Haghani, T. Harko and F. S. N. Lobo, “Static spherically symmetric three-form stars,” [arXiv:2101.04445 [gr-qc]].
- [25] J. W. Moffat, “Modified Gravity (MOG) and Heavy Neutron Star in Mass Gap,” [arXiv:2008.04404 [gr-qc]].
- [26] R. C. Nunes, J. G. Coelho and J. C. N. de Araujo, “Weighing massive neutron star with screening gravity: a look on PSR J0740 + 6620 and GW190814 secondary component,” *Eur. Phys. J. C* **80**, no.12, 1115 (2020) [arXiv:2008.10395 [astro-ph.HE]].
- [27] A. V. Astashenok, S. Capozziello, S. D. Odintsov and V. K. Oikonomou, “Extended Gravity Description for the GW190814 Supermassive Neutron Star,” *Phys. Lett. B* **811**, 135910 (2020) [arXiv:2008.10884 [gr-qc]].
- [28] D. N. Vollick, “Palatini approach to Born-Infeld-Einstein theory and a geometric description of electrodynamics,” *Phys. Rev. D* **69**, 064030 (2004) [arXiv:gr-qc/0309101 [gr-qc]].
- [29] M. Banados and P. G. Ferreira, “Eddington’s theory of gravity and its progeny,” *Phys. Rev. Lett.* **105**, 011101 (2010) [erratum: *Phys. Rev. Lett.* **113**, no.11, 119901 (2014)] [arXiv:1006.1769 [astro-ph.CO]].
- [30] P. Pani, V. Cardoso and T. Delsate, “Compact stars in Eddington inspired gravity,” *Phys. Rev. Lett.* **107**, 031101 (2011) [arXiv:1106.3569 [gr-qc]].
- [31] P. Pani, T. Delsate and V. Cardoso, “Eddington-inspired Born-Infeld gravity. Phenomenology of non-linear gravity-matter coupling,” *Phys. Rev. D* **85**, 084020 (2012) [arXiv:1201.2814 [gr-qc]].
- [32] T. Harko, F. S. N. Lobo, M. K. Mak and S. V. Sushkov, “Structure of neutron, quark and exotic stars in Eddington-inspired Born-Infeld gravity,” *Phys. Rev. D* **88**, 044032 (2013) [arXiv:1305.6770 [gr-qc]].
- [33] A. I. Qauli, M. Iqbal, A. Sulaksono and H. S. Ramadhan, “Hyperons in neutron stars within an Eddington-inspired Born-Infeld theory of gravity,” *Phys. Rev. D* **93**, no.10, 104056 (2016) [arXiv:1605.01152 [astro-ph.SR]].

- [34] B. Kumar, S. K. Singh, B. K. Agrawal and S. K. Patra, “New parameterization of the effective field theory motivated relativistic mean field model,” Nucl. Phys. A **966**, 197-207 (2017) [arXiv:1705.02621 [nucl-th]].
- [35] L. Ryder, *Introduction to general relativity*, Cambridge University Press, UK (2009).
- [36] S. M. Carroll, *Spacetime and Geometry: An Introduction to General Relativity*, Cambridge University Press, UK (2019).
- [37] R. d’Inverno, *Introducing Einstein’s relativity*, Clarendon Press, UK (1992).
- [38] E. Poisson, *A Relativist’s Toolkit: The Mathematics of Black-Hole Mechanics*, Cambridge University Press, UK (2009).
- [39] C. W. Misner, K. S. Thorne and J. A. Wheeler, *Gravitation*, W. H. Freeman and Company, California (1973).
- [40] M. Nakahara, *Geometry, topology and physics*, 2nd ed., IOP Publishing, UK (2003).
- [41] J. Baez and J. P. Muniain, *Gauge fields, knots and gravity*, World Scientific, Singapore (1994).
- [42] R. M. Wald, *General Relativity*, University of Chicago Press, IL (1984).
- [43] S. W. Hawking and G. F. R. Ellis, *The Large Scale Structure of Space-Time*, Cambridge University Press, UK (1973).
- [44] C. Nash and S. Sen, *Topology and Geometry for Physicists*, Academic Press, UK (1983).
- [45] N. D. Birrell and P. C. W. Davies, *Quantum Fields in Curved Space*, Cambridge University Press, UK (1982).
- [46] L. E. Parker and D. Toms, *Quantum Field Theory in Curved Spacetime: Quantized Field and Gravity*, Cambridge University Press, UK (2009).
- [47] R. M. Wald, *Quantum Field Theory in Curved Space-Time and Black Hole Thermodynamics*, University of Chicago Press, IL (1995).
- [48] N. K. Glendenning, *Compact stars: Nuclear physics, particle physics, and general relativity*, 2nd edition, Springer, German (2000).

- [49] F. Weber, *Pulsars as astrophysical laboratories for nuclear and particle physics*, IOP Publishing, UK (1999).
- [50] E. Poisson and C. M. Will, *Gravity: Newtonian, Post-Newtonian, Relativistic*, Cambridge University Press, UK (2014).
- [51] S. Chandrasekhar, *The Mathematical Theory of Black Holes*, Oxford University Press, New York (1983).
- [52] J. Lense and H. Thirring, “Ueber den Einfluss der Eigenrotation der Zentralkoerper auf die Bewegung der Planeten und Monde nach der Einsteinschen Gravitations-theorie,” Phys. Z. **19**, 156-163 (1918)
- [53] A. Urbano and H. Veermäe, “On gravitational echoes from ultracompact exotic stars,” JCAP **04**, 011 (2019) [arXiv:1810.07137 [gr-qc]].
- [54] M. Mannarelli and F. Tonelli, “Gravitational wave echoes from strange stars,” Phys. Rev. D **97**, no.12, 123010 (2018) [arXiv:1805.02278 [gr-qc]].
- [55] J. Abedi and N. Afshordi, “Echoes from the Abyss: A highly spinning black hole remnant for the binary neutron star merger GW170817,” JCAP **11**, 010 (2019) [arXiv:1803.10454 [gr-qc]].
- [56] P. Pani and V. Ferrari, “On gravitational-wave echoes from neutron-star binary coalescences,” Class. Quant. Grav. **35**, no.15, 15LT01 (2018) [arXiv:1804.01444 [gr-qc]].
- [57] P. Landry, R. Essick and K. Chatzioannou, “Nonparametric constraints on neutron star matter with existing and upcoming gravitational wave and pulsar observations,” Phys. Rev. D **101**, no.12, 123007 (2020) [arXiv:2003.04880 [astro-ph.HE]].
- [58] J. L. Jiang, S. P. Tang, Y. Z. Wang, Y. Z. Fan and D. M. Wei, “PSR J0030+0451, GW170817 and the nuclear data: joint constraints on equation of state and bulk properties of neutron stars,” Astrophys. J. **892**, 1 (2020) [arXiv:1912.07467 [astro-ph.HE]].
- [59] C. D. Capano, I. Tews, S. M. Brown, B. Margalit, S. De, S. Kumar, D. A. Brown, B. Krishnan and S. Reddy, “Stringent constraints on neutron-star radii from multimessenger observations and nuclear theory,” Nature Astron. **4**, no.6, 625-632 (2020) [arXiv:1908.10352 [astro-ph.HE]].

- [60] K. Huang, J. Hu, Y. Zhang and H. Shen, “The possibility of the secondary object in GW190814 as a neutron star,” *Astrophys. J.* **904**, no.1, 39 (2020) [arXiv:2008.04491 [nucl-th]].
- [61] H. C. Das, A. Kumar, B. Kumar, S. K. Biswal and S. K. Patra, “The BigApple force and it’s implications to finite nuclei and astrophysical objects,” [arXiv:2009.10690 [nucl-th]].
- [62] C. Drischler, S. Han, J. M. Lattimer, M. Prakash, S. Reddy and T. Zhao, “Limiting masses and radii of neutron stars and their implications,” [arXiv:2009.06441 [nucl-th]].
- [63] V. Dexheimer, R. O. Gomes, T. Klähn, S. Han and M. Salinas, “GW190814 as a massive rapidly rotating neutron star with exotic degrees of freedom,” *Phys. Rev. C* **103**, no.2, 025808 (2021) [arXiv:2007.08493 [astro-ph.HE]].
- [64] A. Kanakis-Pegios, P. S. Koliogiannis and C. C. Moustakidis, “Probing the Nuclear Equation of State from the Existence of a $\sim 2.6 M_{\odot}$ Neutron Star: The GW190814 Puzzle,” *Symmetry* **13**, no.2, 183 (2021) [arXiv:2012.09580 [astro-ph.HE]].
- [65] H. Tan, J. Noronha-Hostler and N. Yunes, “Neutron Star Equation of State in light of GW190814,” *Phys. Rev. Lett.* **125**, no.26, 261104 (2020) [arXiv:2006.16296 [astro-ph.HE]].
- [66] J. E. Horvath and P. H. R. S. Moraes, “Modelling a $2.5 M_{\odot}$ Compact Star with Quark Matter,” arXiv:2012.00917 [astro-ph.HE]
- [67] T. Demircik, C. Ecker and M. Jrvinen, “Rapidly Spinning Compact Stars with Deconfinement Phase Transition,” *Astrophys. J. Lett.* **907**, no. 2, L37 (2021) [arXiv:2009.10731 [astro-ph.HE]].
- [68] Z. Roupas, “Secondary component of gravitational-wave signal GW190814 as an anisotropic neutron star,” *Astrophys. Space Sci.* **366**, no. 1, 9 (2021) [arXiv:2007.10679 [gr-qc]].
- [69] B. V. Lehmann, S. Profumo and J. Yant, “Model-independent discovery prospects for primordial black holes at LIGO,” *MNRAS*, Volume 501, Issue 3, March 2021, Pages 3727-3740 [arXiv:2007.00021 [astro-ph.CO]]
- [70] R. Beradze and M. Gogberashvili, “Unexpected LIGO events and the Mirror World,” arXiv:2101.12532 [astro-ph.CO]

- [71] P. Demorest, T. Pennucci, S. Ransom, M. Roberts and J. Hessels, “Shapiro Delay Measurement of A Two Solar Mass Neutron Star,” *Nature* **467**, 1081-1083 (2010) [arXiv:1010.5788 [astro-ph.HE]].
- [72] E. Fonseca, T. T. Pennucci, J. A. Ellis, I. H. Stairs, D. J. Nice, S. M. Ransom, P. B. Demorest, Z. Arzoumanian, K. Crowter and T. Dolch, *et al.* “The NANOGrav Nine-year Data Set: Mass and Geometric Measurements of Binary Millisecond Pulsars,” *Astrophys. J.* **832**, no.2, 167 (2016) [arXiv:1603.00545 [astro-ph.HE]].
- [73] Z. Arzoumanian *et al.* [NANOGrav], “The NANOGrav 11-year Data Set: High-precision timing of 45 Millisecond Pulsars,” *Astrophys. J. Suppl.* **235**, no.2, 37 (2018) [arXiv:1801.01837 [astro-ph.HE]].
- [74] J. Antoniadis, P. C. C. Freire, N. Wex, T. M. Tauris, R. S. Lynch, M. H. van Kerkwijk, M. Kramer, C. Bassa, V. S. Dhillon and T. Driebe, *et al.* “A Massive Pulsar in a Compact Relativistic Binary,” *Science* **340**, 6131 (2013) [arXiv:1304.6875 [astro-ph.HE]].
- [75] A. L. Watts, N. Andersson, D. Chakrabarty, M. Feroci, K. Hebeler, G. Israel, F. K. Lamb, M. C. Miller, S. Morsink and F. Özel, *et al.* “Colloquium : Measuring the neutron star equation of state using x-ray timing,” *Rev. Mod. Phys.* **88**, no.2, 021001 (2016) [arXiv:1602.01081 [astro-ph.HE]].
- [76] S. Guillot, M. Kerr, P. S. Ray, S. Bogdanov, S. Ransom, J. S. Deneva, Z. Arzoumanian, P. Bult, D. Chakrabarty and K. C. Gendreau, *et al.* “NICER X-ray Observations of Seven Nearby Rotation-Powered Millisecond Pulsars,” *Astrophys. J. Lett.* **887**, no.1, L27 (2019) [arXiv:1912.05708 [astro-ph.HE]].
- [77] S. Bogdanov, S. Guillot, P. S. Ray, M. T. Wolff, D. Chakrabarty, W. C. G. Ho, M. Kerr, F. K. Lamb, A. Lommen and R. M. Ludlam, *et al.* “Constraining the Neutron Star Mass–Radius Relation and Dense Matter Equation of State with NICER. I. The Millisecond Pulsar X-Ray Data Set,” *Astrophys. J. Lett.* **887**, no.1, L25 (2019) [arXiv:1912.05706 [astro-ph.HE]].
- [78] S. Bogdanov, F. K. Lamb, S. Mahmoodifar, M. C. Miller, S. M. Morsink, T. E. Riley, T. E. Strohmayer, A. L. Watts, A. J. Dittmann and D. Chakrabarty, *et al.* “Constraining the Neutron Star Mass–Radius Relation and Dense Matter Equation of State with NICER. II. Emission from Hot Spots on a Rapidly Rotating Neutron Star,” *Astrophys. J. Lett.* **887**, no.1, L26 (2019) [arXiv:1912.05707 [astro-ph.HE]].

- [79] B. P. Abbott *et al.* [LIGO Scientific and Virgo], “GW170817: Observation of Gravitational Waves from a Binary Neutron Star Inspiral,” Phys. Rev. Lett. **119**, no.16, 161101 (2017) [arXiv:1710.05832 [gr-qc]].
- [80] B. P. Abbott *et al.* [LIGO Scientific and Virgo], “GW170817: Measurements of neutron star radii and equation of state,” Phys. Rev. Lett. **121**, no.16, 161101 (2018) [arXiv:1805.11581 [gr-qc]].
- [81] B. P. Abbott *et al.* [LIGO Scientific and Virgo], “Properties of the binary neutron star merger GW170817,” Phys. Rev. X **9**, no.1, 011001 (2019) [arXiv:1805.11579 [gr-qc]].
- [82] B. Kumar and P. Landry, “Inferring neutron star properties from GW170817 with universal relations,” Phys. Rev. D **99**, no.12, 123026 (2019) [arXiv:1902.04557 [gr-qc]].
- [83] Y. Lim, J. W. Holt and R. J. Stahulak, “Predicting the moment of inertia of pulsar J0737-3039A from Bayesian modeling of the nuclear equation of state,” Phys. Rev. C **100**, no.3, 035802 (2019) [arXiv:1810.10992 [nucl-th]].
- [84] J. M. Lattimer and B. F. Schutz, “Constraining the equation of state with moment of inertia measurements,” Astrophys. J. **629**, 979-984 (2005) [arXiv:astro-ph/0411470 [astro-ph]].
- [85] C. Breu and L. Rezzolla, “Maximum mass, moment of inertia and compactness of relativistic stars,” Mon. Not. Roy. Astron. Soc. **459**, no.1, 646-656 (2016) [arXiv:1601.06083 [gr-qc]].
- [86] M. Dutra, O. Lourenço, S. S. Avancini, B. V. Carlson, A. Delfino, D. P. Menezes, C. Providência, S. Typel and J. R. Stone, “Relativistic Mean-Field Hadronic Models under Nuclear Matter Constraints,” Phys. Rev. C **90**, no.5, 055203 (2014) [arXiv:1405.3633 [nucl-th]].
- [87] O. Lourenço, M. Dutra, C. H. Lenzi, C. V. Flores and D. P. Menezes, “Consistent relativistic mean field models constrained by GW170817,” Phys. Rev. C **99**, no.4, 045202 (2019) [arXiv:1812.10533 [nucl-th]].
- [88] A. Rahmansyah, A. Sulaksono, A. B. Wahidin and A. M. Setiawan, “Anisotropic neutron stars with hyperons: implication of the recent nuclear matter data and observations of neutron stars,” Eur. Phys. J. C **80**, no.8, 769 (2020)
- [89] J. P. W. Diener, “Relativistic mean-field theory applied to the study of neutron star properties,” [arXiv:0806.0747 [nucl-th]].

- [90] J. P. W. Diener, “Ferromagnetic Phase Transitions in Neutron Stars,” [arXiv:1305.7346 [nucl-th]].
- [91] A. Sulaksono and B. K. Agrawal, “Existence of hyperons in the pulsar PSRJ1614-2230,” Nucl. Phys. A **895**, 44-58 (2012) [arXiv:1209.6160 [nucl-th]].
- [92] B. K. Agrawal, A. Sulaksono and P. G. Reinhard, “Optimization of relativistic mean field model for finite nuclei to neutron star matter,” Nucl. Phys. A **882**, 1-20 (2012) [arXiv:1204.2644 [nucl-th]].
- [93] H. Shen, F. Ji, J. Hu and K. Sumiyoshi, “Effects of symmetry energy on equation of state for simulations of core-collapse supernovae and neutron-star mergers,” Astrophys. J. **891**, 148 (2020) [arXiv:2001.10143 [nucl-th]].
- [94] L. Tolos, M. Centelles and A. Ramos, “Equation of State for Nucleonic and Hyperonic Neutron Stars with Mass and Radius Constraints,” Astrophys. J. **834**, no.1, 3 (2017) [arXiv:1610.00919 [astro-ph.HE]].
- [95] A. Le Fèvre, Y. Leifels, W. Reisdorf, J. Aichelin and C. Hartnack, “Constraining the nuclear matter equation of state around twice saturation density,” Nucl. Phys. A **945**, 112-133 (2016) [arXiv:1501.05246 [nucl-ex]].
- [96] P. Danielewicz, R. Lacey and W. G. Lynch, “Determination of the equation of state of dense matter,” Science **298**, 1592-1596 (2002) [arXiv:nucl-th/0208016 [nucl-th]].
- [97] C. Drischler, K. Hebeler and A. Schwenk, “Asymmetric nuclear matter based on chiral two- and three-nucleon interactions,” Phys. Rev. C **93**, no.5, 054314 (2016) [arXiv:1510.06728 [nucl-th]].
- [98] I. Tews, J. Carlson, S. Gandolfi and S. Reddy, “Constraining the speed of sound inside neutron stars with chiral effective field theory interactions and observations,” Astrophys. J. **860**, no.2, 149 (2018) [arXiv:1801.01923 [nucl-th]].
- [99] T. Miyatsu, S. Yamamuro and K. Nakazato, “A new equation of state for neutron star matter with nuclei in the crust and hyperons in the core,” Astrophys. J. **777**, 4 (2013) [arXiv:1308.6121 [astro-ph.HE]].
- [100] C. Margaritis, P. S. Koliogiannis and C. C. Moustakidis, “Speed of sound constraints on maximally-rotating neutron stars,” Phys. Rev. D **101**, no.4, 043023 (2020) [arXiv:1910.05767 [nucl-th]].

- [101] I. Prasetyo, H. S. Ramadhan and A. Sulaksono, “Ultra-compact objects from semi-classical gravity,” Phys. Rev. D **103**, no.12, 123536 (2021) [arXiv:2105.11691 [gr-qc]].
- [102] B. S. DeWitt, “Quantum Field Theory in Curved Space-Time,” Phys. Rept. **19**, 295-357 (1975)
- [103] B. A. Juárez-Aubry, “Semi-classical gravity in de Sitter spacetime and the cosmological constant,” Phys. Lett. B **797**, 134912 (2019) [arXiv:1903.03924 [gr-qc]].
- [104] M. Visser, “Gravitational vacuum polarization,” gr-qc/9710034.
- [105] L. C. Barbado, C. Barcelo and L. J. Garay, “Hawking radiation as perceived by different observers,” Class. Quant. Grav. **28**, 125021 (2011) [arXiv:1101.4382 [gr-qc]].
- [106] I. L. Shapiro, “Effective Action of Vacuum: Semiclassical Approach,” Class. Quant. Grav. **25**, 103001 (2008) [arXiv:0801.0216 [gr-qc]].
- [107] C. Barcelo, S. Liberati, S. Sonego and M. Visser, “Fate of gravitational collapse in semiclassical gravity,” Phys. Rev. D **77**, 044032 (2008) [arXiv:0712.1130 [gr-qc]].
- [108] P. M. Ho and Y. Matsuo, “Static Black Hole and Vacuum Energy: Thin Shell and Incompressible Fluid,” JHEP **03**, 096 (2018) [arXiv:1710.10390 [hep-th]].
- [109] P. M. Ho and Y. Matsuo, “Static Black Holes With Back Reaction From Vacuum Energy,” Class. Quant. Grav. **35**, no. 6, 065012 (2018) [arXiv:1703.08662 [hep-th]].
- [110] A. Fabbri and J. Navarro-Salas, “Modeling Black Hole Evaporation,” Imperial College Press, London (2005)
- [111] C. Barcelo, R. Carballo and L. J. Garay, “Two formalisms, one renormalized stress-energy tensor,” Phys. Rev. D **85**, 084001 (2012) [arXiv:1112.0489 [gr-qc]].
- [112] C. C. Moustakidis, T. Gaitanos, C. Margaritis and G. A. Lalazissis, “Bounds on the speed of sound in dense matter, and neutron star structure,” Phys. Rev. C **95**, no.4, 045801 (2017) [erratum: Phys. Rev. C **95**, no.5, 059904 (2017)] [arXiv:1608.00344 [nucl-th]].
- [113] C. Anastopoulos and N. Savvidou, “Classification theorem and properties of singular solutions to the Tolman-Oppenheimer-Volkoff equation,” [arXiv:2010.02279 [gr-qc]].

- [114] I. Prasetyo, H. S. Ramadhan and A. Sulaksono, “ $2.6M_{\odot}$ compact object and neutron stars in Eddington-inspired Born-Infeld theory of gravity,” accepted by PRD, [arXiv:2109.05718 [gr-qc]].
- [115] T. Delsate and J. Steinhoff, “New insights on the matter-gravity coupling paradigm,” Phys. Rev. Lett. **109**, 021101 (2012) [arXiv:1201.4989 [gr-qc]].
- [116] C. Wibisono and A. Sulaksono, “Information-entropic method for studying the stability bound of nonrelativistic polytropic stars within modified gravity theories,” Int. J. Mod. Phys. D **27**, no. 05, 1850051 (2018) [arXiv:1712.07587 [gr-qc]].
- [117] M. D. Danarianto and A. Sulaksono, “Overturning and apparent anisotropic pressure in Eddington-inspired Born-Infeld theory on compact stars,” Phys. Rev. D **100**, no. 6, 064042 (2019).
- [118] A. S. Rosyadi, A. Sulaksono, H. A. Kassim and N. Yusof, “Brown dwarfs in Eddington-inspired Born-Infeld and beyond Horndeski theories,” Eur. Phys. J. C **79**, no. 12, 1030 (2019).
- [119] J. Beltran Jimenez, L. Heisenberg, G. J. Olmo and D. Rubiera-Garcia, “Born-Infeld inspired modifications of gravity,” Phys. Rept. **727**, 1-129 (2018) [arXiv:1704.03351 [gr-qc]].
- [120] E. Berti, E. Barausse, V. Cardoso, L. Gualtieri, P. Pani, U. Sperhake, L. C. Stein, N. Wex, K. Yagi and T. Baker, *et al.* “Testing General Relativity with Present and Future Astrophysical Observations,” Class. Quant. Grav. **32**, 243001 (2015) [arXiv:1501.07274 [gr-qc]].
- [121] I. Prasetyo, I. Husin, A. I. Qauli, H. S. Ramadhan and A. Sulaksono, “Neutron stars in the braneworld within the Eddington-inspired Born-Infeld gravity,” JCAP **01**, 027 (2018) [arXiv:1708.04837 [astro-ph.CO]].
- [122] A. I. Qauli, A. Sulaksono, H. S. Ramadhan and I. Husin, “Compactness, masses and radii of compact stars within the Eddington-inspired Born-Infeld theory,” arXiv:1710.03988 [gr-qc]
- [123] Y.-H. Sham, L.-M. Lin and P. T. Leung, “Radial oscillations and stability of compact stars in Eddington inspired Born-Infeld gravity,” Phys. Rev. D **86**, 064015 (2012) [arXiv:1208.1314 [gr-qc]].
- [124] Y. H. Sham, P. T. Leung and L. M. Lin, “Compact stars in Eddington-inspired Born-Infeld gravity: Anomalies associated with phase transitions,” Phys. Rev. D **87**, no. 6, 061503 (2013) [arXiv:1304.0550 [gr-qc]].

- [125] E. Barausse, T. P. Sotiriou and J. C. Miller, “A No-go theorem for polytropic spheres in Palatini f(R) gravity,” *Class. Quant. Grav.* **25**, 062001 (2008) [[gr-qc/0703132 \[GR-QC\]](#)].
- [126] Y. H. Sham, L. M. Lin and P. T. Leung, “Testing universal relations of neutron stars with a nonlinear matter-gravity coupling theory,” *Astrophys. J.* **781**, 66 (2014) [[arXiv:1312.1011 \[gr-qc\]](#)].
- [127] P. Pani and T. P. Sotiriou, “Surface singularities in Eddington-inspired Born-Infeld gravity,” *Phys. Rev. Lett.* **109**, 251102 (2012) [[arXiv:1209.2972 \[gr-qc\]](#)].
- [128] P. Pani, T. P. Sotiriou and D. Vernieri, “Gravity with Auxiliary Fields,” *Phys. Rev. D* **88**, no. 12, 121502 (2013) [[arXiv:1306.1835 \[gr-qc\]](#)].
- [129] H. C. Kim, “Physics at the surface of a star in Eddington-inspired Born-Infeld gravity,” *Phys. Rev. D* **89**, no. 6, 064001 (2014) [[arXiv:1312.0705 \[gr-qc\]](#)].
- [130] J. B. Hartle, “Slowly rotating relativistic stars. 1. Equations of structure,” *Astrophys. J.* **150**, 1005-1029 (1967)
- [131] T. Regge and J. A. Wheeler, “Stability of a Schwarzschild singularity,” *Phys. Rev.* **108**, 1063-1069 (1957)
- [132] T. Hinderer, “Tidal Love numbers of neutron stars,” *Astrophys. J.* **677**, 1216-1220 (2008) [[arXiv:0711.2420 \[astro-ph\]](#)].
- [133] T. Damour and A. Nagar, “Relativistic tidal properties of neutron stars,” *Phys. Rev. D* **80**, 084035 (2009) [[arXiv:0906.0096 \[gr-qc\]](#)].
- [134] S. Weinberg, “The Cosmological Constant Problem,” *Rev. Mod. Phys.* **61**, 1-23 (1989)
- [135] S. M. Carroll, “The Cosmological constant,” *Living Rev. Rel.* **4**, 1 (2001) [[arXiv:astro-ph/0004075 \[astro-ph\]](#)].
- [136] T. Padmanabhan, “Cosmological constant: The Weight of the vacuum,” *Phys. Rept.* **380**, 235-320 (2003) [[arXiv:hep-th/0212290 \[hep-th\]](#)].
- [137] J. Frieman, M. Turner and D. Huterer, “Dark Energy and the Accelerating Universe,” *Ann. Rev. Astron. Astrophys.* **46**, 385-432 (2008) [[arXiv:0803.0982 \[astro-ph\]](#)].

APPENDIX

This page intentionally left blank

APPENDIX A

TETRAD METHOD

This section is a part of our second work. The purpose of writing this Appendix is so that readers will be familiar with the tetrad method, a method used in advanced books on GR, e.g., Chandrasekhar [51].

Here, we show the algorithm to obtain the Einstein tensor components. Since calculating using Christoffel symbol is tedious, people usually use a tensor manipulations package in *Mathematica*, such as *diffgeo*¹. But, for a metric whose form is simple, it might be beneficial to show how to do it by hand using the so-called *tetrad method*. The steps are shown explicitly up to a point where the mathematical calculation will be too long.

First, we consider the following metric

$$\mathbf{g} = -e^\nu dt^2 + e^\lambda dr^2 + r^2[d\theta^2 + \sin^2 \theta(d\varphi - \omega dt)^2]. \quad (\text{A.1})$$

Introducing only one small but non-zero function ω in the off-diagonal term of the metric (actually two, but they are related to each other since $g_{t\varphi} = g_{\varphi t}$), readers will see that the calculation is getting larger quite rapidly. For simplicity, we shall ignore $\mathcal{O}(\omega^2)$.² This metric can be easily diagonalized into $\eta_{mn} = \text{diag}(-1, 1, 1, 1)$ by

$$g_{\mu\nu} = \eta_{mn} e_\mu^m e_\nu^n, \quad (\text{A.2})$$

where e_μ^m is the components of a 1-form $\mathbf{e}^m = e_\mu^m dx^\mu$. \mathbf{e}^m is usually called as *tetrad basis* with $m = \{0, 1, 2, 3\}$ called as tetrad indices. This new indices correspond to the coordinate indices $\mu = \{t, r, \theta, \varphi\}$. In matrix form, e_μ^m can be written as

$$e_\mu^m = \begin{pmatrix} e^{\lambda/2} & 0 & 0 & 0 \\ 0 & r & 0 & 0 \\ 0 & 0 & r \sin(\theta) & -r\omega \sin(\theta) \\ 0 & 0 & 0 & e^{\nu/2} \end{pmatrix}. \quad (\text{A.3})$$

Notice that its upper index m and lower index μ denotes the row and column. The order

¹M. Headrick, *Mathematica packages* by Matthew Headrick available at <http://people.brandeis.edu/~headrick/Mathematica/>.

²For explicit expressions of the Riemann, Ricci, and Einstein tensors without omission of any terms such as $\mathcal{O}(\omega^2)$, readers can check Appendix G of Ref. [49]. The metric used there is in Chapter 15, which is more general than what we use here.

in the indices is also altered a bit, i.e., $m = (1, 2, 3, 0)$ and $\mu = (r, \theta, \varphi, t)$. In this form, it is easy to find the inverse of e_μ^m :

$$e_m^\mu = \begin{pmatrix} e^{-\frac{\lambda}{2}} & 0 & 0 & 0 \\ 0 & \frac{1}{r} & 0 & 0 \\ 0 & 0 & \frac{\csc(\theta)}{r} & e^{-\frac{\nu}{2}}\omega \\ 0 & 0 & 0 & e^{-\frac{\nu}{2}} \end{pmatrix}. \quad (\text{A.4})$$

In general, we can calculate this by

$$e_\mu^m e_n^\nu = \delta_n^m, \quad (\text{A.5})$$

$$q^{\mu\nu} = \eta^{mn} e_m^\mu e_n^\nu. \quad (\text{A.6})$$

Then, the tetrad basis are

$$e^0 = e^{\nu/2} dt, \quad (\text{A.7a})$$

$$e^1 = e^{\lambda/2} dr, \quad (\text{A.7b})$$

$$e^2 = r d\theta, \quad (\text{A.7c})$$

$$e^3 = r \sin \theta (d\varphi - \omega dt). \quad (\text{A.7d})$$

The next step is using the so-called the so-called *Cartan structure equations*

$$\mathbf{T}^m = d\mathbf{e}^m + \boldsymbol{\omega}_n^m \wedge \mathbf{e}^n, \quad (\text{A.8})$$

$$\mathbf{R}_n^m = d\boldsymbol{\omega}_n^m + \boldsymbol{\omega}_o^m \wedge \boldsymbol{\omega}_n^o. \quad (\text{A.9})$$

The 1-form $\boldsymbol{\omega}_n^m$ called is (spin-)connection 1-form

$$\boldsymbol{\omega}_n^m = \omega_{\mu n}^m dx^\mu. \quad (\text{A.10})$$

Similar to the potential vector A_μ in Maxwell or Yang-Mills electrodynamics, $\omega_{\mu n}^m$ is related to the Christoffel symbol by [36]

$$\Gamma_{\mu\lambda}^\nu = e_m^\nu e_\lambda^n \omega_{\mu n}^m + e_m^\nu \partial_\mu e_\lambda^m. \quad (\text{A.11})$$

The components of the 2-form \mathbf{T}^m is actually just the torsion tensor. We set $\mathbf{T}^m = 0$ since the GR theory is torsionless. The components of the curvature 2-form \mathbf{R}_n^m is also just the Riemann tensor:

$$\mathbf{R}_n^m = \frac{1}{2} R_{n\mu\nu}^m dx^\mu \wedge dx^\nu. \quad (\text{A.12})$$

Notice that there are two tetrad indices and two coordinate indices in $R_{n\mu\nu}^m$. To make all indices becomes coordinate indices, it is more economical if we lower one of the indices of curvature 2-form, then use the tetrad basis components to convert the indices, and lastly extract the Riemann tensor:

$$\mathbf{R}_{mn} = \eta_{mp} \mathbf{R}_n^p, \quad (\text{A.13a})$$

$$\mathbf{R}_{\mu\nu} = \mathbf{R}_{mn} e_\mu^m e_\nu^n, \quad (\text{A.13b})$$

$$\mathbf{R}_{\mu\nu} = \frac{1}{2} R_{\mu\nu\alpha\beta} dx^\alpha \wedge dx^\beta. \quad (\text{A.13c})$$

Using the Cartan structure equations, the algorithm is as follows. From the torsionless condition, we calculate the connection 1-form. Then, from the curvature 2-form, we infer the components of the Riemann tensor.

We calculate the connection 1-form first. Before that, the rule is that the indices of ω_{mn} antisymmetric $\omega_{mn} = -\omega_{nm}$, with $\omega_{mn} = \omega_n^o \eta_{mo}$. This then implies $\omega_i^0 = \omega_0^i$, $\omega_j^i = -\omega_i^j$ with $i, j = \{1, 2, 3\}$. Then, we shape the arbitrary form of ω_n^m as

$$\omega_1^0 = Adt + Bdr + Cd\theta + Dd\varphi, \quad (\text{A.14a})$$

$$\omega_2^0 = Edt + Fdr + Gd\theta + Hd\varphi, \quad (\text{A.14b})$$

$$\omega_3^0 = Idt + Jdr + Kd\theta + Ld\varphi, \quad (\text{A.14c})$$

$$\omega_2^1 = Mdt + Ndr + Od\theta + Pd\varphi, \quad (\text{A.14d})$$

$$\omega_3^1 = Qdt + Rdr + Sd\theta + Td\varphi, \quad (\text{A.14e})$$

$$\omega_3^2 = Udt + Vdr + Wd\theta + Xd\varphi, \quad (\text{A.14f})$$

where A, \dots, X are undetermined. The exterior derivative d acts like a partial derivative

$$df = \partial_\nu f dx^\nu, \quad (\text{A.15})$$

$$de^m = \partial_\nu (e_\mu^m) dx^\nu \wedge dx^\mu. \quad (\text{A.16})$$

This makes an n -form becomes an $(n+1)$ -form. The wedge symbol \wedge is a way to tell that the basis of any n -form are fully anti-symmetric, e.g.,

$$dx^\mu \wedge dx^\nu = -dx^\nu \wedge dx^\mu, \quad (\text{A.17})$$

which is similar to the property of the Levi-Civita symbol $\epsilon_{\mu\nu}$.

Next, we use Eq. (A.8) to calculate all A, \dots, X . Substituting all e^m and ω_n^m into

Eq. (A.8) gives us

$$\begin{aligned} \mathbf{T}^0 = 0 : \quad 0 &= dt \wedge dr \left(\frac{\partial_r \nu}{2} e^{\nu/2} - A e^{\lambda/2} - J r \omega \sin \theta \right) \\ &+ dt \wedge d\theta (-E r - K r \omega \sin \theta) \\ &+ dt \wedge d\varphi (-I r \sin \theta - L \omega r \sin \theta) + dr \wedge d\theta (C e^{\lambda/2} - F r) \\ &+ dr \wedge d\varphi (-J r \sin \theta + D e^{\lambda/2}) + d\theta \wedge d\varphi (H r - K r \sin \theta), \end{aligned} \quad (\text{A.18a})$$

$$\begin{aligned} \mathbf{T}^1 = 0 : \quad 0 &= dt \wedge dr (-B e^{\nu/2} + R \omega r \sin \theta) + dt \wedge d\theta (-C e^{\nu/2} + M r + S \omega r \sin \theta) \\ &+ dt \wedge d\varphi (-D e^{\nu/2} + Q r \sin \theta + T \omega r \sin \theta) + dr \wedge d\theta (N r) \\ &+ dr \wedge d\varphi (r R \sin \theta) + d\theta \wedge d\varphi (-P r + S r \sin \theta), \end{aligned} \quad (\text{A.18b})$$

$$\begin{aligned} \mathbf{T}^2 = 0 : \quad 0 &= dt \wedge dr (-F e^{\nu/2} - M e^{\lambda/2} + V \omega r \sin \theta) \\ &+ dt \wedge d\theta (-G e^{\nu/2} + W \omega r \sin \theta) \\ &+ dt \wedge d\varphi (-H e^{\nu/2} + U r \sin \theta + X \omega r \sin \theta) + dr \wedge d\theta (1 - O e^{\lambda/2}) \\ &+ dr \wedge d\varphi (P e^{\lambda/2} + V r \sin \theta) + d\theta \wedge d\varphi (W r \sin \theta), \end{aligned} \quad (\text{A.18c})$$

$$\begin{aligned} \mathbf{T}^3 = 0 : \quad 0 &= dt \wedge dr (\sin \theta \partial_r (r \omega) - J e^{\nu/2} - Q e^{\lambda/2}) \\ &+ dt \wedge d\theta (r \partial_\theta (\sin \theta \omega) - K e^{\nu/2} - U r) \\ &+ dt \wedge d\varphi (-L e^{\nu/2}) + dr \wedge d\theta (S e^{\lambda/2} - V r) \\ &+ dr \wedge d\varphi (T e^{\lambda/2} + \sin \theta) + d\theta \wedge d\varphi (r \cos \theta + X r). \end{aligned} \quad (\text{A.18d})$$

These imply 24 equations that need to be solved, whose solutions are

$$A = \frac{\partial_r \nu}{2} e^{(\nu-\lambda)/2} - J e^{-\lambda/2} \omega r \sin \theta = \frac{\partial_r \nu}{2} e^{(\nu-\lambda)/2} + \mathcal{O}(\omega^2), \quad (\text{A.19a})$$

$$D = J r \sin \theta e^{-\lambda/2}, \quad (\text{A.19b})$$

$$E = -K \omega \sin \theta = \mathcal{O}(\omega^2), \quad (\text{A.19c})$$

$$H = K \sin \theta, \quad (\text{A.19d})$$

$$J = \frac{\partial_r \omega}{2} r \sin \theta e^{-\nu/2}, \quad (\text{A.19e})$$

$$K = \frac{\partial_\theta \omega}{2} r \sin \theta e^{-\nu/2}, \quad (\text{A.19f})$$

$$O = -e^{-\lambda/2}, \quad (\text{A.19g})$$

$$Q = \sin \theta \partial_r (\omega r) e^{-\lambda/2} - J e^{(\nu-\lambda)/2}, \quad (\text{A.19h})$$

$$T = -e^{-\lambda/2} \sin \theta, \quad (\text{A.19i})$$

$$U = \frac{K e^{\nu/2}}{r} + \omega \cos \theta, \quad (\text{A.19j})$$

$$X = -\cos \theta, \quad (\text{A.19k})$$

and $B = C = F = G = I = L = M = N = P = R = S = V = W = 0$.

Next, we calculate $R_{n\mu\nu}^m$. This is relatively fast but still tedious because the explicit expression is quite long. To do this, we calculate the curvature 2-form first:

$$\begin{aligned} \mathbf{R}_1^0 = \mathbf{R}_0^1 &= dt \wedge dr (-\partial_r A + JQ) + dt \wedge d\theta (-EO + KQ) \\ &\quad + dt \wedge d\varphi (0) + dr \wedge d\theta (0) \\ &\quad + dr \wedge d\varphi (\partial_r D - JT) + d\theta \wedge d\varphi (\partial_\theta D + HO - KT), \end{aligned} \quad (\text{A.20a})$$

$$\begin{aligned} \mathbf{R}_2^0 = \mathbf{R}_0^2 &= dt \wedge dr (-\partial_r E + JU) + dt \wedge d\theta (-\partial_\theta E + AO + KU) \\ &\quad + dt \wedge d\varphi (0) + dr \wedge d\theta (0) \\ &\quad + dr \wedge d\varphi (\partial_r H - JX) + d\theta \wedge d\varphi (\partial_\theta H - DO - KX), \end{aligned} \quad (\text{A.20b})$$

$$\begin{aligned} \mathbf{R}_3^0 = \mathbf{R}_0^3 &= dt \wedge dr (0) + dt \wedge d\theta (0) \\ &\quad + dt \wedge d\varphi (AT - DQ + EX - HU) + dr \wedge d\theta (-\partial_\theta J + \partial_r K) \\ &\quad + dr \wedge d\varphi (0) + d\theta \wedge d\varphi (0), \end{aligned} \quad (\text{A.20c})$$

$$\begin{aligned} \mathbf{R}_2^1 = -\mathbf{R}_1^2 &= dt \wedge dr (0) + dt \wedge d\theta (0) \\ &\quad + dt \wedge d\varphi (AH - DE - QX + TU) + dr \wedge d\theta (\partial_r O) \\ &\quad + dr \wedge d\varphi (0) + d\theta \wedge d\varphi (0), \end{aligned} \quad (\text{A.20d})$$

$$\begin{aligned} \mathbf{R}_3^1 = -\mathbf{R}_1^3 &= dt \wedge dr (-\partial_r Q + AJ) + dt \wedge d\theta (-\partial_\theta Q + AK + OU) \\ &\quad + dt \wedge d\varphi (0) + dr \wedge d\theta (0) \\ &\quad + dr \wedge d\varphi (\partial_r T - DJ) + d\theta \wedge d\varphi (\partial_\theta T - DK + OX), \end{aligned} \quad (\text{A.20e})$$

$$\begin{aligned} \mathbf{R}_3^2 = -\mathbf{R}_2^3 &= dt \wedge dr (-\partial_r U + EJ) + dt \wedge d\theta (-\partial_\theta U + EK + OQ) \\ &\quad + dt \wedge d\varphi (0) + dr \wedge d\theta (0) \\ &\quad + dr \wedge d\varphi (\partial_r X - HJ) + d\theta \wedge d\varphi (\partial_\theta X - HK - OT). \end{aligned} \quad (\text{A.20f})$$

Then, $R_{n\mu\nu}^m$ are just the terms in the round brackets. So, the non-zero ones are R_{1tr}^0 , $R_{1t\theta}^0$, $R_{1r\varphi}^0$, $R_{1\theta\varphi}^0$, R_{2tr}^0 , $R_{2t\theta}^0$, $R_{2r\varphi}^0$, $R_{2\theta\varphi}^0$, R_{3tr}^0 , $R_{3t\theta}^0$, $R_{3r\varphi}^1$, $R_{2t\varphi}^1$, $R_{2r\theta}^1$, R_{3tr}^1 , $R_{3t\theta}^1$, $R_{3r\varphi}^1$, $R_{3\theta\varphi}^1$, R_{3tr}^2 , $R_{3t\theta}^2$, $R_{3r\varphi}^2$ and $R_{3\theta\varphi}^2$. For instance,

$$R_{1r\varphi}^0 = \partial_r D - JT = \partial_r \left(\frac{\partial_r \omega}{2} r^2 \sin^2 \theta e^{-(\lambda+\nu)/2} \right) - \frac{\partial_r \omega}{2} r \sin^2 \theta e^{-(\lambda+\nu)/2}, \quad (\text{A.21})$$

$$\begin{aligned} R_{2\theta\varphi}^0 &= \partial_\theta H - DO - KX \\ &= \partial_\theta \left(\frac{\partial_\theta \omega}{2} r \sin^2 \theta e^{-\nu/2} \right) + \frac{\partial_r \omega}{2} r^2 \sin^2 \theta e^{-\lambda-\nu/2} + \frac{\partial_\theta \omega}{4} r \sin(2\theta) e^{-\nu/2}, \end{aligned} \quad (\text{A.22})$$

$$R_{3t\varphi}^0 = AT - DQ + EX - HU = -\frac{\partial_r \nu}{2} \sin \theta e^{(\nu-2\lambda)/2} + \mathcal{O}(\omega^2). \quad (\text{A.23})$$

Lastly, we use Eq. (A.13) to convert all tetrad indices into coordinate indices. Notice that $R_{t\mu\nu}^t$ and $R_{\varphi\mu\nu}^\varphi$ are non-zero, because $e_t^3 = -r\omega \sin \theta \neq 0$ and $e_0^\varphi = e^{-\nu/2}\omega \neq 0$.

The steps are straightforward so we do not show them here.

After we obtain the components of the Riemann tensor, we can calculate the Ricci tensor. We recommend calculating the Riemann tensor first using Eq. (A.13) then moving to the Ricci tensor. We **do not** recommend calculating Ricci tensor directly because it will be very tedious. To illustrate the nightmare, this is an example:

$$\begin{aligned}
R_{\varphi}^t &= R_{\mu\varphi\nu}^t q^{\mu\nu} = R_{n\varphi\nu}^m e_m^t e_{\mu}^n q^{\mu\nu} = R_{n\varphi\nu}^0 e_0^t e_{\mu}^n q^{\mu\nu} \\
&= R_{1\varphi\nu}^0 e_0^t e_{\mu}^1 q^{\mu\nu} + R_{2\varphi\nu}^0 e_0^t e_{\mu}^2 q^{\mu\nu} + R_{3\varphi\nu}^0 e_0^t e_{\mu}^3 q^{\mu\nu} \\
&= R_{1\varphi\nu}^0 e_r^t e_0^1 q^{r\nu} + R_{2\varphi\nu}^0 e_{\theta}^t e_0^2 q^{\theta\nu} + R_{3\varphi\nu}^0 e_{\varphi}^t e_0^3 q^{\varphi\nu} + R_{3\varphi\nu}^0 e_0^t e_t^3 q^{t\nu} \\
&= R_{1\varphi r}^0 e_r^t e_0^1 q^{rr} + R_{2\varphi\theta}^0 e_0^t e_{\theta}^2 q^{\theta\theta} + R_{3\varphi t}^0 e_0^t e_{\varphi}^3 q^{\varphi t} + R_{3\varphi t}^0 e_0^t e_t^3 q^{tt} \\
&= -R_{1r\varphi}^0 e_0^t e_r^1 q^{rr} - R_{2\theta\varphi}^0 e_0^t e_{\theta}^2 q^{\theta\theta} - R_{3t\varphi}^0 e_{\varphi}^t e_0^3 q^{\varphi t} - R_{3t\varphi}^0 e_0^t e_t^3 q^{tt} \\
&= -R_{1r\varphi}^0 e_0^t e_r^1 q^{rr} - R_{2\theta\varphi}^0 e_0^t e_{\theta}^2 q^{\theta\theta} - R_{3t\varphi}^0 e_0^t (e_{\varphi}^3 q^{\varphi t} + e_t^3 q^{tt}) \\
&= -R_{1r\varphi}^0 e^{-(\lambda+\nu)/2} - R_{2\theta\varphi}^0 e^{-\nu/2} \frac{1}{r} - R_{3t\varphi}^0 e^{-\nu/2} (-wr \sin \theta e^{-\nu} + wr \sin \theta e^{-\nu}) \\
&= -\left(\partial_r \left(\frac{\partial_r \omega}{2} r^2 \sin^2 \theta e^{-(\lambda+\nu)/2} \right) + \frac{\partial_r \omega}{2} r \sin^2 \theta e^{-(\lambda+\nu)/2} \right) e^{-(\lambda+\nu)/2} \\
&\quad - \left(\partial_\theta \left(\frac{\partial_\theta \omega}{2} r \sin^2 \theta e^{-\nu/2} \right) + \frac{\partial_\theta \omega}{2} r^2 \sin^2 \theta e^{-\lambda-\nu/2} \right. \\
&\quad \left. + \frac{\partial_\theta \omega}{2} r \sin \theta \cos \theta e^{-\nu/2} \right) e^{-\nu/2} \frac{1}{r} \\
&= -\frac{e^{-(\nu+\lambda)/2}}{2r^2 \sin \theta} [\partial_r (e^{-(\nu+\lambda)/2} r^4 \sin^3 \theta \partial_r \omega) + \partial_\theta (e^{(\lambda-\nu)/2} r^2 \sin^3 \theta \partial_\theta \omega)]. \quad (\text{A.24})
\end{aligned}$$

Now, we can calculate the components of the Einstein tensor from the Ricci tensor. The final results are as follows:

$$G_t^t = -\frac{e^{-\lambda} (r\lambda' + e^\lambda - 1)}{r^2} + \mathcal{O}(\omega), \quad (\text{A.25a})$$

$$G_r^r = \frac{e^{-\lambda} (-e^\lambda + r\nu' + 1)}{r^2} + \mathcal{O}(\omega), \quad (\text{A.25b})$$

$$G_\theta^\theta = G_\varphi^\varphi = \frac{e^{-\lambda} (-\lambda' (r\nu' + 2) + 2r\nu'' + r\nu'^2 + 2\nu')}{4r} + \mathcal{O}(\omega), \quad (\text{A.25c})$$

$$\begin{aligned}
G_t^\varphi &= R_t^\varphi = -\frac{e^{-\lambda}}{4r^2} [\omega (2r^2 \nu'' + r^2 \nu'^2 + r\lambda' (2 - r\nu') + 4e^\lambda + 2r\nu' - 4) \\
&\quad + r^2 \lambda' \partial_r \omega + r^2 \nu' \partial_r \omega - 2r^2 \partial_r^2 \omega - 2e^\lambda \partial_\theta^2 \omega - 6 \cot(\theta) e^\lambda \partial_\theta \omega - 8r \partial_r \omega] \\
&\quad + \mathcal{O}(\omega^2), \quad (\text{A.25d})
\end{aligned}$$

$$G_\varphi^t = R_\varphi^t. \quad (\text{A.25e})$$

PENYANDANG DANA DAN PUBLIKASI ILMIAH TERKAIT DISERTASI

PENYANDANG DANA

Disertasi ini didanai oleh:

- DRPM UIs Publikasi Terindeks Internasional (PUTI) Doktor 2020 grant No. NKB-614/UN2.RST/HKP.05.00/2020.
- Kemenristek/BRINs Penelitian Disertasi Doktor (PDD) 2021 grant No. NKB-314/UN2.RST/HKP.05.00/2021.

PUBLIKASI ILMIAH

Disertasi ini merupakan kumpulan dari berbagai publikasi berikut:

- I. Prasetyo, H. S. Ramadhan and A. Sulaksono, “Ultra-compact objects from semi-classical gravity,” Phys. Rev. D **103**, no.12, 123536 (2021) [arXiv:2105.11691 [gr-qc]],
- I. Prasetyo, H. Maulana, H. S. Ramadhan and A. Sulaksono, “2.6 M \odot compact object and neutron stars in Eddington-inspired Born-Infeld theory of gravity,” Phys. Rev. D **104**, no.8, 084029 (2021) [arXiv:2109.05718 [gr-qc]].
- I. Prasetyo, H. S. Ramadhan, and A. Sulaksono, “Exterior solutions of ultra-compact object candidate from semi-classical gravity,” AIP Conference Proceedings **2320**, 050024 (2021).
- I. Prasetyo, H. S. Ramadhan, and A. Sulaksono, “Moment of Inertia of a Slowly Rotating Compact Star in Eddington-inspired Born Infeld Theory,” AIP Conference Proceedings **2374**, 020001 (2021).

BIOGRAFI PENULIS



Ilham Prasetyo dilahirkan di Tangerang, Banten pada tanggal 28 Desember 1992. Anak kedua dari dua bersaudara pasangan Bapak Aba Badrudin dan Ibu Sri Susilowati. Penulis menamatkan pendidikan SMA di SMAI Al-Azhar 1, Kebayoran Baru, DKI Jakarta pada tahun 2010. Penulis lulus sarjana di Jurusan Fisika Universitas Indonesia pada tahun 2015. Selanjutnya, penulis lulus magister di Jurusan Ilmu Fisika Universitas Indonesia pada tahun 2017. Penulis kemudian magang sebagai *Research Assistant* di Pusat Penelitian Fisika LIPI pada tahun 2017-2018 di bawah bimbingan Dr. Ardian Nata Atmaja. Tahun 2019 penulis melanjutkan program doktor di Jurusan Ilmu Fisika FMIPA Universitas Indonesia dengan bantuan biaya pendidikan dari DRPM UI dan Ristek/BRIN.